8 Atmospheric Nanoparticles

Cort Anastasio

Atmospheric Science Program
Department of Land, Air & Water Resources
University of California-Davis
One Shields Avenue
Davis, California 95616

Scot T. Martin

Division of Engineering and Applied Sciences
29 Oxford Street, Pierce Hall
Harvard University
Cambridge, Massachusetts 02138

INTRODUCTION

Atmospheric nanoparticles are of growing interest to many investigators for two main reasons. First, nanoparticles are important precursors for the formation of larger particles, which are known to strongly influence global climate, atmospheric chemistry, visibility, and the regional and global transport of pollutants and biological nutrients. Second, atmospheric nanoparticles may play critical roles in the deleterious human health effects associated with air pollution. In addition to these two well-recognized roles, nanoparticles may also significantly influence the chemistry of the atmosphere. Because their composition and reactivity can be quite different from larger particles, the presence of nanoparticles may open novel chemical transformation pathways in the atmosphere. There is possibly also an important role for nanostructures within larger particles, which often contain nanoscale features such as mineral grain agglomerates, soot spherules, or layer coatings of sulfates and nitrates. These complex morphological features likely influence a number of properties. For example, nanostructures probably affect water uptake via capillary condensation and nanoscale aqueous surface films may provide a medium for heterogeneous chemistry. In addition, nanoscale active sites on surfaces may influence particle phase transitions through heterogeneous nucleation. However, with a few notable exceptions, the potential roles and implications in atmospheric chemistry for nanoparticles and nanostructures have not been quantitatively examined.

The goal of this chapter is to provide a survey of what is currently known about nanoparticles in the atmosphere, especially in terms of their formation and growth, number concentrations and chemical composition, and chemical, physical, and mechanical properties. Although combustion sources are important sources of nanoparticles, we do not discuss the special conditions (e.g., in terms of particle dynamics) encountered in combustion plumes. This chapter complements two recent journal issues, one focused on nano- and ultrafine particles in the atmosphere (*Philosphical Transactions of the Royal Society of London* A, vol. 358, no. 1775, 2000) and the other containing papers related to nanoparticles in technology and in the atmosphere (*Journal of Aerosol Science*, vol. 29, no. 5-6, 1998). Given the mineralogy context of the volume in which this chapter appears, we also provide a general introduction to the occurrence and physicochemical properties of atmospheric particles.

At the outset of this chapter, one point of distinction is necessary regarding the term "nano" in the context of atmo spheric particles. In contemporary scientific usage in many fields such as materials science, chemistry, and physics, nanoscale is understood to mean

1529-6466/01/0044-0008$10.00 DOI:10.2138/rmg.2001.44.08

at a lengthscale where properties diverge from the bulk. In this chapter, we also adopt this definition on occasion. However, there is a second usage employed by aerosol scientists, who in recent years have pushed the detection limits of their instrumentation to particles as small as 3 nm. In this framework, a nanoparticle is defined solely by size. A common contemporary understanding is that a nanoparticle has a diameter under 50 nm, and we will generally use this definition in this chapter. The exact usage in each case should be clear from its context.

As this review will show, much must still be elucidated in the field of atmospheric nanoparticles and many important unknowns remain. However, a recent surge of research activities in this area should greatly contribute to our knowledge in the coming years.

BACKGROUND CONCEPTS

This section provides a general overview on the physicochemical properties of atmospheric aerosols. An aerosol is defined as a suspension of solid or liquid particles in a gas, though sometimes the term is used in the vernacular to refer solely to the suspended particles or particulate matter. Excellent references on atmospheric aerosols include Finlayson-Pitts and Pitts (2000), Seinfeld and Pandis (1998), Kreidenweis et al. (1999), and Friedlander (2000).

Size distributions of atmospheric particles

Atmospheric particles have spherical equivalent diameters (D_p) ranging from 1 nm to 100 μm. Plots of particle number concentration (as well as surface area and volume) as a function of particle size usually show that an atmospheric aerosol is composed of three or more modes, as illustrated in Figure 1. By convention, particles are classified into three approximate categories according to their size: Aitken (or transient) nuclei mode ($D_p < 0.1$ μm), accumulation mode ($0.1 < D_p < 2.5$ μm), and coarse mode ($D_p > 2.5$ μm) (Seinfeld and Pandis 1998). Particles smaller than 2.5 μm are generally classified as fine. The terms $PM_{2.5}$ and PM_{10} refer to particulate matter with aerodynamic equivalent diameters under 2.5 and 10 μm, respectively. These terms are often used to describe the total mass of particles with diameters smaller than the cutoff size.

In addition to the three modes described above, recent measurements have shown that there is often a distinct particle mode under 10-nm diameter (Fig. 2). There is no current agreement for the name of particles in this mode, which are interchangeably called ultrafine particles, nanoparticles, or nucleation mode particles. There are also alternative definitions for these terms, which can be a source of confusion. For example, the term ultrafine particles is sometimes employed to refer solely to particles with D_p = 3 -10 nm (e.g., in nucleation studies) or to all particles with $D_p < 100$ nm (e.g., in health and emission studies). Similarly, the term nanoparticles is sometimes employed as a description for all particles of $D_p < 50$ nm (regardless of mode), sometimes for particles of 10-nm diameter or less, and occasionally for any particle with $D_p < 1$ μm. In this review we use the common current definitions of ultrafine particles as those with $D_p < 100$ nm and nanoparticles as those with $D_p < 50$ nm.

The different size modes reflect differences in particle sources, transformations, and sinks (Finlayson-Pitts and Pitts 2000). For example, coarse particles are generated by mechanical processes such as wind erosion of soil, wave action in the oceans, and abrasion of plant material. In contrast, many of the fine particles in the atmosphere are produced from either primary emissions from combustion sources or via atmospheric gas-to-particle conversions (i.e., new particle formation). The relative and absolute sizes of particle modes, as well as the number of modes, can vary greatly in different locations and at different times. In addition, the chemical composition of particles within one size

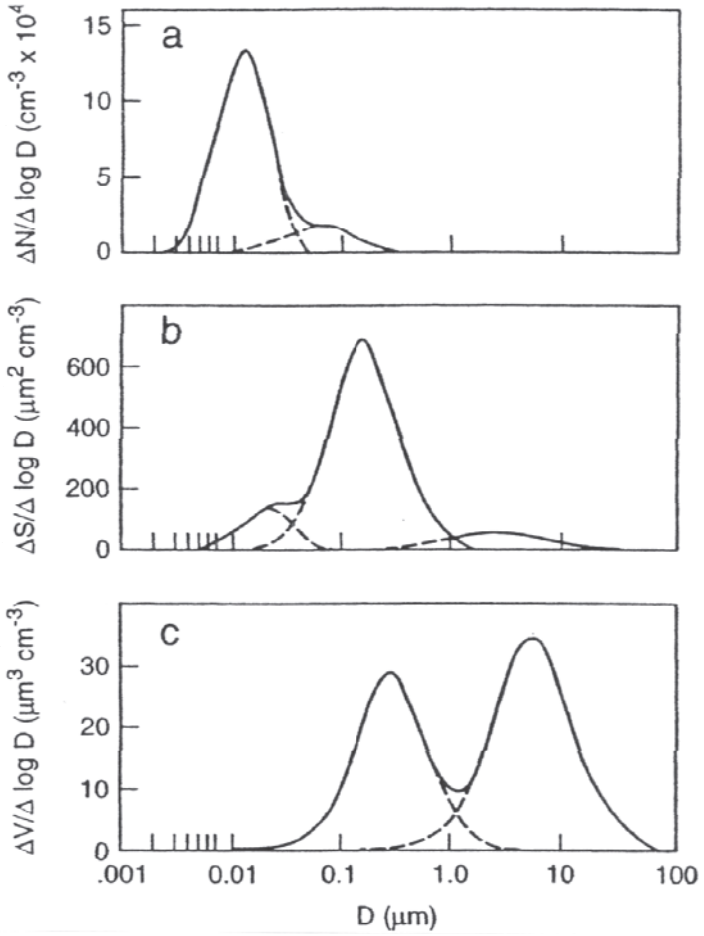

Figure 1. Number (ΔN/Δlog D), surface area (ΔS/Δlog D), and volume (ΔV/Δlog D) distributions for a typical urban aerosol. The solid lines are the size distributions, while the dashed lines show the tails between intersecting modes. The total number concentration, surface area, and volume equal the areas under the curves of each mode. From Finlayson-Pitts and Pitts (2000). Used by permission of Academic Press.

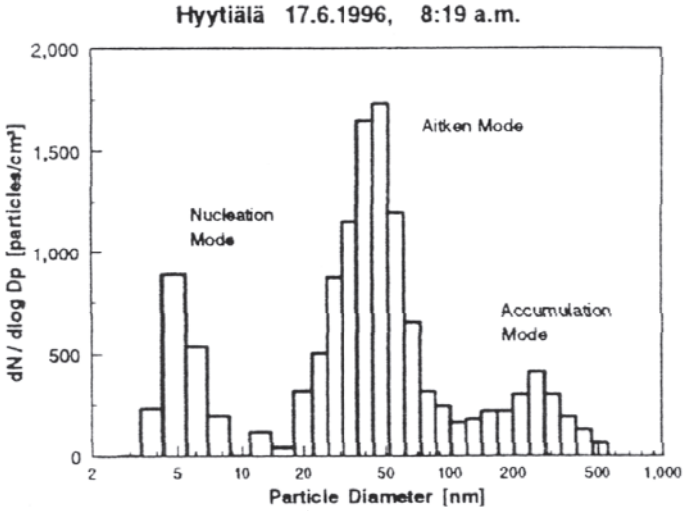

Figure 2. Trimodal structure of the submicron particle number size distribution observed at a boreal forest in Hyytiä lä , Finland on June 17, 1996, 08:09-08:19. The total particle number concentration of the submicron aerosol is 1011 particles cm^{-3}. From Mä kelä et al. (1997). Used by permission of the American Geophysical Union.

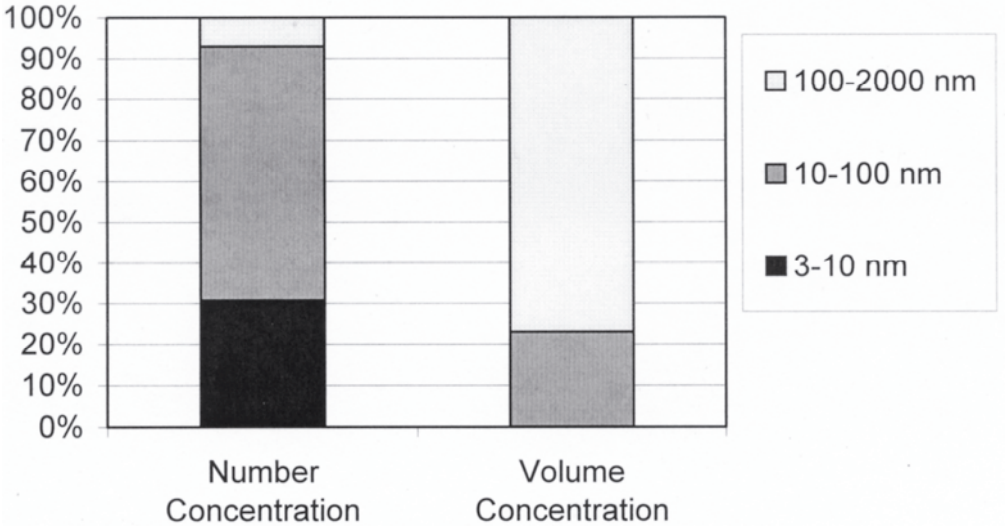

Figure 3. Percent of total ($D_p \leq 2$ μm) particle number and volume concentrations in three size ranges in Atlanta, Georgia. From Woo et al. (2001). Used by permission of Taylor & Francis, Inc.

mode often differs considerably from those in other size modes. Even within one size mode, there is often a wide variety of particle compositions, i.e., the aerosol is externally mixed (Noble and Prather 1996). The opposite situation, where all particles have the same composition, is called an internally mixed aerosol.

As shown in Figure 1, within an atmospheric aerosol the smallest particles usually dominate the total number of particles, while the accumulation and coarse modes often determine the total surface area and volume (i.e., mass), respectively. For example, Figure 3 shows results from a study in Atlanta where nanoparticles (D_p = 3-10 nm) and nano- and ultrafine particles (D_p = 10-100 nm) contributed approximately 30 and 60%, respectively, to the total particle number concentration ($D_p \leq 2$ μm). However, in terms of particle mass, the accumulation mode particles were dominant, and nanoparticles with $D_p < 10$ nm contributed insignificantly.

Sources and sinks of atmospheric particles

Atmospheric particles are classified as primary when they are emitted directly into the atmosphere and as secondary when they form in the atmosphere from reactions of atmospheric gases. The dominant particle sources by mass are mineral dust from wind-blown soils and sea-salt particles from wave breaking (Table 1). These primary sources produce high numbers of coarse particles that dominate the mass distribution of the aerosol, but measurements during the last decade show that these sources can also produce appreciable numbers of nanoparticles. The dominant sources of fine particles include anthropogenic primary emissions from combustion processes and secondary aerosol formation from the oxidation of species such as gaseous SO_2 or organic compounds (Table 1). The estimates in Table 1 show that anthropogenic emissions of particles and their gaseous precursors have more than doubled the flux of fine particles into the atmosphere. This fact suggests that the burden of nanoparticles in the atmosphere has also greatly increased because of anthropogenic emissions.

There are three major sinks that act to remove particles from the atmosphere: diffusion (Brownian motion), wet deposition, and gravitational settling. The relative importance of each mechanism depends primarily upon particle size (Seinfeld and Pandis 1998; Kreidenweis et al. 1999; Friedlander 2000). As shown in Figure 4, diffusion is the

Table 1. Global emission estimates for major aerosol types in the 1980s. From Seinfeld and Pandis (1998). Used by permission of Wiley-Interscience.

Source	*Estimated flux* (Tg yr $^{-1}$) *Low*	*High*	*Best*	*Particle size category*[a]
NATURAL				
Primary				
Soil dust (mineral aerosol)	1000	3000	1500	Mainly coarse[b]
Sea salt	1000	10000	1300	Mianly coarse[b]
Volcanic dust	4	10000	30	Coarse
Biological debris	26	80	50	Coarse
Secondary				
Sulfates from biogenic gases	80	150	130	Fine
Sulfates from volcanic SO_2	5	60	20	Fine
Organics from biogenic gases	40	200	60	Fine
Nitrates from NO_x	15	50	30	Fine and coarse
Total natural	2200	23500	3100	
ANTHROPOGENIC				
Primary				
Industrial dust, etc. (except soot)	40	130	100	Fine and Coarse
Soot	5	20	10	Mainly Coarse
Secondary				
Sulfates from SO_2	170	250	190	Fine
Biomass burning	60	150	90	Fine
Nitrates from NO_x	25	65	50	Mainly Coarse
Organics from anthropogenic gases	5	25	10	Fine
Total anthropogenic	300	650	450	
TOTAL	2500	24000	3600	

[a] Coarse and fine size categories refer to mean D_p above and below 1 μm, respectively.

[b] By mass, coarse particles dominate. By number the fine mode may dominate.

Note that sulfates and nitrates are assumed to occur as ammonium salts.

Flux units: 10^{12} g yr $^{-1}$ (dry mass).

dominant removal mechanism for nanoparticles (D_p < 50 nm) because of their small sizes. Nanoparticles can be removed by diffusing to the Earth's surface (dry deposition), diffusing and colliding with larger particles (intermodal coagulation), or by growing out of the nanoparticle size range (through condensation of gases). Nanoparticle residence times thus depend both upon diameter (which affects the diffusion rate) and upon the atmospheric aerosol surface area. Under typical conditions, nanoparticles are believed to have residence times ranging from minutes to a few days. Coarse particles also have atmospheric residence times that vary from minutes to days, but due to their relatively large sizes, gravitational settling is their dominant removal mechanism. Intermediate between these sizes are the accumulation mode particles. These particles are removed efficiently neither by diffusion nor by settling, and thus they tend to have the longest atmospheric lifetimes (typically days to weeks). The dominant sink for accumulation

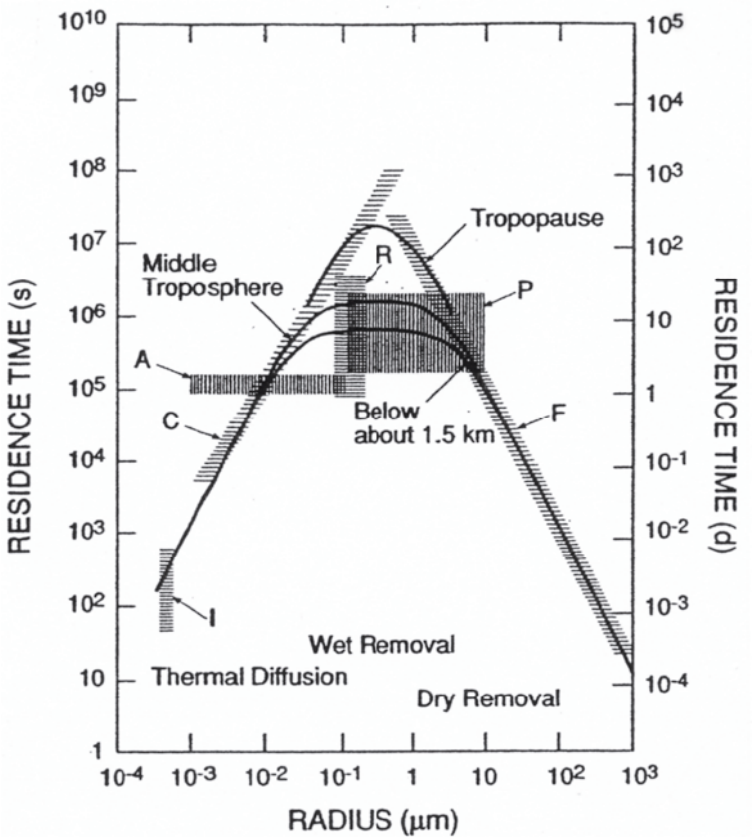

Figure 4. Residence time of particles in seconds (left axis) and days (right axis) as a function of particle radius. The shaded areas represent estimates of the lifetimes made as follows: I, molecular or ionic clusters; C, coagulation of particles; P, removal by precipitation; F, gravitational settling; A, derived from spatial distribution of Aitken particles; R, derived from the distribution of small radioactive particles. From Kreidenweis et al. (1999) in *Atmospheric Chemistry and Global Change* by Brasseur et al. © 1999 by Oxford University Press, Inc. Used by permission.

mode particles is generally removal by precipitation, either as rain-out or wash-out (Finlayson-Pitts and Pitts 2000).

Visibility reduction

One of the most widely recognized aspects of atmospheric pollution is reduced visibility, which is due primarily to light extinction by particles. A common measure of visibility is visual range (V_R), which is defined as the maximum distance at which a black object can be seen against the horizon, as follows:

$$V_R = \frac{\ln(C / C_0)}{b_{est}} \tag{1}$$

where C/C_0 is the contrast that can be discerned by an observer (typically 0.02-0.05) and b_{ext} is the extinction coefficient (units of length^{-1}) (Pilinis 1989; Finlayson-Pitts and Pitts 2000). Thus regions with greater extinction coefficients have lower visual ranges and visibility. Four components contribute to b_{ext}: scattering of light by particles (b_{sp}), absorption of light by particles (b_{ap}), scattering by gases (b_{sg}), and absorption by gases (b_{ag}).

In areas with reduced visibility, scattering of light by particles is usually the dominant extinction term. Typical values of b_{sp} are 10^{-5} to 10^{-3} m^{-1} (Mathai 1990; Sloane et al. 1991; Eldering et al. 1994; Finlayson-Pitts and Pitts 2000; Pryor and Barthelmie 2000). Light scattering is conveniently classified into three regimes based on the size parameter, α, expressed as $\alpha = 2D_p/\lambda$ where λ is the wavelength of light. Rayleigh scattering occurs for small α, Mie scattering for $\alpha \sim 1$, and geometric scattering occurs for large α (Friedlander 2000; Finlayson-Pitts and Pitts 2000). For visible wavelengths, which are relevant for visibility reductions as well as the direct climate effects discussed

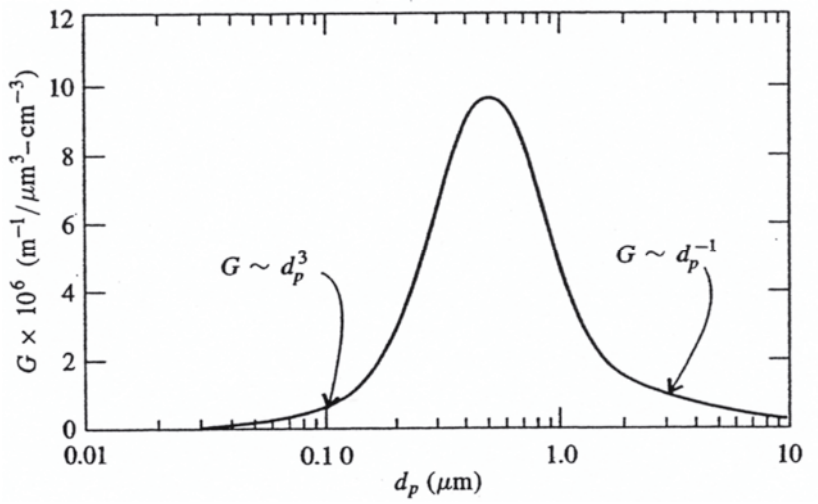

Figure 5. Light scattering per unit volume of aerosol material (G) as a function of particle diameter (d_p), integrated over the wavelengths 360-680 nm for a refractive index of 1.5. The curve is independent of the particle size distribution. From Friedlander (2000) © by Oxford University Press, Inc. Used by permission.

below, Mie scattering is typically the most important mechanism for scattering by atmospheric aerosols. In this regime accumulation mode particles are the most efficient at scattering visible light (Friedlander 2000), as shown in Figure 5. Because of this, and because accumulation mode particles typically dominate fine particle mass, values of b_{ext} for atmospheric aerosols often correlate well with the mass of the fine particle fraction (Finlayson-Pitts and Pitts 2000). Fine particulate components such as sulfate, nitrate, and organic carbon often contribute significantly to b_{sp} (Pilinis 1989; Eldering et al. 1994; Pryor and Barthelmie 2000). In contrast, ultrafine and nanoparticles make small contributions to the scattering of visible light (cf. Fig. 5) (Friedlander 2000).

Absorption of light by particles (b_{ap}) is sometimes an important contribution to the value of b_{ext}. In urban areas, b_{ap} can account for approximately 13-42% of the total extinction coefficient (Finlayson-Pitts and Pitts 2000). The chemical components that contribute most substantially to b_{ap} are soot, organic carbon, and soil dust (Finlayson-Pitts and Pitts 2000). It is unclear whether nano- and ultrafine particles contribute significantly to light absorption by particles. On the one hand, these particle sizes account for an appreciable number fraction of the soot emitted from combustion sources such as diesel engines. On the other hand, unless the particles are highly absorbing, light absorption scales with particle mass, which for atmospheric aerosol contains an insignificant contribution from nanoparticles.

Radiative forcing and climate change

Over the course of the past century, human activities have significantly changed the composition of the atmosphere, which in turn has apparently altered the Earth's climate (IPCC 2001). For example, anthropogenic emissions of long-lived greenhouse gases, such as CO_2, have made the atmosphere less transparent to longwave radiation. Consequently, the atmosphere more efficiently traps longwave radiation emitted by the Earth, which is expected to lead to increased surface temperatures (Crowley 2000; IPCC 2001). However, it is unclear to what extent this increase in temperature might be damped, or possibly enhanced, by climate feedbacks involving clouds, desertification, or changes in ocean circulation. Overall, anthropogenic increases in directly emitted greenhouse gases since pre-industrial times have caused a global-mean radiative forcing

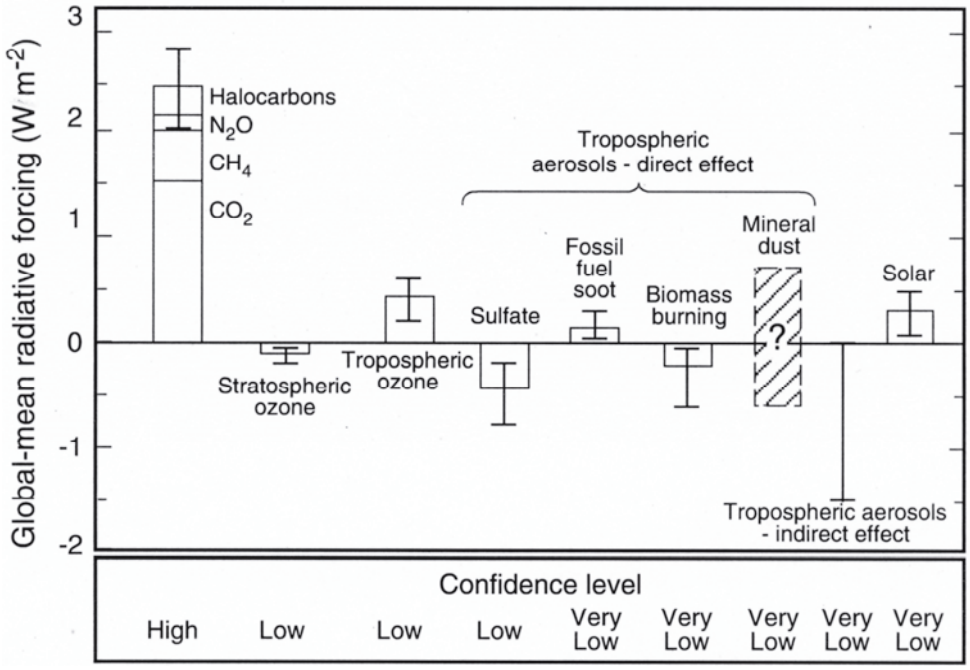

Figure 6. Estimates of globally averaged radiative forcings at the tropopause as a result of changes in greenhouse gases, aerosol particles, and solar activity from pre-industrial times to the present. From Buseck et al. (2000). Used by permission of the editor of *International Geology Review*.

of ca. +2.5 W m^{-2} (Fig. 6). According to most current models, this greenhouse gas forcing is primarily responsible for the globally averaged 0.6°C increase in temperature that has occurred over the past century (Barnett et al. 1999; Crowley 2000; IPCC 2001).

Based on our current understanding, this greenhouse warming would have been larger if not for the effects of atmospheric particles (IPCC 2001). Anthropogenic increases in atmospheric particle loadings have provided a net cooling effect as a result of both direct (i.e., backscatter of incoming solar radiation to space) and indirect effects (i.e., by their effects on clouds) (Boer et al. 2000a,b; Schwartz and Buseck 2000; IPCC 2001). One of the most investigated direct effects is the scattering of incoming solar radiation by sulfate particles. This scattering is believed to cause a negative radiative forcing of approximately -0.5 W m^{-2}, though the exact value is uncertain (Fig. 6) (Penner et al. 1998; Harvey 2000; Kiehl et al. 2000). Anthropogenic sulfate particles are derived primarily from fossil fuel combustion, which releases SO_2 that is subsequently oxidized in the atmosphere to H_2SO_4 (Finlayson-Pitts and Pitts 2000). The combustion of fossil fuels, especially coal, has approximately doubled the mass of sulfate particles in the atmosphere (Table 1).

Other types of particles also contribute significantly to changes in radiative forcing (Fig. 6). Carbonaceous aerosols from biomass burning are thought to cause a net negative forcing due to scattering from organic components. In contrast, soot from fossil fuel combustion is believed to have a net positive forcing because of light absorption (Penner et al. 1998). Recent work by Jacobson (2001) estimates the forcing from soot particles to be +0.55 W m^{-2}. This value is much larger than previously thought (e.g., Fig. 6) and arises from the internal mixing of soot with other particle types such as sulfate. It has been suggested that this atmospheric warming by soot particles could reduce cloud cover (Ackerman et al. 2000). However, modeling by Lohmann and Feichter (2001) indicates

that on a global scale this "semi-direct" effect is small compared to the indirect effects of aerosols.

Another important particle type is mineral dust. The atmospheric loading of mineral dust is increasing due to land-use changes accompanying anthropogenic activities. These particles may have significant climatic effects, though the sign and the magnitude of this forcing are not known (Fig. 6) (Buseck and Pó sfai 1999; Buseck et al. 2000). This uncertainty arises because mineral dusts both scatter incoming solar radiation (a negative forcing) and absorb solar and longwave radiation (a positive forcing) (Miller and Tegen 1998; Buseck and Pó sfai 1999).

In addition to their direct effects, particles also affect climate indirectly by modifying the optical properties, frequencies, and lifetimes of clouds (IPCC 2001). This indirect effect is estimated to have a very large negative forcing, though the magnitude of the effect is highly uncertain (Fig. 6). The indirect effect is a result of anthropogenic increases in the number of cloud condensation nuclei (CCN), which are hygroscopic particles that serve as centers for water condensation and thus the formation of cloud droplets (Finlayson-Pitts and Pitts 2000). For a fixed cloud liquid water content, an increase in the number of CCN yields smaller cloud drops. This causes an increase in the albedo (reflectivity) of the cloud and thereby enhances its efficiency for scattering incoming solar radiation (Twomey 1977; Charlson et al. 1992). In addition, clouds with smaller drops precipitate less frequently and thus have longer lifetimes, which amplifies the climatic impact (Albrecht 1989; Borys et al. 2000; Rosenfeld 2000). Because nanoparticles are important precursors for CCN, there is much current research activity aimed at understanding how nanoparticles form and grow into CCN.

Health effects

Epidemiologic analyses link ambient atmospheric particles with acute and chronic adverse health effects, including respiratory disease, reduced lung function, cardiovascular effects, and mortality (Pope et al. 1995a; Pope 2000; Schlesinger 2000). The associations found in these analyses are particularly strong for susceptible populations such as the elderly, children with asthma, and others with pre-existing respiratory problems (Utell and Frampton 2000). There is no consensus on what types or sizes of atmospheric particles are most responsible for these effects. While a number of epidemiological studies find that fine particle mass (i.e., $PM_{2.5}$) is strongly associated with adverse health effects (Dockery et al. 1993; Pope et al. 1995b; Brunekreef 2000; Pope 2000), other studies indicate coarse particles (e.g., PM_{10}) are more strongly associated (Pope et al. 1995a; Pekkanen et al. 1997; Brunekreef 2000; Loomis 2000). In addition, a few epidemiological studies have shown that impairment in pulmonary function is best correlated to the number of ultrafine ($D_p < 100$ nm) particles (Peters et al. 1997; Hauser et al. 2001).

There are numerous hypotheses—but few definitive results—as to what physicochemical characteristics of atmospheric particles are responsible for adverse health effects (Samet 2000; Schlesinger 2000). Hypotheses include general properties such as mass, surface area, or size, as well as more specific chemical properties such as acidity or elevated concentrations of transition metals (Dreher et al. 1997; Samet 2000). For example, it has been suggested that particulate iron is toxic due to its ability to generate the strongly oxidizing hydroxyl radical through the Fenton reaction (Ghio et al. 1996; Smith and Aust 1997; Donaldson et al. 1998; van Maanen et al. 1999):

$$\mathrm{Fe(II) + HOOH \longrightarrow Fe(III) + {}^{\bullet}OH + {}^{-}OH} \qquad (2)$$

In biological systems the hydroxyl radical can lead to damage such as lipid peroxidation and DNA breakage (van Maanen et al. 1999). In support of this hypothesis, iron is often the most abundant transition metal in atmospheric particles, and there are numerous reports that particulate Fe(III) can be reduced to Fe(II) as a result of atmospheric reactions (Faust 1994).

Animal studies provide additional evidence that ultrafine or nanoparticles might be at least partially responsible for the health effects associated with atmospheric particles. For example, for the same mass of particles instilled into rat lungs, TiO_2 nanoparticles (D_p = 20 nm) yield a greater inflammatory response compared to that from fine TiO_2 particles (250 nm) (Oberdörster 2001). However, when the doses are normalized to particle surface area, the inflammatory response is the same, suggesting that surface reactions might have been responsible for the observed effects. These results also indicate that there is no special reactivity for the TiO_2 nanoparticles compared to the larger particles. In contrast, Donaldson et al. (2000) suggest that, in terms of adverse health effects, nanoparticle surfaces might be more active than the surfaces of larger particles. A number of other studies show that inhaled or instilled nanoparticles give a greater inflammatory response and cause more oxidative stress than fine particles, though the confounding role of surface area is not evaluated (Donaldson et al. 1998, 2000, 2001). Not all studies, however, show that nanoparticles cause measurable responses. For example, in one study rats and mice exposed to nanoparticles of black carbon ($D_p \sim 40$ nm; 10^5-10^6 cm^{-3}) show no signs of lung injury, while those animals exposed to greater masses of fine particles ($D_p \sim 400$ nm; 10^4-10^5 cm^{-3}) show some adverse effects (Arts et al. 2000).

In addition to the greater surface area discussed above, a number of other hypotheses have been presented as potential explanations for the possibly greater toxicity associated with nano- and ultrafine particles. First, these particles could have increased toxicity because of their high number concentrations in the atmosphere and significant deposition in the lungs. Hughes et al. (1998) have estimated that ca. 10^{11} ultrafine particles are deposited daily in the lungs of a typical person in the Los Angeles area during winter. Ultrafines are efficiently deposited in human lungs (e.g., 40-50% deposition fraction for inhaled 40-nm particles (Jaques and Kim 2000)), and a large fraction of this deposition occurs in the alveoli (i.e., the deepest reaches of the lungs) (Oberdörster 2001). By contrast, accumulation mode particles typically have lower number concentrations, a lower overall lung deposition rate, and a smaller fraction deposited in the alveoli (Oberdörster 2001). Second, there is some evidence that nanoparticles inhibit or overwhelm phagocytosis, perhaps because of their great numbers, and thus decrease the ability of alveolar macrophages to clear out foreign particles (Donaldson et al. 2001). This causes an increased contact time between particles and lung epithelial cells (Donaldson et al. 1998). In conjunction with the small size of nanoparticles, this might allow these particles to cross the alveolar epithelial barrier and enter interstitial spaces (Donaldson et al. 2001). Subsequent transport to other organs could then be possible (Oberdörster 2001). Finally, at least one study indicates that nanoparticles act synergistically or additively with ozone to cause adverse health effects, especially in older rats and mice pre-treated with endotoxin to simulate the compromised lungs of susceptible groups (Elder et al. 2000). This result suggests that health effects from particles are strongly tied with co-exposure to other pollutants (Samet 2000; Oberdörster 2001).

The evidence of adverse health effects from respirable particles, and perhaps nanoparticles in particular, raises the question of what regulatory strategy would be most effective to protect human health. In response to the epidemiological evidence linking

fine particles with adverse health effects, the EPA in 1997 proposed a new mass-based $PM_{2.5}$ standard for ambient air quality (Seinfeld and Pandis 1998). However, in light of the limited evidence that nanoparticles in particular, and perhaps particle number in general, are more important components of particle toxicity, there is concern that the $PM_{2.5}$ standard is not the most effective or economic regulatory approach to protect human health. This is because most of the $PM_{2.5}$ mass results from the larger accumulation mode particles, but most of the aerosol particle number generally results from the nano- and ultrafine particles. The result is that particle number and mass are expected to generally be unrelated (Fig. 7) (Keywood et al. 1999; Woo et al. 2001). Thus control of fine particle mass is likely to have little effect upon nanoparticle number concentrations in the atmosphere. Similarly, a mass-based standard is unlikely to be effective or economic if specific chemical species within atmospheric particles are responsible for the observed adverse health effects.

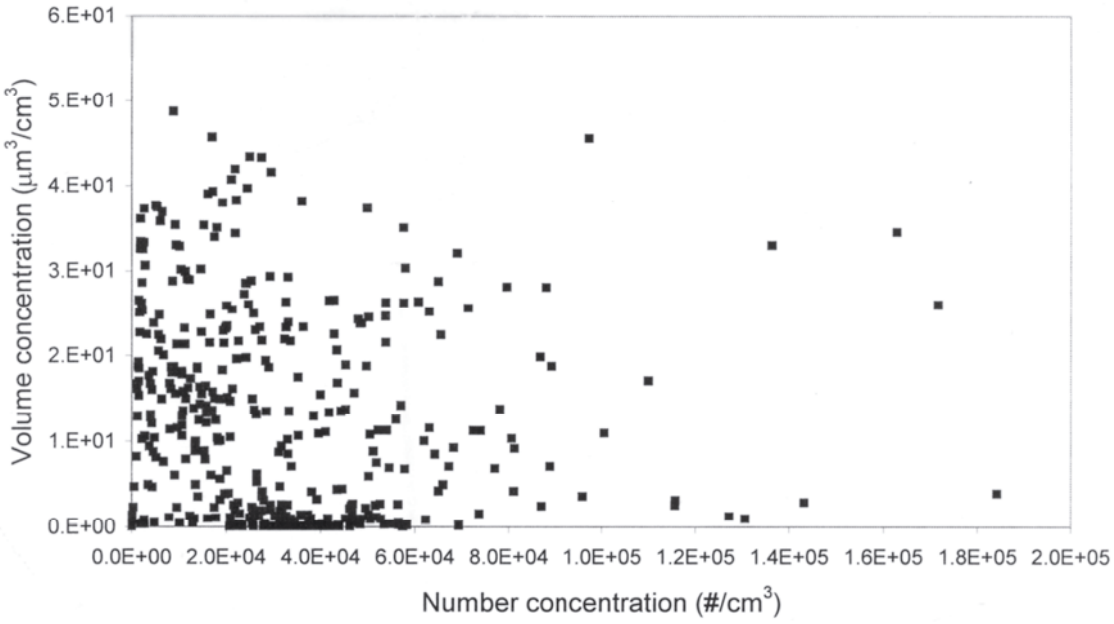

Figure 7. Relationship between volume and number concentrations for particles with D_p = 3 nm to 2 μm in Atlanta, Georgia, during August 1998 through August 1999. From Woo et al. (2001). Used by permission of Taylor & Francis, Inc.

Chemical reactions of atmospheric particles

Reactions involving atmospheric particles have significant effects upon the composition of the atmosphere (Andreae and Crutzen 1997). Perhaps the most well known example is the particle-catalyzed springtime destruction of stratospheric ozone over the Antarctic. Particle reactions in the troposphere are also significant and affect concentrations of important gaseous pollutants such as ozone, nitric acid, and sulfur dioxide. These reactions often alter the composition of the particles as well, which can alter the ability of particles to act as cloud condensation nuclei, change their efficiency for scattering and absorbing light, and perhaps influence their health effects.

Three examples of chemistry occurring on or in atmospheric particles are provided below. These examples demonstrate how particulate-based chemical reactions can alter the composition both of particles and of the gas phase. However, the examples are by no means comprehensive of all chemical processes that occur in the troposphere. The particles involved in these examples are generally accumulation or coarse mode, though

in some cases similar reactions on nanoparticles of the same material might also occur. The chemistry of nanoparticles is discussed separately later in this chapter.

Mineral dusts. The northern African and Gobi deserts are large sources of mineral dusts (Pye 1987; Charlson and Heintzenberg 1994; Prospero 1999a), which are regularly carried by atmospheric circulation patterns to the eastern USA and Brazil as well as the Pacific Ocean (Swap et al. 1992; Leinen et al 1994; Prospero 1999a). The dusts are monitored both by analysis of collected aerosol particles (Prospero 1999b) and by satellite observations (Husar et al. 1997; Herman et al. 1997; Chiapello et al. 1999) (Fig. 8). In addition to these global sources, there are also regional emissions of mineral dusts. In total, nearly one-third of the Earth's land surface is arid and hence a possible dust source (Tegen and Fung 1994), and land use changes associated with human activities are expected to increase the global burden of mineral dusts (Tegen and Fung 1995; Tegen et al. 1996). In addition to the chemistry described below, mineral dusts are also important as an essential component of open ocean fertility, primarily as a source of iron (Duce et al. 1980; Martin and Gordon 1998; Boyd et al. 2000).

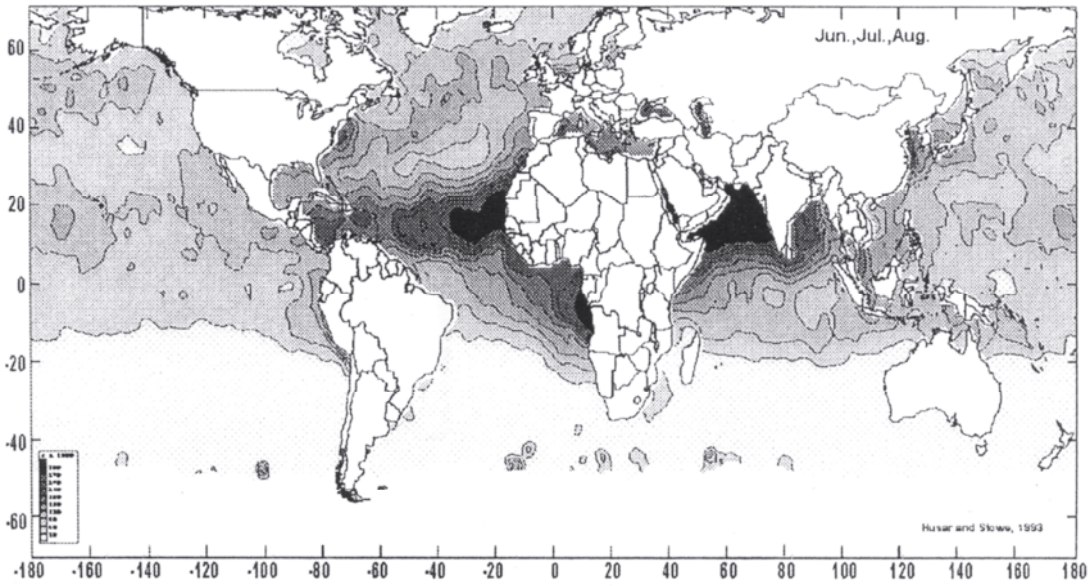

Figure 8. Radiatively equivalent aerosol optical thickness (EAOT × 1000) over the oceans derived from NOAA AVHRR satellites for summer. Darker shades indicate greater values of EAOT. Adapted from Husar et al. (1997). Used by permission of the American Geophysical Union.

The mode of the number size distributions of mineral dusts outside of source regions (i.e., after long-range transport) is approximately 100 nm, though the mass mode typically lies between diameters of 2 to 5 μm (D'Almedia and Schütz 1983). The small particles usually arise from submicron clay particles that are initially attached to larger mineral grains but break free during the abrasive events of a dust storm. Analysis of mineral dust indicates the particles are largely composed of silicates (clay minerals, feldspars, and quartz) and occasionally carbonates and sulfates (Schütz and Sebert 1987; Schütz 1989, 1997; Merrill et al. 1994; Claquin et al. 1999). Dominant clays are illite and kaolinite with contributions by smectite (montmorillonite) and chlorite. Iron and aluminum oxides and hydroxides also contribute, especially as surface coatings, which then dominate the surface chemistry of agglomerated mineral particles (Dixon and Weed 1989). On average, dust composition reflects that of the Earth's crust, though northern Saharan dust contains an unusually high proportion of calcite and gypsum. Submicron

dust arises from heavily weathered soil components.

During their residence time in the atmosphere, mineral dusts become coated by sulfates, nitrates, and other species (Dentener et al. 1996; Buseck and Pó sfai 1999; Zhang and Carmichael 1999; Song and Carmichael 1999; Buseck et al. 2000). These coatings are formed through chemical reactions such as the oxidation of SO_2 and NO_2 at the gas-solid interface, as well as by condensation of sulfuric and nitric acids. Once coated, the hygroscopic dusts act as cloud condensation nuclei and further oxidation reactions can take place in the aqueous medium (Wurzler et al. 2000). Subsequent evaporation of the cloud droplet yields a coated particle.

Recent work has investigated whether surfaces of mineral dusts may provide stoichiometric or catalytic reaction centers that are significant enough to perturb important gas-phase cycles (Dentener et al. 1996; Zhang and Carmichael 1999; Song and Carmichael 1999; de Reus et al. 2000a). For example, the kinetics of the oxidation of SO_2 and NO_2 in the atmosphere may be enhanced by mineral surface reactions. Compared to the gas-phase oxidation of SO_2 and subsequent formation of new submicron sulfate particles, the scavenging of SO_2 by mineral surfaces reduces the climate cooling effect of sulfate aerosol by reducing particle number. In addition, interactions of O_3, HNO_3, and $HO_2^{\bullet}$-radicals with mineral surfaces may perturb the photooxidant cycle downwind of dust sources and lead to reduced levels of tropospheric ozone. A number of studies have examined the uptake of HNO_3 and O_3 on mineral dusts or surrogate surfaces (Fenter et al. 1995; Dentener et al. 1996; Goodman et al. 2000; Hanisch and Crowley 2001; Underwood et al 2001). In some cases values range widely, as discussed by Underwood et al. (2000) and Hanisch and Crowley (2001). The uptake coefficients for NO_2 reaction on alumina and other crustal constituents are regarded as too low to have an impact on gas-phase NO_2, HNO_3, or O_3 (Borensen et al. 2000; Underwood et al. 2001), though coating of mineral surfaces may still be significant. The uptake coefficients for low molecular weight organic molecules such as acetaldehyde, acetone, and propionaldehyde have been measured on SiO_2, Al_2O_3, Fe_2O_3, TiO_2, and CaO. Model results with these uptake values suggest that heterogeneous loss of these organics to mineral dusts is comparable to their loss by direct photolysis or through reaction with hydroxyl radical ($^{\bullet}OH$) in the middle to upper troposphere (Li et al. 2001). In contrast to nitrate, a critical unknown is the rate of SO_2 uptake (and oxidation) on mineral surfaces. More laboratory work is necessary to reduce these uncertainties; current modeling studies must employ assumed values.

Polar stratospheric clouds. During winter over the polar regions of the Earth, temperatures are cold enough that polar stratospheric cloud (PSC) particles composed of sulfuric and nitric acids and water are present (Peter 1997, 1999; Zondlo et al. 2000). The PSC particles form on background H_2SO_4 particles, which have diameters of approximately 50 nm, and grow by condensation of gaseous H_2O and HNO_3 to form particles with diameters of up to several micrometers. Particles as large as 25 μm have recently been reported (Fahey et al. 2001). The chemical constituents of PSC particles may be arranged in several possible phases, including aqueous, ice, and hydrates of sulfuric and nitric acid (Kolb et al. 1995; Martin 2000). Common hydrates include $H_2SO_4 \cdot 4H_2O$ (sulfuric acid tetrahydrate, SAT), $HNO_3 \cdot 2H_2O$ (nitric acid dihydrate, NAD), and $HNO_3 \cdot 3H_2O$ (nitric acid trihydrate, NAT).

A critical step in the annual depletion of polar ozone is the activation of chlorine on the surface of PSC particles, i.e., the conversion of non-ozone-destroying chlorine forms such as $ClONO_2$ into reactive, ozone-destroying chlorine compounds (Abbatt and Molina 1993; Anderson 1995). Critical heterogeneous reactions, for example, are:

$$ClONO_2 + H_2O \xrightarrow{PSC} HOCl + HNO_3 \quad (3)$$

$$ClONO_2 + HCl \xrightarrow{PSC} Cl_2 + HNO_3 \quad (4)$$

HOCl and Cl_2 both rapidly photolyze during polar spring to yield Cl radicals which catalytically destroy O_3. In addition, the HNO_3-containing PSC particles sediment out of the stratosphere, thus removing HNO_3 and serving as a sink for NO_x (i.e., NO and NO_2). This denitrification contributes to sustaining Cl as an active radical because it slows several important chlorine deactivation pathways such as:

$$ClO + NO_2 \xrightarrow{PSC} ClONO_2 \quad (5)$$

One critical research question relates to the kinetics of PSC formation (e.g., nucleation rates of ice and the various acid hydrates) from supercooled aqueous droplets of sulfuric and nitric acids (Tolbert and Toon 2001). Nucleation rates measured in the laboratory appear too slow in many cases to explain the occurrence of PSC particles observed in the polar stratosphere. The obvious hypothesis, that the particles contain heterogeneous nuclei, has not found support because of the low occurrence of nuclei in the stratosphere and the low activity of candidate materials tested in the laboratory. An active area of research remains investigating mechanisms that could explain the formation of PSCs.

Sea-salt particles. Particles formed from sea spray initially have a composition that is similar to bulk seawater but with enhanced levels of organic compounds. The inorganic species in sea-salt particles are chiefly Na^+ and Cl^- with contributions from SO_4^{2-}, Ca^{2+}, Mg^{2+}, and K^+ (Holland 1978). The organics include surfactants and other compounds that are enriched in the surface layer of the ocean. It has been suggested that these compounds form organic layers on the surfaces of sea-salt particles that might impede the transport of gases to and from the largely inorganic core (Ellison et al. 1999). Although most sea-salt particle mass occurs in the coarse mode, there are also significant numbers of sea-salt particles at sizes below 100 nm (Gong et al 1997). For example, Berg et al. (1998) report the occurrence of sea-salt particles in the smallest size mode (35 nm) of their measurements.

Atmospheric processing alters the chemical composition of sea-salt particles, for example by increasing the amounts of SO_4^{2-} and NO_3^- and depleting Cl^- (Duce, 1969; Finlayson-Pitts et al. 1989; Chameides and Stelson 1992; McInnes et al. 1994). One pathway in this processing is:

$$NaCl(s,aq) + HNO_3(g) \longrightarrow NaNO_3(s,aq) + HCl(g) \quad (6)$$

An analogous reaction occurs with sulfuric acid. H_2SO_4 also forms within deliquesced sea-salt particles by the oxidation of aqueous SO_2 species by ozone (Sievering et al. 1992). Figure 9 provides an example of a 100-nm atmospheric sea-salt particle enriched in sulfate due to atmospheric processing. In addition to this chemistry, sea-salt particles are also important sources of reactive halogen species (e.g., Br_2 or BrCl) in the marine boundary layer (Pszenny et al. 1993; De Haan et al. 1999; Foster et al. 2001). These reactive halogens evaporate from sea-salt particles and undergo direct photolysis to yield gas-phase bromine and chlorine radicals, which in turn affect the chemistry of tropospheric ozone, dimethyl sulfide, and hydrocarbons (Vogt et al. 1996; Keene et al. 1998).

Many characteristics of sea-salt particles, such as chemical reactivity and light scattering properties, depend on the particle phase. At sufficiently low relative humidity

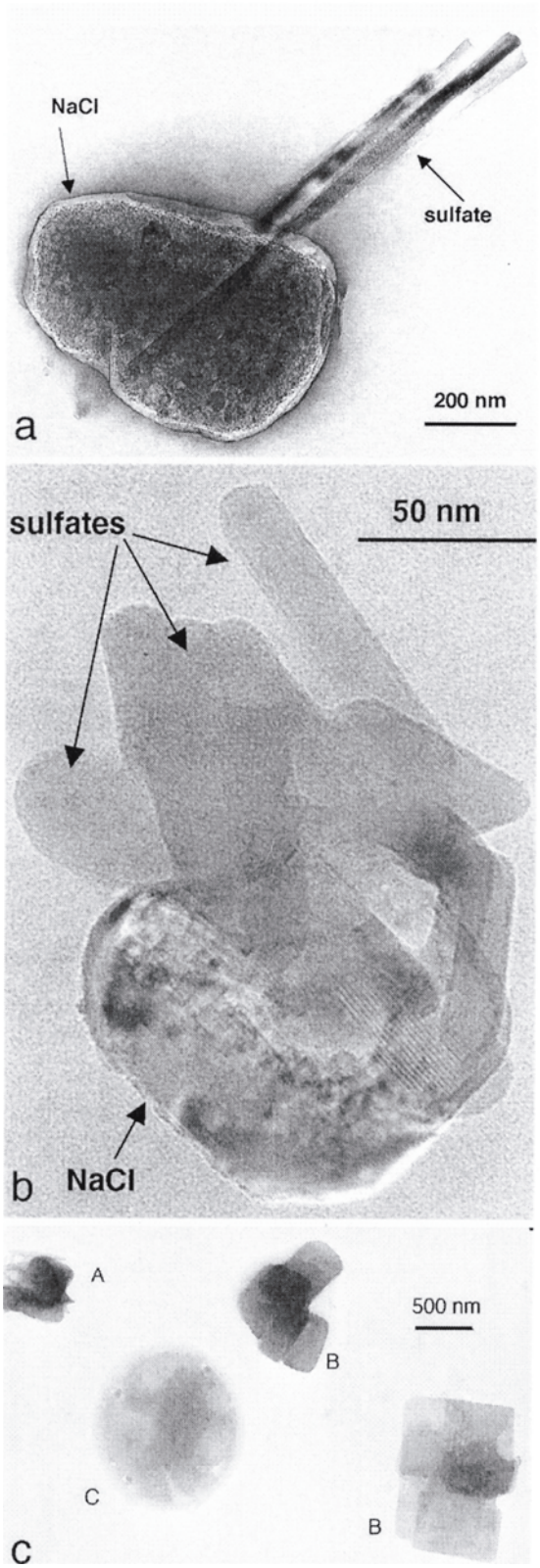

(RH), crystalline phases precipitate from the aqueous droplets (Martin 2000). Solid formation during the evaporation of relatively large volumes of seawater begins with $CaSO_4 \cdot 2H_2O$, which is followed by NaCl and finally $Na_2Ca(SO_4)_2$ at lower RH (McCaffrey et al. 1987; Marion and Farren 1999). However, at the smaller volumes characteristic of atmospheric particles, significant supersaturation is possible and even likely according to laboratory studies (Tang et al. 1997). A critical uncertainty in the laboratory work to date, especially for aerosols, is that ambiguity remains as to which phases nucleate rapidly and thus crystallize in atmospheric sea-salt particles and in what relative order they do so. It is not known, for example, if $CaSO_4 \cdot 2H_2O$ is the first salt to crystallize. It is important to emphasize that laboratory studies on NaCl surfaces indicate that several monolayers of water coat the surface even at low RH (Barraclough and Hall 1974; Peters and Ewing 1997a; Hemminger 1999). Thus chemical transformations of gas-phase species at the surfaces of crystalline sea-salt particles usually have reactivity and pathways similar to an aqueous environment (Finlayson-Pitts and Hemminger 2000). However, the optical properties of these particles are described well by consideration of the crystalline core, which is much more massive than the aqueous surface coating.

NUCLEATION

The formation of nanoparticles from gaseous precursors is the dominant mechanism for new particle formation in the atmosphere. Secondary mechanical effects, such as shattering of ice or rain particles or abrasion of mineral dust, also lead to increases in particle number density but at sizes larger than the nanoparticle range. As illustrated in Figure 10, the first step in nanoparticle formation is generally the oxidation of precursor gases such as SO_2 or

Figure 9. TEM images of sea salt. (*a* and *b*) Subhedral halite (NaCl) and euhedral sulfate crystals. The particle in *b* belongs to the smallest sea-salt particles that occur in the ACE-1 samples (Southern Ocean, Cape Grim, ACE-1); (c) Halite particles in various stages of conversion to sulfate and nitrate. Grain A is partly converted, whereas C has been completely converted to nitrate and grains B to sulfates. (Azores, North Atlantic, ASTEX/MAGE.) Images by Mihaly Pó sfai. Figure adapted from Buseck and Pó sfai (1999). Used by permission of the editor of *Proceedings of the National Academy of Sciences, USA.*.

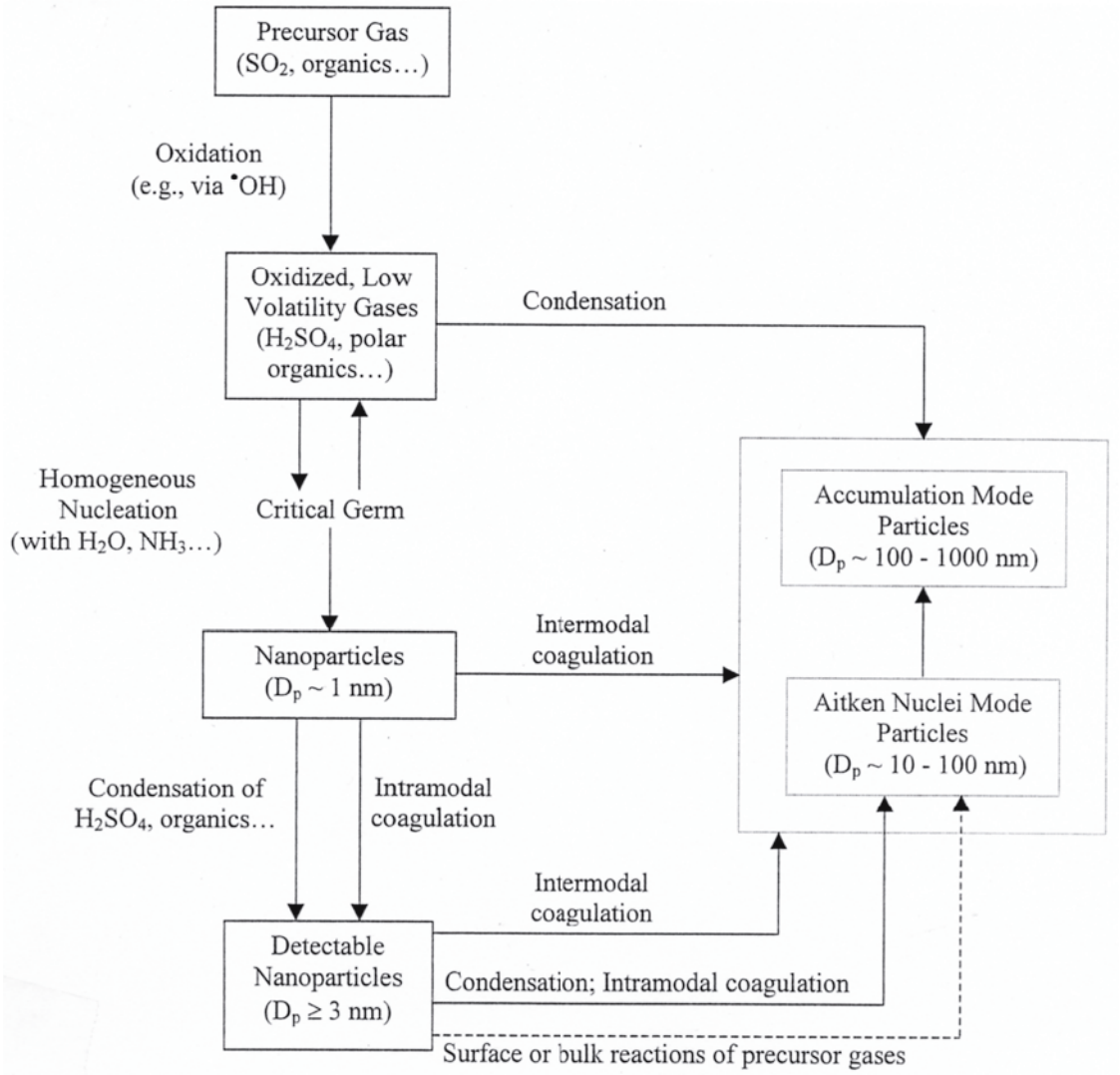

Figure 10. Schematic diagram of nanoparticle formation and growth.

organic compounds to form low-volatility products such as H_2SO_4 or polar organics. At sufficient supersaturations, these products condense to form a critical germ (also called a critical nucleus), which is a polymeric unit just sufficient in size to begin growth into a larger particle. Growth of the critical germ by condensation of low-volatility gases yields a nanoparticle (diameter of ~1 nm). These fresh nanoparticles can eventually join the accumulation mode via further growth, e.g., through continued condensation of vapors.

Nucleation is the science investigating the kinetics and thermodynamics of the formation of a new phase of a material at a size just sufficient to be stable. In addition to their role in new particle formation, nucleation processes are also critical to an accurate understanding of a number of other atmospheric events, including cloud droplet activation on CCN, ice formation, and the deliquescence/efflorescence of particles. In this section we focus on the nucleation of new particles through homogeneous nucleation, i.e., from gaseous precursors. The theoretical treatment of new particle nucleation, as well as field and laboratory measurements of nanoparticle formation, are addressed.

Theoretical treatment of critical germ formation

The process of new particle formation is a first-order transition from a disordered to

an ordered atomic arrangement (Doremus, 1985; Oxtoby 1992; Laaksonen et al. 1995; Martin 2000). Gas-to-liquid and liquid-to-crystalline conversions both proceed via first-order transitions, which require activated nucleation. Although the overall transformation is favored by a negative change in the Gibbs free energy, each microscopic step along the route is not. Thermal fluctuations in the medium must assist in overcoming the positive free energy change in a microscopic region. As an example, liquid water has a driving force to freeze below 273 K, but in fact submicron droplets readily supercool to 233 K. Liquid water monomers are dynamically associating in larger polymeric networks resembling ice. Most of these networks dissipate, however, without forming ice because the surface free energy of small networks exceeds the volume free energy. At this microscopic step in the freezing process (i.e., the *n*-mer or cluster level), the Gibbs free energy change is positive and unfavorable. However, the liquid is incessantly exploring possible configurations of its spatial and energy coordinates through thermal fluctuations, and at some time point an *n*-mer forms that is large enough such that the negative volume free energy just offsets the positive surface free energy. This large *n*-mer, called a critical germ, then grows freely into a large crystal. These ideas have been developed quantitatively by classical nucleation theory and more recently by density functional theory and cluster kinetic theory (Laaksonen 1995; Kusaka et al. 1998a,b, 1999; Bowles et al. 2000).

Classical homogeneous nucleation theory is widely employed to describe the formation of new particles in the atmosphere (Pruppacher and Klett 1997; Seinfeld and Pandis 1998). The free energy of germ formation, ΔG_{germ}, in classical homogeneous nucleation theory is described as follows:

$$\Delta \mathrm{G}_{\mathrm{germ}} = \frac{16\pi \mathrm{v}^2 \sigma_{\mathrm{germ}}^3}{3(\mathrm{kT}\ln \mathrm{S})^2} \tag{7}$$

where v is the molecular volume, σ_{germ} is the surface tension of the germ in the medium, k is the Boltzmann constant, T is temperature, and S is the saturation ratio of a metastable phase with respect to a stable phase. The third-order dependence on σ_{germ} makes this term a critical factor in calculations. The volume nucleation rate, J, is as follows:

$$J = n\frac{kT}{h}\exp\left(-\frac{\Delta G_{germ}}{kT}\right) \tag{8}$$

where n is the molecular concentration in the liquid phase and h is the Planck constant. The probability, P, of a chemical system forming a critical nucleus after time t is:

$$P(t) = 1 - \exp(-JVt) \tag{9}$$

where V is the system volume.

Nucleation of an ordered phase is often favored when there is an available surface of foreign matter. The free energy of germ formation is then reduced by a favorable interaction of the critical germ with the foreign surface. Classical heterogeneous nucleation theory provides the surface nucleation rate as follows:

$$j = n_s \frac{kT}{h}\exp\left(-f(m)\frac{\Delta G_{germ}}{kT}\right) \tag{10}$$

where n_s is the number of monomer units per unit surface area. An important assumption inherent in this theory is an undifferentiated surface (i.e., a large terrace structure). $f(m)$ describes the favorability of the interaction between the germ and the foreign surface, as

follows:

$$f(m) = \frac{(2+m)(1-m)^2}{4} \tag{11}$$

The term m follows from $m = \cos\theta$ where θ is the contact angle, as given by the surface tension relationships of Young's equation. Because $-1 \le m \le 1$, it follows that $1 \ge f \ge 0$. The probability of a chemical system forming a critical nucleus is:

$$P(t) = 1 - \exp(-jAt) \tag{12}$$

where A is the area of the foreign surface.

Chemical composition of critical germ

The chemical composition of a critical germ often differs significantly from both the constitution of the supersaturated mother liquor and the equilibrium composition of the stable phase. For example, for $J = 1$ cm^{-3} s^{-1} at 298 K, 2.2×10^9 molecules H_2SO_4 cm^{-3} and 4.2×10^{17} molecules H_2O cm^{-3} (50% RH) in the gas phase are calculated to yield a critical germ containing 39 molecules and a H_2SO_4 mole fraction of 0.205, in contrast to the gas-phase H_2SO_4 mole fraction of 5.0×10^{-9} (Jaecker-Voirol and Mirabel 1988). The chemical composition of the germ depends on the details of the energy surface, as specified by $\Delta G(n_1, n_2, \ldots, n_i)$ for an i-component system (e.g., $i = 2$ for H_2SO_4/H_2O) where n_i denotes the number of molecules in a candidate germ. Experimental studies on cluster formation are useful in elucidating the shape of the energy surface (Jaecker-Voirol et al. 1987; Mirabel and Ponche 1991; MacTaylor and Castleman 2000). Movement across the surface from monomers to a macroscopic particle requires surmounting an activation barrier denoted by $\Delta G_{germ}(n_1^*, n_2^*, \ldots, n_i^*)$, where n_i^* is the number of molecules of component i in the critical germ. The height of the barrier is specified by the condition:

$$\left(\frac{\Delta G_{germ}}{n_1^*}\right)_{n_i;i\neq 1} = \left(\frac{\Delta G_{germ}}{n_2^*}\right)_{n_i;i\neq 2} = \ldots = \left(\frac{\Delta G_{germ}}{n_i^*}\right)_{n_i;i\neq i} = 0 \tag{13}$$

Experimental data of the dependence of J on concentration can yield an estimate of n_i^*, especially for the conversion of vapors to condensed phases. The essential relation is provided in the nucleation theorem, as follows (Oxtoby and Kashchiev 1994):

$$\frac{\partial \Delta G_{germ}}{\partial \mu_{o,i}} = -\Delta n_i^* \tag{14}$$

This equation states that the change in the free energy of the critical germ with the chemical potential $\mu_{o,i}$ per molecule of species i in the *original* phase (i.e., the mother liquor) equals the negative of the excess number Δn_i^* of molecules of type i in the nucleus over that present in the same volume of original space. The nucleation theorem is independent of the model and of the transition: it holds true for classical nucleation theory, density functional theory, or cluster kinetic analysis and for gas-to-liquid or liquid-to-solid conversions.

In the particular case of gas-to-condensed-phase transitions, Equations 8 and 14 can be developed together to yield the following accurate approximation for isothermal binary nucleation (e.g., for H_2SO_4/H_2O):

$$\Delta n_i^* = \frac{\partial(kT \ln J)}{\partial \mu_{oj}} - \delta \tag{15}$$

where δ is a small correction factor (typically between 0 and 1) related to the dependence of the preexponential factor on chemical potentials (i.e., usually small). The chemical potential relates to chemical composition by $\mu_{o,i} = \mu^0_{o,i} + kT \ln f_i x_{o,i}$ where f_i is the activity coefficient and $x_{o,i}$ is the mole fraction composition. When the activity coefficient is unity or otherwise ignored, Equation (15) yields:

$$\partial(\ln J) = (\Delta n_i^* + \delta)\partial(\ln x_{o,i}) \tag{16}$$

Under the assumption that Δn_i^* is independent of $x_{o,i}$, the slope of a log-log plot of the experimental dependence of J on the composition of component i in the mother liquor yields the composition of the germ component i. It should be emphasized that $\Delta n_i^* = f(x_{o,1}, x_{o,2}, .., x_{o,i})$, which is factorable as $\Delta n_i^* = N_i f(x_{o,1}, x_{o,2}, .., x_{o,i-1})$ under the assumption of independence in $x_{o,i}$. The point is that Δn_i^* has a specific value N_i when $x_{o,1}, x_{o,2}, .., x_{o,i-1}$ are held constant. When these values vary, N_i also varies.

Employing Equation (16), Ball et al. (1999) analyze their data of particle formation rates from vapors of H_2SO_4/H_2O to determine that there are 13 H_2SO_4 monomers in a critical germ at 2 to 12×10^9 molecules H_2SO_4 cm^{-3} and 2.3% RH at 295 K. As RH increases to 15.3%, the number of H_2SO_4 monomers drops to 7. While the H_2SO_4 monomers drop from 13 to 7, the H_2O monomers in the critical germ increase from 4 to 6, and the acid mole fraction in the critical germ shifts from 0.76 to 0.53. In breakthrough work, Eisele and Hanson (2000) succeed in directly measuring H_2SO_4/H_2O clusters containing 3 to 8 H_2SO_4 molecules by mass spectrometric techniques. The measurements are under conditions where new particle formation is not rapid, i.e., the dynamic cluster distribution is being observed. Kulmala et al. (1998a) provide a parameterization, which is convenient for inclusion in computer codes, of the mole fraction composition of the critical germ and the nucleation rate of new particles from H_2SO_4/H_2O gases.

In the Ball et al. (1999) work mentioned above, addition of NH_3 at levels of tens of parts per trillion by volume (pptv) increases the particle nucleation rate and at 15% RH reduces the number of H_2SO_4 monomers in the critical germ from 8 to 5. It would be desirable in future studies to extend this experimental work to higher RH values because the strongly nonlinear dependencies make extrapolations very uncertain, although modeling work by Korhonen et al. (1999) suggests the nucleation rate from $H_2SO_4/H_2O/NH_3$ could be approximately independent of RH under atmospheric conditions. According to this model description (Korhonen et al. 1999), a critical germ contains 8 H_2SO_4, 4 NH_3, and 6 H_2O molecules at 298 K, 52.3% RH, 5 pptv NH_3, and 10^8 molecules H_2SO_4 cm^{-3}. In this model the presence of NH_3 increases the nucleation rate by several orders of magnitude.

Equations 15 and 16 develop Equation (14) for gas-to-condensed-phase transitions. It would also be desirable to develop Equation (14) for liquid-to-crystalline nucleation to assign physical meaning to Δn_i^*. However, development of Equation (14) is difficult both because δ can be a large correction factor for liquid/solid interfaces and because the molecular density differences between liquids and solids are smaller than between gases and condensed phases (Kashchiev 1982).

New particle formation in the atmosphere

Understanding new particle formation has been a focus of field, laboratory, and modeling efforts in recent years. This research has been driven by observations that rates of new particle production in field studies often exceed modeled rates that are based upon laboratory studies of nucleation (Covert et al. 1992; Weber et al. 1996, 1997, 1998a, 1999; Clarke et al. 1998; Kulmala et al. 1998b).

Nanoparticle formation in the atmosphere is initiated by the process of homogenous nucleation from gas-phase precursors (Eqn. 8). As shown in Figure 10, the first step in this process is the conversion of gases to lower volatility products, via reactions with species such as hydroxyl radical ($^{\bullet}OH$). When the resulting partial pressures of low volatility vapors exceed saturation, vapor condensation to form new particles with diameters of approximately 1 nm is thermodynamically favored (Seinfeld and Pandis 1998; Friedlander 2000). However, new particle formation is in competition with scavenging of the low volatility gas by condensation to pre-existing particles (Kulmala et al. 1995; Weber et al. 1997; de Reus et al. 1998; Pirjola and Kulmala 1998; Pirjola et al. 1999; Kerminen et al. 2000; Clement et al. 2001). Thus new particle formation is not constant in time but instead occurs in bursts under conditions where there is little pre-existing aerosol but sufficient concentrations of (generally) photochemically produced low volatility vapors, as illustrated in Figure 11.

Sulfuric acid. New particle formation involving H_2SO_4 has been investigated most intensively because there is strong evidence that sulfuric acid can be an important particle precursor. Gaseous sulfuric acid is formed via the oxidation of sulfur dioxide (SO_2) by hydroxyl radical in the following multistep reaction:

$$SO_2 + {}^{\bullet}OH + O_2 + H_2O \longrightarrow H_2SO_4 + HO_2{}^{\bullet} \qquad (17)$$

where the rate-limiting elementary step is the attack of $^{\bullet}OH$ on SO_2 (Finlayson-Pitts and Pitts 2000). Since hydroxyl radical is primarily formed via reactions that require sunlight,

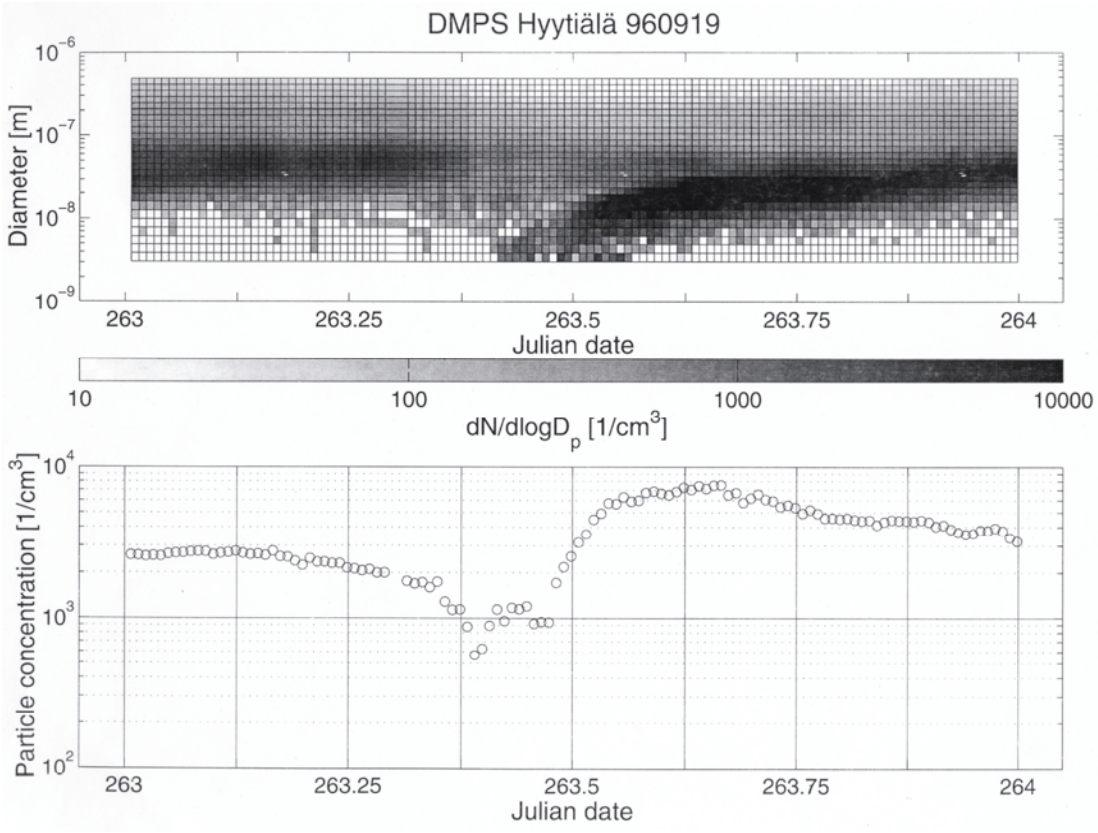

Figure 11. Particle size distributions (top panel) and particle number concentrations (bottom panel) at Hyytiä lä , Finland as a function of time of day (Julian day 263.5 = noon on September 19, 1996). Note the burst of nanoparticle nucleation occurring near noon and its subsequent growth. From Clement et al. (2001). Used by permission of the editor of *The Journal of Aerosol Science*.

the formation of gaseous H_2SO_4 (and many other secondary low-volatility gases) has a strong diurnal dependence. Correspondingly, new particle formation also shows a diurnal dependence (e.g., Fig. 11).

The photochemical dependence for the production of $^{\bullet}OH$, H_2SO_4, and new particles is apparent in Figure 12 for data from Idaho Hill, Colorado, which is a remote continental site (Weber et al. 1997). As seen in the top panel (a), $^{\bullet}OH$ formation begins at sunrise, and concentrations correlate well with the UV irradiance. H_2SO_4 concentrations (c) also rise at sunrise and correlate with UV irradiance, which follows from Equation (17). On the other hand, SO_2 mixing ratios (b) show no diurnal trends because SO_2 has a long lifetime (days) with respect to reaction with $^{\bullet}OH$. The bottom panel in this sequence (d) reveals that the formation of 3- to 4-nm diameter particles is associated with the photochemical cycle and that the greatest particle number concentrations occur near solar noon. However, the appearance of these particles does not begin until approximately an hour after sunrise. This induction period is attributed to the time required for the initial particle nuclei ($D_p \sim 1$ nm) to grow to measurable size (3 nm) (Weber et al. 1997).

In the Idaho Hill study described above, measured concentrations of gaseous H_2SO_4 and H_2O are much lower than the levels required for rapid new particle formation based on classical nucleation theory (Weber et al. 1997). Similar results are reported in several other studies (Wiedensohler et al. 1997; Pirjola et al. 1998, 2000; O'Dowd et al. 1999; Weber et al. 1999). These measurements show that homogeneous classical nucleation theory for H_2SO_4/H_2O generally underpredicts measured rates of new particle formation in the boundary layer. In contrast, in studies of high-altitude regions near cloud venting, observed rates of nucleation are similar to those predicted from binary nucleation theory (Clarke et al. 1999; Weber et al. 1999). In addition, a study of polluted air masses with high SO_2 concentrations in the Finnish Arctic found that application of classical nucleation theory to H_2SO_4 and H_2O can explain measured new particle formation rates reasonably well (Pirjola et al. 1998). Overall, these results suggest that binary nucleation of H_2SO_4 and H_2O is sometimes responsible for new particle formation in the atmosphere, but that other mechanisms are often more important. However, even in these latter cases there is evidence that sulfuric acid plays a role in nucleation, such as the correlation of gaseous H_2SO_4 with nanoparticle number concentrations at Idaho Hill (Fig. 12). Despite this evidence, it is also possible that H_2SO_4 is not a nucleating agent in these studies, but instead that its concentration co-varies with another, as yet unknown, photochemically produced agent (Weber et al. 1999).

Numerous authors suggest that a plausible alternative to H_2SO_4/H_2O binary nucleation is ternary nucleation involving H_2SO_4, H_2O, and NH_3 (Coffman and Hegg 1995; Weber et al. 1997, 1999; Kim et al. 1998; Korhonen et al. 1999). Ammonia is a common gas in the troposphere with mixing ratios that are typically under 50 pptv in remote regions and on the order of ppbv (parts per billion by volume) in regions near sources such as animal operations (Finlayson-Pitts and Pitts 2000). The H_2SO_4 vapor pressure is much smaller over aqueous ammonium sulfate solutions, as compared to over H_2SO_4/H_2O solutions, which suggests that NH_3 stabilizes H_2SO_4-H_2O clusters (Marti et al. 1997a). In addition, as described earlier, several recent laboratory and modeling studies show that the presence of pptv levels of NH_3 greatly reduces the critical concentration of H_2SO_4 required to form new particles (Ball et al. 1999; Korhonen et al. 1999; Pirjola et al. 2000). Whether the ternary $H_2SO_4/H_2O/NH_3$ system correctly predicts nucleation rates in a wide range of atmospheric conditions remains to be tested.

Recent work by Kulmala et al. (2000) indicates that the $H_2SO_4/H_2O/NH_3$ ternary nucleation mechanism yields nanoparticle ($D_p > 3$ nm) concentrations that match field observations at a Finnish study site. In addition, the authors present the interesting

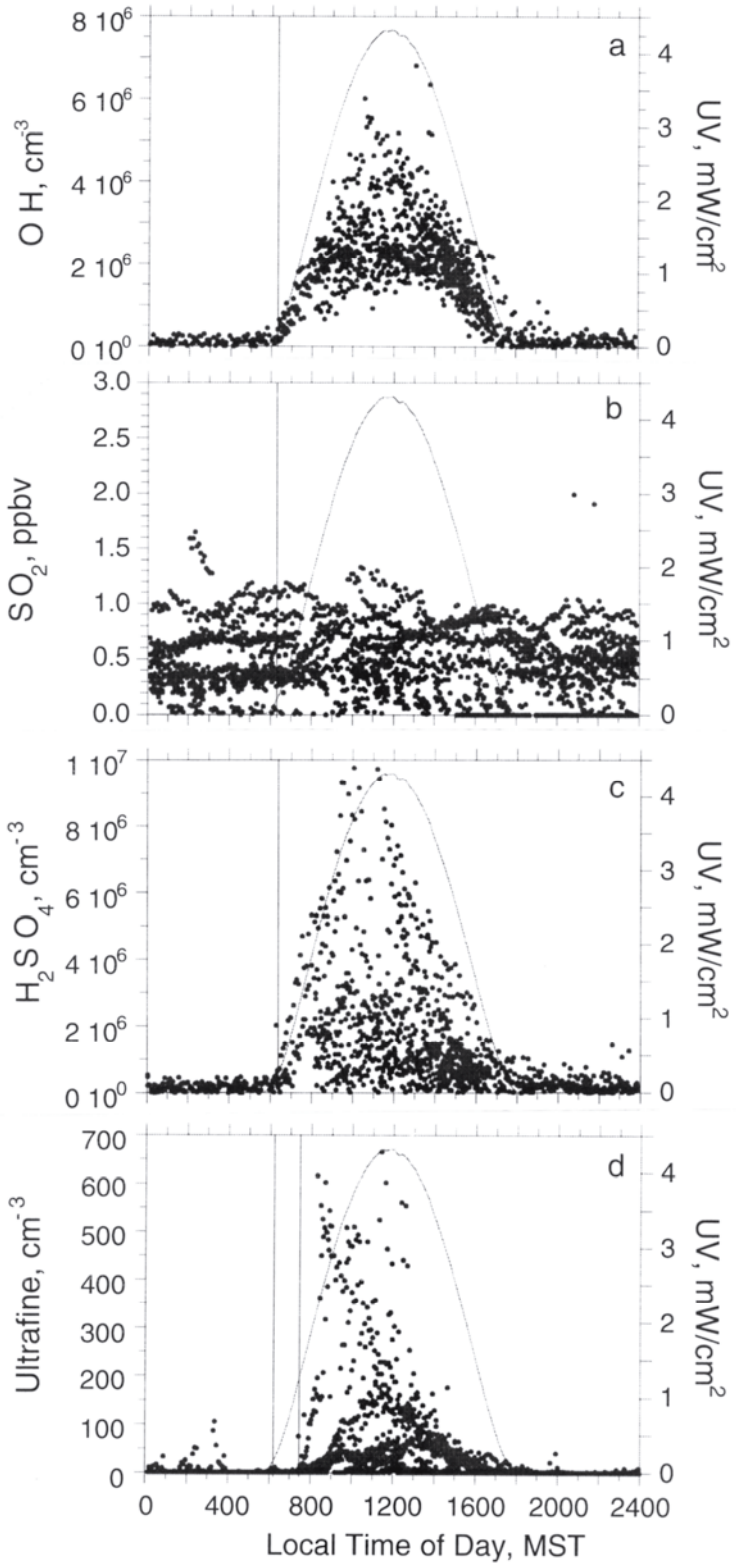

Figure 12. Concentrations of (a) $^{\bullet}OH$, (b) SO_2, (c) H_2SO_4, and (d) nanoparticles (D_p = 2.7-4 nm) measured at Idaho Hill, Colorado, from September 5 to 29, 1993, during periods of relatively clean (downslope) air flow. The solid curve on each plot (right axis) is the UV irradiance measured on a clear day (September 26) during the study. The vertical line at approximately 06:15 in each plot indicates sunrise. The second vertical line at approximately 07:30 in plot *d* indicates the beginning of measurable number concentrations of nanoparticles. From Weber et al. (1997). Used by permission of the American Geophysical Union.

hypothesis that 1- to 3-nm particles ("thermodynamic stable clusters") nucleate from $H_2SO_4/NH_3/H_2O$ continuously and are present in the atmosphere undetected. According to this hypothesis, these small particles are formed daily to yield peak number concentrations of approximately 10^5 cm^{-3}. However, their growth is slow due to the absence of condensable H_2SO_4. Their lifetime is also relatively short in areas with heavy loadings of larger particles due to intermodal coagulation. A measurement challenge (Eisele and Hanson 2000) remains to observe in situ these thermodynamically stable clusters and thus refute or support the hypothesis.

Organic compounds. Low volatility organic gases are also believed to be precursors for the formation of new particles. As in the case of SO_2 oxidation to H_2SO_4, the first step in the formation of an organic nanoparticle appears to be the oxidation of a precursor gas to a more polar, lower volatility gas (Fig. 10). While there are thousands of natural and anthropogenic organic gases present in the atmosphere (Graedel et al. 1986), only those that are emitted in significant quantities, react quickly in the atmosphere, and form very low volatility products are expected to be significant in particle nucleation. Examples of these potentially significant precursor gases include biogenic monoterpenes such as α- and β-pinene (Griffin et al. 1999; Kavouras et al. 1999) and, in urban areas, anthropogenic aromatics such as alkyl benzenes (Odum et al. 1997). Reactions of these organic gases with oxidants, such as $^{\bullet}OH$ and O_3, yield more oxygenated compounds, such as carboxylic acids and peroxides. These oxygenated species have lower volatilities than their parent compounds and thus increase the likelihood of forming new particles (e.g., Forstner et al. 1997; Barthelmie and Pryor 1999; Tobias and Ziemann 2000). The critical germs in these cases probably contain several different types of interacting organic species.

The Idaho Hill study discussed earlier also assesses the possible roles of biogenic terpenes and anthropogenic organic gases in nucleation (Weber et al. 1997; Marti et al. 1997b). The conclusions reached are that H_2SO_4 is generally a more important nucleating species than the measured organic gases but that there are possibly a few events where organics participate in nucleation. There is indirect evidence from other field studies that organic compounds at times lead to new particle formation in the boundary layer. For example, several studies find new particle formation in forests under conditions where organic species should be abundant (Mäkelä et al. 1997; Kulmala et al. 1998b; Becker et al. 1999; Kavouras et al. 1999). In addition, species such as carboxylic acids from terpene oxidation have been measured in accumulation mode or larger particles in forested regions (Kavouras et al. 1999; Yu et al. 1999). However, the most abundant secondary organic compounds in accumulation mode particles are likely to be the compounds condensed during particle growth, rather than any putatitive organics contributing to the critical germ (Kerminen et al. 2000). Thus while organic compounds are a major component of ultrafine particles in the atmosphere (Cass et al. 2000), much more work remains to identify and to evaluate the organic compounds that might serve as nucleating agents.

Primary emissions

In addition to the formation of new secondary nanoparticles, there are also primary emissions of nanoparticles to the atmosphere, most importantly from high temperature combustion. While there are no published emissions inventories specifically for nanoparticles, Cass et al. (2000) estimate that approximately 85% of the mass of primary ultrafine particles (D_p < 100 nm) in the Los Angeles area is emitted from combustion sources. On-road vehicles are estimated to account for approximately 40% of ultrafine particle mass. Similar results are reported for the United Kingdom, with a somewhat greater contribution (60% of total) from vehicles (Harrison et al. 2000). Observations in

Birmingham, where the number of nanoparticles decreases rapidly with distance from roads, also suggest that vehicles are an important source of primary nanoparticles (Shi et al. 1999).

Diesel engines are a particular research focus because they emit approximately 10-100 times more particles by mass than spark-ignition (gasoline) engines (Kittelson 1998). As shown in Figure 13, particulate matter from diesel engines generally contains both a nanoparticle mode (D_p < 50 nm) as well as an accumulation mode (D_p = 100-300 nm) (Kittelson 1998; Collings and Graskow 2000). The nanoparticle mode typically accounts for more than 90% of the total number of particles emitted from diesel engines, but less than 20% of the total particle mass (Kittelson 1998). The nanoparticle number size distributions recorded in laboratory measurements of vehicle emissions depend strongly upon the dilution process of the exhaust prior to analysis (Kittelson 1998; Shi and Harrison 1999; Collings and Graskow 2000). Even so, chase-car roadway measurements of particles reveal number size distributions similar to the laboratory measurements shown in Figure 13 (Collings and Graskow 2000). In an attempt to reduce diesel particle emissions in the United States, the EPA has enforced a series of increasingly strict mass-based standards (Kittelson 1998). It is unclear whether these regulations will impact the number of particles emitted from diesel engines. In fact, initial evidence suggests that new diesel engines designed to reduce emissions of particle mass might emit higher number concentrations of nanoparticles (Bagley et al. 1996; Kittelson 1998).

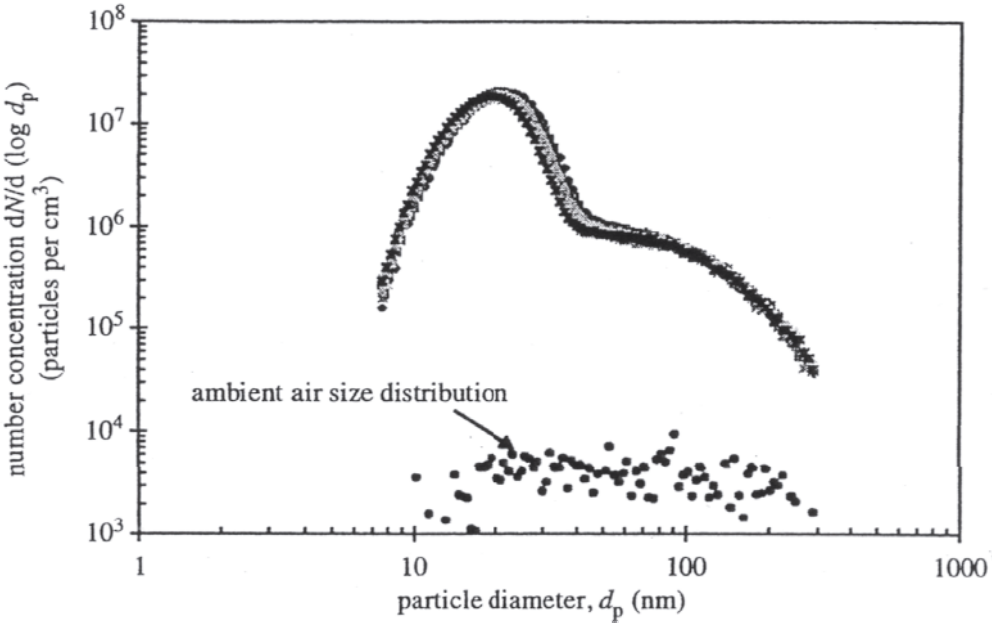

Figure 13. Particle number distributions for a diesel engine (2.5 L displacement, direct injection, 4-cylinder, 1500 rpm, 7.5 kW) run with 300 ppm sulfur content diesel fuel. Distributions are measured using a dilution tunnel with conditions simulating those expected in the environment (final dilution ratio of approximately 100:1). From Collings and Graskow (2000). Used by permission of the Royal Society.

Most of the nanoparticles emitted from diesel vehicles appear to nucleate from sulfuric acid and water during the cooling and dilution of the exhaust with ambient air (Kittelson 1998; Shi and Harrison 1999; Collings and Graskow 2000; Tobias et al. 2001). However, based on results from Shi and Harrison (1999), the measured rate of particle formation in diesel exhaust is much greater than the rate calculated from binary

homogeneous nucleation of H_2SO_4 and H_2O. The implication is that other species are also participating. As the vehicle exhaust further cools, unburned fuel and lubricating oil condense upon the sulfuric acid nucleus, increasing its size and changing its composition (Burtscher et al. 1998; Kittelson 1998; Tobias et al. 2001). The organic composition of diesel nanoparticles varies with particle size, with a higher proportion of larger and less volatile organics present in the smaller particles (Tobias et al. 2001).

The accumulation mode of diesel particles consists primarily of elemental carbon in addition to significant amounts of organic carbon (including PAHs), sulfate, nitrate, ammonium, chloride, and sodium (Kittelson 1998; Schauer et al. 1999; Kleeman et al. 2000; Richter and Howard 2000). Many other species are also present in trace amounts, including Si, Fe, Ti, Zn, and Al (Schauer et al. 1999; Kleeman et al. 2000). Based on extrapolation of the size-resolved chemical composition measurements for particles with $D_p > 50$ nm (Kleeman et al. 2000), it appears that many of these same accumulation mode components are also present in diesel nanoparticles.

In addition to diesel vehicles, gasoline (spark ignition) vehicles also emit significant numbers of nanoparticles (Burtscher et al. 1998; Kittelson 1998; Kleeman et al. 2000). Although the total mass emission rate of particles from diesel engines is much greater than from gasoline engines, under highway cruise conditions diesel and gasoline engines have similar nanoparticle emission rates (Kittelson 1998). Other combustion sources of primary nanoparticles include the burning of coal and fuel oil (Huffman et al. 2000; Linak and Miller 2000; Senior et al. 2000; Fan and Zhang 2001; Zhuang and Biswas 2001), combustion of wood and other biomass (Rogge et al. 1998; Kleeman et al. 1999), aircraft (Brock et al. 2000; Kä rcher et al2000), meat charbroiling (Rogge et al. 1991; Kleeman et al. 1999), and cigarettes (Rogge et al. 1994; Kleeman et al. 1999). The particles produced from these processes contain elemental carbon as well as a complex suite of organic compounds and numerous trace metals.

GROWTH

This section provides a conceptual framework and several examples of modeling and fieldwork on the growth of atmospheric nanoparticles. The growth of nanoparticles is an important source of Aitken mode and accumulation mode particles, including cloud condensation nuclei, especially in remote regions with few primary particle sources. For more quantitative descriptions of growth processes, as well as their parameterizations in models, see Kulmala (1993), Kulmala et al. (1993), Kerminen et al. (1997), Mattila et al. (1997), Vesala et al. (1997), Seinfeld and Pandis (1998), and Friedlander (2000).

The processes involved in nanoparticle growth are depicted in Figure 10. Phenomenological descriptions of early growth are presently limited because the formation of new nanoparticles, which have diameters of around 1 nm, cannot be detected by current state-of-the-art field-deployable instruments, which can measure particles with diameters of 3 nm and above. Model descriptions, however, indicate that growth is accomplished through one of three pathways: the condensation of low volatility gases such as sulfuric acid, coagulation with other newly formed nanoparticles (i.e., intramodal coagulation), or surface or bulk reactions that increase particle mass (i.e., reactive condensation) (Kerminen 1999). The growth of nanoparticles changes their chemical composition, especially at the surface, and therefore likely alters their health effects and chemical reactivity.

The rates and relative importance of condensation and intramodal coagulation depend upon the number concentration and size of nanoparticles, the partial pressures of condensable gases, and the accommodation coefficients of the gases onto the particles

(Friedlander 2000). While intramodal coagulation can be important under some conditions (e.g., in regions with very high nanoparticle number concentrations), condensation is the dominant growth mechanism under typical atmospheric conditions (Wexler et al. 1994; Kerminen et al. 1997). In addition, the growth of nanoparticles is influenced by the presence of larger particles in the aerosol due to collisions with these particles (i.e., intermodal coagulation) and a competition between the nanoparticles and larger particles in scavenging the condensable gases. All other factors being equal, the vapor pressures of chemical species over nanoparticles are greater than over larger particles due to the Kelvin effect. The Kelvin effect states that the vapor pressure over a curved surface, P, increases relative to that over a flat surface, P^0, as follows: $P = P^0 \exp(4\sigma v / kTD_p)$, where σ is the surface tension and v is the condensed-phase molecular volume (Seinfeld and Pandis 1998). The overall effect of these factors is that insignificant growth, and possibly even evaporation, of nanoparticles occurs in the presence of high number concentrations of larger particles. The third growth mechanism, reactive condensation, is important for the growth of accumulation mode particles through reactions such as the aqueous oxidation of SO_2 by HOOH or O_3 (Finlayson-Pitts and Pitts 2000). However, these same reactions are calculated to be too slow to be significant for nanoparticle growth (Kerminen et al. 1997; Kerminen 1999).

In the remaining part of this section we focus on nonreactive condensation because this process usually contributes more to nanoparticle growth than does intramodal coagulation (except perhaps in urban environments). In most field studies, observed nanoparticle growth rates are much faster than can be explained by the condensation of H_2SO_4 and H_2O (Weber et al. 1997,1998a; O'Dowd et al. 1999; de Reus et al. 2000b). Models yield similar results, especially for conditions where particle formation occurs via $H_2SO_4/H_2O/NH_3$ ternary nucleation (Kerminen et al. 1997; Kulmala et al. 2000). In contrast to its effect on nucleation, the presence of NH_3 has little effect on growth rates in the H_2SO_4/H_2O system (Kerminen et al. 1997; O'Dowd et al. 1999). Model results reveal that the addition of HNO_3 or HCl to the ternary $H_2SO_4/H_2O/NH_3$ system greatly enhances growth rates under conditions found in continental regions, though not at the lower levels of gas-phase HNO_3 and HCl found in remote marine systems (Kerminen et al. 1997).

Several lines of evidence suggest that organic compounds play a significant role in nanoparticle growth. For example, terpenoic acids and other terpene oxidation products are present in accumulation mode particles in forested regions (Kavouras et al. 1999; Yu et al. 1999). In addition, Marti et al. (1997b) report that measured total particle surface areas and volumes ($D_p < 500$ nm) at a remote continental location roughly correlate with the estimated rates of formation of condensable products from terpene oxidation. Finally, measurements at two field sites where biogenic organic gases are likely prevalent (namely, a boreal forest in Finland during spring and summer (Kulmala et al. 1998b) and a coastal site during low tide (O'Dowd et al. 1999)) show that measured growth rates require unidentified condensable species with peak concentrations of greater than 10^7 molecules cm^{-3}.

These unidentified species might be organic compounds. Modeling by Kerminen and co-workers shows that condensation of organic gases leads to the growth of 5-nm nanoparticles to CCN size ($D_p > 50$ nm) in under 24 hours. The simulations employ realistic amounts of precursor organic gases and assume that at least some of the organic oxidation products have extremely low saturation vapor pressures on the order of 0.01 pptv or less (Kerminen 1999; Kerminen et al. 2000). These nonvolatile organics are required for the initial stage of growth where the nanoparticle radius is very small and thus the Kelvin effect is very large. As the particle grows, low volatility (rather than nonvolatile) organic gases are increasingly important as particle components, which is a

combined result of a reduced Kelvin effect and the dependence of gas-particle partitioning of organics on particle mass (Kerminen et al. 2000). These results imply that the chemical composition of organic particles changes dramatically during growth and that the composition of the original nonvolatile nanoparticle nucleus is lost as a result of subsequent condensation of other products.

CHARACTERIZATION

Number concentrations

Observations of atmospheric nanoparticle number concentrations have increased greatly during the last five years. This advance has been made possible by new instruments and techniques that can measure particles with diameters as small as 3 nm. The new approaches include pulse height analysis of data from an ultrafine condensation particle counter (UCPC) (Stolzenburg and McMurry 1991; Wiedensohler et al. 1994; Weber et al. 1998b) and the combination of a nano-differential mobility analyzer (nano-DMA) (Chen and Pui 1997; Seto et al. 1997) with a UCPC.

There are large differences in nanoparticle number concentrations between remote and polluted regions: measured values in remote continental and marine areas are typically under 100 cm^{-3} (Weber et al. 1995, 1997; Covert et al. 1996) whereas number concentrations in urban areas are typically 10^4 cm^{-3} (Shi et al. 1999; McMurry et al. 2000). Higher concentrations (~10^5 cm^{-3}) occur near roads (Shi et al. 1999) and during bursts of new particle formation (McMurry et al. 2000; Woo et al. 2001). At a given location concentrations of the smallest measurable particles (D_p < 10 nm) are usually highly variable in time, occurring in bursts most commonly seen during periods of high solar radiation (e.g., Figs. 11 and 12). Figure 11 also shows that new nanoparticles (3 nm) grow into larger nanoparticles and nuclei mode particles over the course of several hours when conditions are favorable.

New particle formation in an urban site (Atlanta) is illustrated in Figure 14, which shows an afternoon burst of 3- to 10-nm particles during a period with high levels of SO_2. At its peak, this burst nearly quadruples the total number of particles present at the sampling site (Woo et al. 2001). Overall, number concentrations of the smallest nanoparticles (under 10 nm) are highest in Atlanta during midday, while concentrations of the larger nano- and ultrafine particles (10-100 nm) are typically higher during the morning and evening. These results suggest that vehicular emissions might be a significant source of the larger nanoparticles (Woo et al. 2001). An unexplained observation is that appreciable numbers of 3- to 10-nm particles are present in Atlanta even after sunset (Fig. 14), which is unlike the case for the remote Idaho Hill site (Fig. 12) or the Finnish boreal forest site (Fig. 11). These nighttime particles might be the result of vehicular emissions or other anthropogenic sources of primary nanoparticles in Atlanta.

Particle number distributions over the course of a year in Atlanta are shown in Figure 15. During the period August 1998 to April 1999, the number mode size of the aerosol number distribution typically occurs between 10- and 40-nm diameter. However, during the latter part of this study (April to August 1999), the smallest particles (those under 10 nm) dominate the particle number concentrations. During these months, the number of particles increases with decreasing particle size, suggesting that new particle formation events are common in this region (McMurry et al. 2000; Woo et al. 2001).

Chemical composition

Knowledge of the chemical composition of atmospheric nanoparticles is limited.

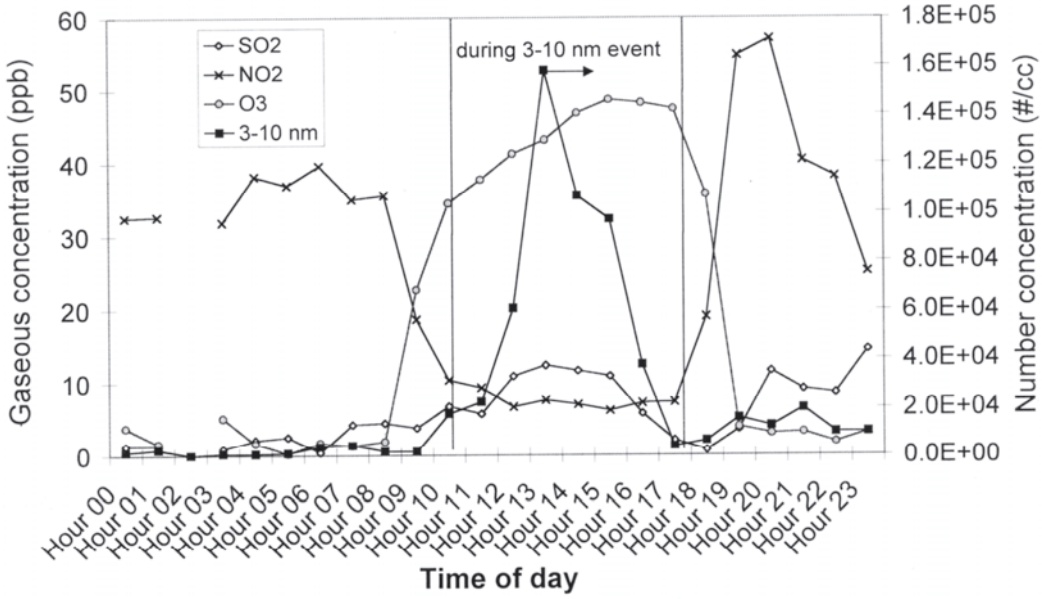

Figure 14. Nucleation burst of nanoparticles (D_p = 3-10 nm) and associated mixing ratios of gases in Atlanta, Georgia, on April 1, 1999. The vertical lines represent the period of enhanced number concentrations of 3-10 nm nanoparticles. Note, however, that the number concentrations of these particles are often still appreciable outside of this period, especially at night. From Woo et al. (2001). Used by permission of Taylor & Francis, Inc.

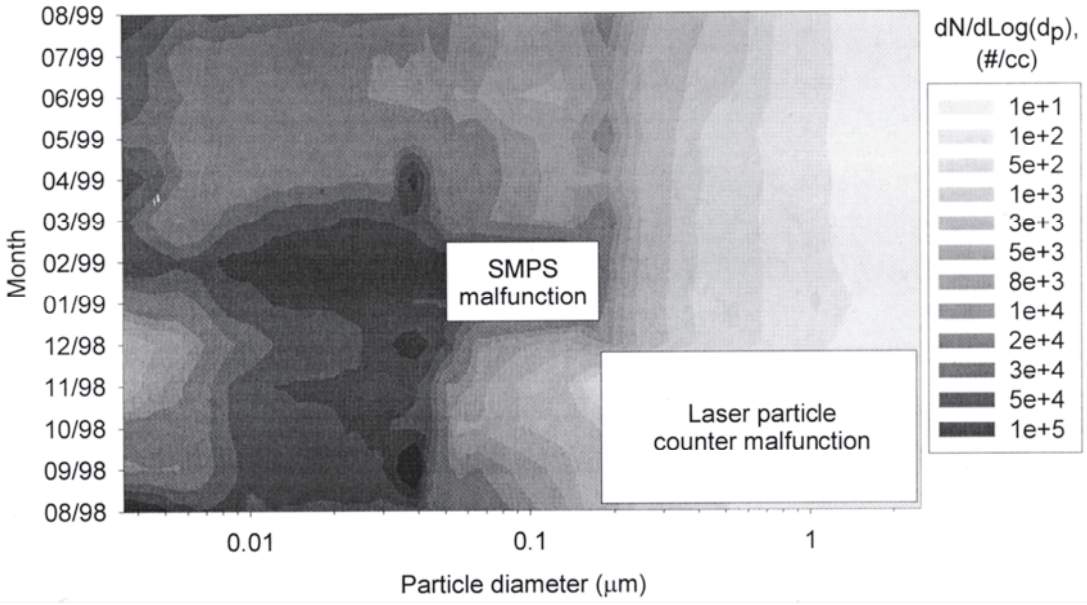

Figure 15. Contour plot of monthly average particle number distributions measured in Atlanta, Georgia. SMPS = scanning mobility particle sizer, used to measure numbers of particles with D_p = 20-250 nm. A laser particle counter is employed to measure particles with diameters of 0.1-2 μm. Nanoparticles with D_p = 3-50 nm are measured with a nano-DMA in conjunction with a UCPC. The white boxes without data indicate times of eqipment failure. From Woo et al. (2001). Used by permission of Taylor & Francis, Inc.

Measurements are difficult both because these particles have very little mass and because their composition varies significantly from particle-to-particle, as well as temporally and spatially. As a first step in a description, the chemical composition of new particles should relate directly to their routes of origin and subsequent growth. For example, new

particles that form from the condensation of H_2SO_4 should clearly contain significant amounts of sulfuric acid as well as any other species involved in the nucleation event (e.g., H_2O, NH_4^+, and perhaps organic species). Similarly, ammonium nitrate and low volatility organic species, when involved in nucleation, should also be important chemical components of new particles.

For fresh nanoparticles arising from primary emissions, it should be possible to roughly infer their composition based on studies that have characterized fine particles from the same emission source. For example, ultrafine and accumulation mode particles from medium duty diesel vehicles mainly contain elemental and organic carbon (Kleeman et al. 2000). Most individual molecules composing this particulate organic carbon have not been identified, but investigated compound classes include large *n*-alkanes, alkanoic acids, and polycyclic aromatic hydrocarbons (Schauer et al. 1999). Though not yet characterized, it is likely that nanoparticles from diesel engines contain similar types of compounds. Likewise, fresh nanoparticles from wood combustion should have compositions somewhat similar to larger wood smoke particles, which contain inorganic compounds as well as hundreds of organic species including levoglucosan, substituted methoxyphenols, and PAHs (Rogge et al. 1998; Simoneit et al. 1999; Nolte et al. 2001; Schauer et al. 2001). One caveat to this argument is that the relatively volatile components (e.g., many of the organics) present in the larger particles should be much less prevalent in nanoparticles from the same source (e.g., Kerminen et al. 2000; Tobias et al. 2001).

As discussed previously, growth and chemical reactions of nanoparticles lead to changes in their compositions. Thus the inferences in composition described above should hold only for fresh nanoparticles; correlations should weaken with atmospheric aging of the particles. It would be desirable to compare these expectations against actual field measurements of particle compositions. However, quantitative measurements of the chemical composition of ambient ultrafine particles are available only for the larger members of this class ($D_p \approx$ 50-100 nm). Available data, from urban areas in Southern California, indicate that organic compounds represent approximately half of the ultrafine particle mass. The remaining mass is contributed by trace metal oxides, elemental carbon, sulfate, nitrate, ammonium, sodium, and chloride (Cass et al. 2000).

Some examples of the composition of 50- to 100-nm particles from different locations in Southern California are given in Figure 16. These data indicate that the relative amounts of ultrafine particle components vary widely at different locations, a reflection of differences in particle sources and the condensation of low-volatility species. It is unknown what fraction of each chemical component in these samples was present at the point of primary emission (or initial formation) and what fraction resulted from atmospheric aging. Condensation likely contributes most significantly for chemical species that have strong vapor sources, such as organic carbon, sulfate, nitrate and ammonium. In contrast, condensation should contribute insignificantly for nonvolatile components such as metals. As shown in Table 2, Fe, Na, K, and Ti are the most abundant metals in the ultrafine particles measured, and there are also significant concentrations of Cr, Zn, and Ba. These metals are potentially significant because of their possible catalytic chemical activities and potential to contribute to the adverse human health effects associated with particles. Other metals of possible significance, such as Pt, Pd, and Rh, are not determined in the samples because of limitations of the analytical method (Hughes et al. 1998).

Future measurements should greatly increase our knowledge of the chemical composition of nanoparticles. The recent development of a novel laser desorption/ionization single-particle mass spectrometer (RSMS-II) (Carson et al. 1997; Ge et al. 1998; Phares

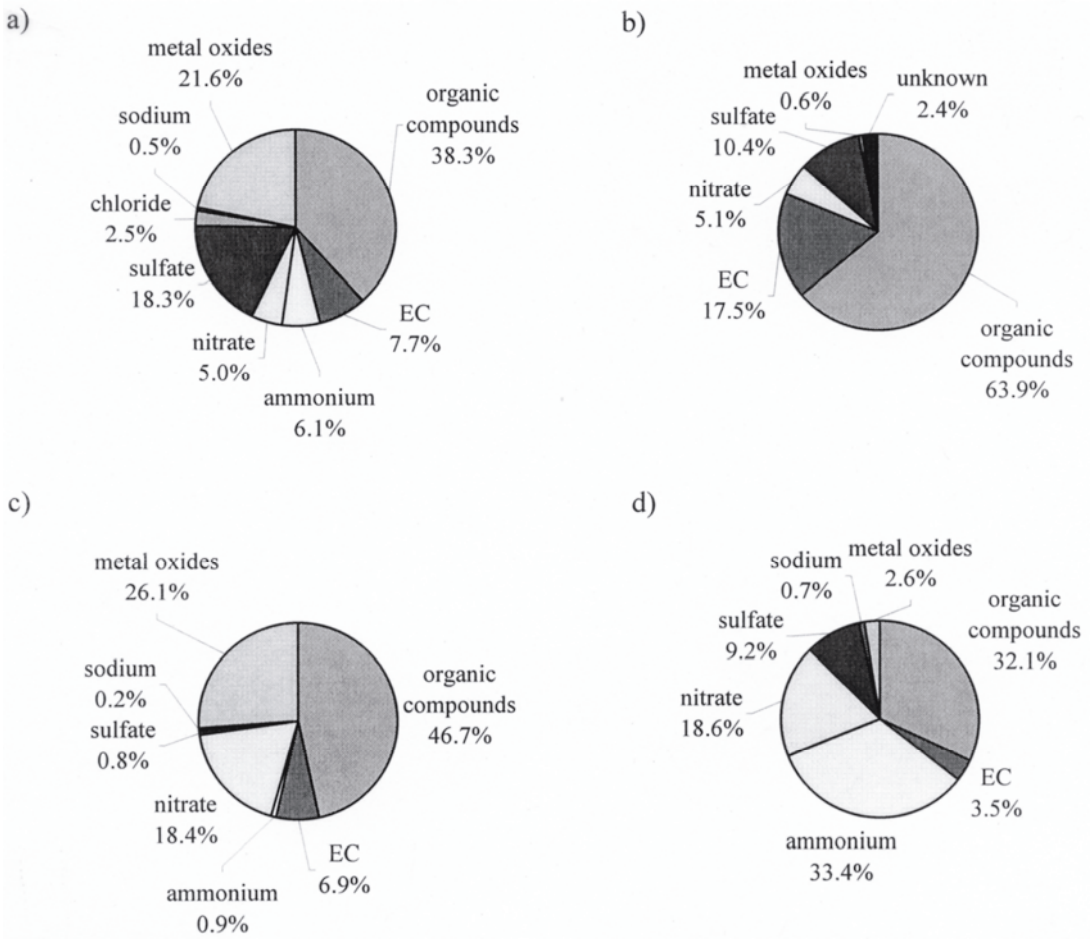

Figure 16. Chemical composition of atmospheric ultrafine particles (D_p = 56-100 nm) measured in four cities in Southern California: (a) Fullerton, September-October, 1996 (average mass concentration of 56-100 nm particles = 0.64 μg m^{-3}), (b) Diamond Bar, September-November, 1997 (0.55 μg m^{-3}), (c) Mira Loma, September-November 1997 (0.58 μg m^{-3}), and (d) Riverside, August-November, 1997 (0.91 μg m^{-3}). Note that elemental carbon is abbreviated as "EC". Adapted from Cass et al. (2000). Used by permission of the Royal Society.

et al. 2001a) enables real-time measurements of the chemical components of ambient nanoparticles (aerodynamic $D_p \geq 10$ nm). At this time, this instrument does not quantitatively determine chemical composition because the detection of particles, and the efficiency with which they are ablated by the laser, depend upon particle size and composition (Kane and Johnston 2000; Phares et al. 2001a). Even so, the instrument provides insight into the elements and compound classes present in ambient nanoparticles. As configured in the two studies described below, the instrument measures particles in 9 or 13 size bins ranging from $D_p > 1$ μm down to nanoparticles as small as 14 nm.

Results are discussed here for the RSMS-II deployed in Atlanta during August 1999 and in Houston during August-September 2000 (Rhoades et al. 2001; Phares et al. 2001b). In the Atlanta study, approximately 16,000 particles, including both nanoparticles and larger particles, are classified into nine major composition classes. Organic carbon is the most abundant class (representing 74% of all particles). Organic particles are even more prevalent among the measured nanoparticles, accounting for 85-90% of the total number of detected particles with diameters under 50 nm (Rhoades et al. 2001). This class of particles is dominated by C^+-ions and other carbon fragments, but it

Table 2.
Concentrations (ng m^{-3}-air) of trace metals in ultrafine particles ($D_p \approx$ 50-100 nm)

	Pasadena, CA [a] (Jan.–Feb., 1996)		*Central Los Angeles, CA* [b] (Aug.– Sept., 1997)	
Element	*Mean*	*Range*	*Mean*	*Range*
Group I and II metals				
Na	27.0	0.75 - 34.8	85	bdl - 249
K	bdl	bdl	88	bdl - 93
Cs	0.016	0.0081 - 0.028	0.100	bdl - 0.34
Ba	1.04	bdl - 2.8	19	bdl - 19
Transition metals				
Sc	0.0046	bdl - 0.0081	0.028	bdl - 0.054
Ti	7.65	4.07 - 10.2	43	bdl - 43
V	0.059	bdl - 0.14	bbl	--
Cr	7.32	bdl - 26.2	6.7	bdl - 15
Mn	0.74	bdl - 2.43	bbl	bbl - 0.056
Fe	67.5	bdl - 148.3	186	bdl - 470
Zn	3.68	bdl - 6.56	3.8	bbl - 10
Mo	0.072	bdl - 0.19	0.48	bdl - 0.68
Cd	0.061	bdl - 0.12	0.19	bbl - 0.49
Au	bdl	bdl	bdl	--
Hg	0.0052	0.00014 - 0.012	0.09	0.038 - 0.14
Lanthanides				
La	0.11	0.00082 - 0.51	0.021	bdl - 0.021
Ce	0.19	bdl - 0.82	1.2	bdl - 2.3
Sm	0.015	0.00030 - 0.73	0.012	bdl - 0.019
Eu	0.013	bdl - 0.023	0.20	bdl - 0.37
Yb	0.0028	bdl - 0.0059	0.26	bbl - 0.5
Lu	0.00038	bdl - 0.0013	0.014	0.0011 - 0.028
Actinides				
Th	0.0065	bdl - 0.018	bbl	—
U	0.0057	bdl - 0.019	bdl	—

bdl denotes 'below detection limit' bbl denotes 'below blank levels'

[a] Data from Hughes et al. (1998). Used by permission of the American Chemical Society.

[b] Data from Cass et al. (2000). Used by permission of the Royal Society.

also includes Si and K ions. These observations are consistent with a high temperature combustion source of primary particles. Given the high biogenic emissions in Atlanta during the summer (Chameides et al. 1988), gas-to-particle conversion of oxidation products from biogenic hydrocarbons also likely contributes to the organic aerosol. Other important particle classes of nanoparticles in Atlanta include potassium (a class with contributions from C, Ca, Na, Si and Al), calcium (with C, Fe, and Si), nitrate (with C, Si, and NH_4^+), and elemental carbon.

The compositions of nanoparticles in Houston differ markedly from those observed in Atlanta. In particular, the dominant composition in Houston is a Si-based particle rather than an organic type (Phares et al. 2001b). The Si particle type is also prevalent

among the nanoparticles measured, accounting for approximately 70% and 60% of the number of detected particles with diameters of 35 and 50 nm, respectively. Because atmospheric Si is normally associated with coarse particles derived from crustal material (Finlayson-Pitts and Pitts 2000), the presence of nanoparticulate silica suggests an alternative source, possibly involving high temperature combustion (Wooldridge 1998; Wooldridge et al. 1999). The presence of Si in particles of 35-nm diameter, and perhaps smaller, also lends support to speculation that reactions on silica nanoparticles might occur in the troposphere. Other types of 35-nm particles prevalent in Houston include carbon (including several types of aliphatic amines), iron, mixed organic/mineral, potassium, and aluminum (Phares et al. 2001b). Sea-salt particles of 35-nm diameter are also present in Houston when the wind direction follows from the ocean, in agreement with previous observations of 35-nm diameter sea-salt nanoparticles in the Pacific Ocean (Berg et al. 1998).

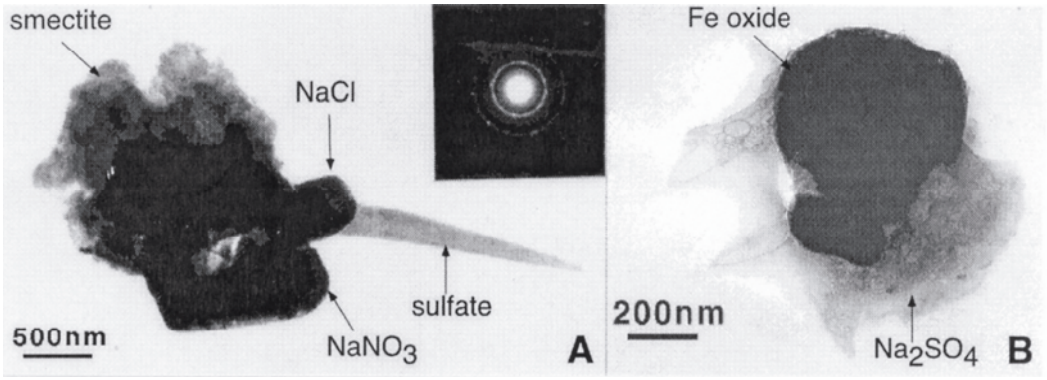

Figure 17. TEM images of internally mixed terrestrial and marine aerosol particles. (a) Terrestrial smectite with sea-salt particles. The selected-area electron diffraction pattern (upper right) confirms the identification of smectite (Azores, North Atlantic Ocean, ASTEX/MAGE). (b) Fe oxide emitted from coal burning, with Na_2SO_4 (Sagres, Portugal, ACE-2). Images by Mihaly Pósfai. Figure adapted from Buseck et al. (2000). Used by permission of the editor of *Proceedings of the National Academy of Sciences, USA*.

Morphology

The shape of atmospheric particles and the arrangement of chemically distinct components within a single particle have been investigated by sampling onto transmission electron microscopy (TEM) grids followed by imaging in the laboratory (Buseck and Pósfai 1999; Buseck et al. 2000).Figures 9 and 17 provide several examples of inorganic particles collected in different locations. A large inventory of images confirms what these figures suggest, i.e., that atmospheric particles in the large submicron to supermicron sizes are usually composed of grains of material in the nanoparticle regime. Nanoscale sulfate coatings, which are presumed to arise from SO_2 oxidation on mineral surfaces or from the condensation of H_2SO_4, are another common feature. Another particularly good example of morphology at the nanoscale is found in soot particles, which are commonly composed of ca. 50-nm spherical units agglomerated in chains to form larger particles. *In situ* mass spectrometric analysis of single atmospheric particles also confirms extensive internal mixing of chemical components (Noble and Prather, 2000). An understanding of atmospheric nanoparticles is thus incomplete without recognizing that many, if not most, larger atmospheric particles are agglomerated domains of nanophase materials.

Although environmental TEM instruments are now beginning to come on-line, a drawback of the TEM imaging completed to date is that they required operation at very

low pressures. Thus the effect of volatile components on particle morphology is unknown; water is of particular importance. Deliquescent components (e.g., NaCl and $NaNO_3$) likely form an aqueous layer around insoluble minerals (e.g., smectite), at least at some of the higher RH values common in the atmosphere. At lower RH values, complex morphological shapes at the nanoscale increase hygroscopic response by reducing the chemical potentials of aqueous solutions in interstices between particles (Xie and Marlow 1997). Organic surfactant layers may be present in some particles (Gill et al. 1983; Ellison et al. 1999), and one property of this interfacial nanostructure is believed to be a decrease in the water evaporation rate (Xiong et al. 1998).

At sufficiently low RH values, crystallization occurs. The result is rarely nonporous particles of idealized shapes such as spheres or cubes (Charlesworth and Marshall 1960; Leong 1981). Laboratory studies on the morphological characteristics of evaporatively dried salt particles provide some insight into possible processes affecting the morphology of atmospheric particles. Cziczo et al. (1997) and Weiss and Ewing (1999) show from infrared studies that submicron $NaCl/H_2O$ aerosols dried by passage through a diffusion dryer retain nanoscale pockets of water to 0% RH. These studies, however, are unable to provide information on the overall particle shape. Even NaCl particles generated by high-temperature aerosol condensation methods fail to yield nonporous cubic particles. Matteson et al. (1972) report that the density of particles generated by such methods are different from the bulk materials. The differences arise from nanoscale structural features. Craig et al. (1952) and Krämer et al. (2000) report that chain agglomerates of NaCl particles produced by condensation rearrange to cubic particles upon exposure to sub-deliquescent RH values. Although evaporation in diffusion dryers has been modeled, these studies omit the effects of the detailed microphysical structuring of the particles that accompanies drying (Xiong and Kodas 1993). Ge et al. (1996) study multicomponent aerosol crystallization by rapid evaporative drying of particles containing $KCl/NaCl/H_2O$, $KCl/KI/H_2O$, $(NH_4)_2SO_4/NH_4NO_3/H_2O$ followed by collection of the mass spectra of the surface layers by single-particle mass spectrometry. They find that nanoscale surface layers are enriched in the minor component. The implication is that the particle morphology consists of some kind of layering with the initially crystallized phase towards the core of the particle and the minor components, which precipitate later, in the surface layers.

The detailed morphology (including overall particle shape, grain sizes and relative juxtapositions, and possible water inclusions) adopted by dried atmospheric particles probably depends on the temperature and the rate of evaporation. For these reasons, it cannot be certain that morphological features observed by TEM for particles dried by exposure to vacuum are the same as those adopted by particles dried by atmospheric processes. A critical need is the development of techniques capable of in situ characterization of particle morphology. Because the particles themselves are often no larger than 1 μm, the heterogeneity of their features occurs on the 10 to 100-nm scale.

PROPERTIES

Motion

On a large scale, particles (as well as gases) are moved through the atmosphere by advection and turbulence, i.e., horizontal and vertical winds (Wexler et al. 1994; Seinfeld and Pandis 1998). Simultaneous with these large-scale motions are the smaller-scale processes that can transport particles across surface boundary layers (e.g., at the Earth's surface) and thus remove them. As discussed earlier, diffusion is the dominant removal mechanism for small particles because of their high diffusion coefficients and low gravitational settling velocities. Because of their very small sizes, nanoparticles can slip

between gas molecules, with the result that diffusion coefficients for nanoparticles are much larger than predicted based on continuum fluid mechanics (Seinfeld and Pandis 1998; Friedlander 2000). The diffusion coefficient (D, cm^2 s^{-1}) for particles in air is given by:

$$D = \left(\frac{kT}{3\pi\mu \mathrm{D}_p} \right) C_c \tag{18}$$

where μ is the gas viscosity and C_c is the Cunningham slip correction factor. The term in parentheses is the Stokes-Einstein relation, which is the diffusion coefficient for particles large enough such that the surrounding gas behaves as a continuous fluid (i.e., C_c = 1) (Seinfeld and Pandis 1998).

The Cunningham correction factor has been empirically determined to be (Seinfeld and Pandis 1998):

$$C_c = 1 + \frac{2\lambda}{\mathrm{D}_p} \left[1.257 + 0.4 \exp\left(-\frac{1.1 \mathrm{D}_p}{2\lambda} \right) \right] \tag{19}$$

where λ is the mean free path. As shown in Figure 18, C_c = 22 for a 10-nm particle and is 216 for a 1-nm particle. This slip correction is small (under 1.08) for particles 2 μm and greater. Limit analysis of Equations 18 and 19 shows that the diffusion coefficient for nanoparticles goes as $D \propto 1/D_p^2$.

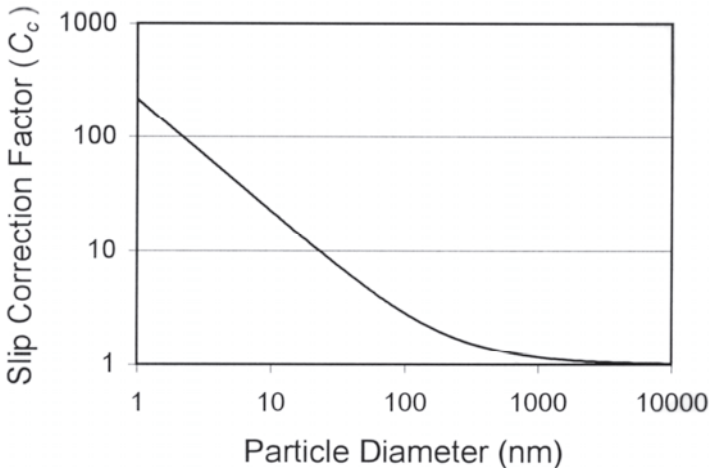

Figure 18. Cunningham slip correction factors (C_c) for spherical particles in air as calculated from Equation (19) at 298 K and 1 atm.

Although the terminal settling velocities for nanoparticles are extremely small and of little consequence, it is interesting to note that they are also much faster than predicted from continuum fluid dynamics. As with nanoparticle diffusion, this is a result of particle slip between gas molecules. The terminal settling velocity for particles ($\mathrm{D_p} \leq 20$ μm) in air is given by the following equation (Seinfeld and Pandis 1998):

$$v_t = \left(\frac{\mathrm{D}_p^2 \rho_p g}{18\mu} \right) C_c \tag{20}$$

where ρ_p is the particle density and g is the gravitational acceleration (9.8 m s^{-2}). Thus the terminal settling velocities of nanoparticles are enhanced by the same factor (C_c) as are their diffusion coefficients.

Hygroscopic behavior

The phases of particles (e.g., aqueous or crystalline) affect their roles in atmospheric

processes (Martin 2000). For example, light scattering is affected by both changes in refractive indices and particle sizes that accompany cycling between aqueous and crystalline states. Heterogeneous chemistry is also strongly influenced by the presence or absence of an aqueous phase. In atmospheric particles, salts comprise one important component in the hygroscopic response, though particulate organics are also increasingly recognized as playing a role (Pitchford and McMurry 1994; Saxena et al. 1995; Cruz and Pandis 2000).

In the lower troposphere, the dominant cycling of the inorganic component of particles is between aqueous and crystalline states as the relative humidity (RH) changes. At sufficiently high RH values, crystalline salts uptake water and deliquesce to form aqueous particles (Martin, 2000). With decreasing RH, crystallization (efflorescence) is often inhibited kinetically and high supersaturations are possible. For example, at 298 K deliquescence of $(NH_4)_2SO_4$ particles occurs at 80% RH but crystallization of the $(NH_4)_2SO_4/H_2O$ particles via homogeneous nucleation does not occur until 35% RH. Two ongoing research efforts focus on how this hysteresis cycle is altered by the presence of nanosized foreign surfaces such as mineral dusts inside the particle (Han and Martin 1999; Martin et al. 2001) and on how the deliquescence behavior is altered when the salt particles have a significant contribution from surface energies, i.e., nano-sized particles.

Effect of size on heterogeneous nucleation. Figure 17 shows an example of a mineral dust particle coated by hygroscopic salts. The deliquescence/efflorescence hysteresis cycle is reduced due to heterogeneous nucleation when foreign material, such

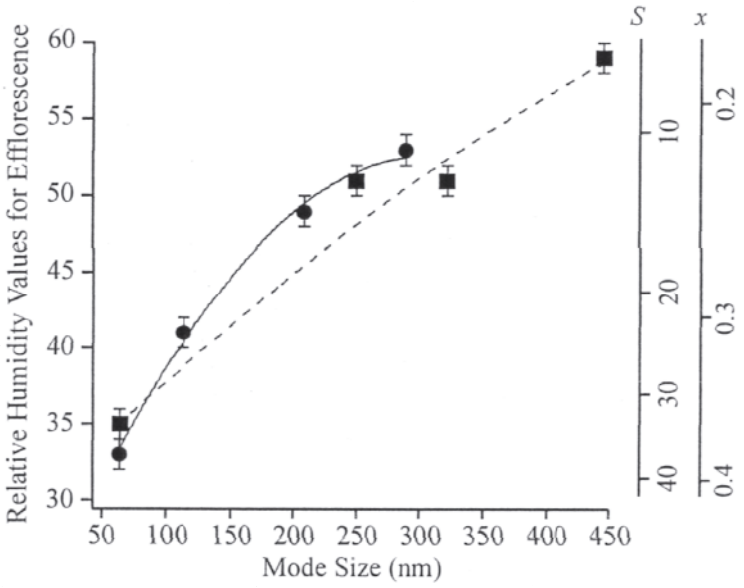

Figure 19. RH values observed for the efflorescence of ammonium sulfate (120 sec residence time) by heterogeneous nucleation as a function of mode diameter of the inclusions for corundum (●) and hematite (■). The lines show $\mathbb{F} = 0.50$ of the optimized fit to the active site model (Eqn. 24). Right axes show saturation ratios, *S*, of the aqueous phase with respect to crystalline ammonium sulfate and salt mole fractions, *x*, of the aqueous phase, as calculated from the model of Clegg et al. (1998) when assuming equilibrium between RH and water activity and omitting Kelvin effects. Adapted from Martin et al. (2001). Used by permission of the American Geophysical Union.

as mineral dusts, are present (Han and Martin 1999; Martin et al. 2001). Figure 19 shows that the RH value for $(NH_4)_2SO_4$ efflorescence increases with the size of submicron hematite and corundum inclusions (Martin et al. 2001). Rationalization of these data based upon changes in surface area is not possible within the framework of classical heterogeneous nucleation theory (Eqns. 10-12) when a reasonable range of physical parameters is employed. According to this theory, the dependence $d\mathrm{RH}_{\mathrm{eff}}/d\mathrm{D}_{\mathrm{p}}$ is nearly vertical. One critical assumption of classical theory is that the surface is everywhere the same, i.e., an infinitely extending terrace. An alternative theory, based on the occurrence of specific active sites, succeeds in explaining the size-dependence shown in Figure 19. According to the active-site theory (Fletcher 1969; Gorbunov and Kakutkina 1982), a surface is populated by nanoscale step edges, pits, kinks, and so on, of which each is possibly a heterogeneous nucleation center. This chapter follows the development by Han et al. (2001).

The central point of the active-site theory is that the areal density of nanoscale surface features is small and approaches the same scale as individual particle surface areas, especially in the regime of nanoparticles. The probability that a particle bears *i* active-sites is given by the Poisson distribution, as follows:

$$P_i = \exp(-4\pi R^2 n_0)\frac{(4\pi R^2 n_0)^i}{i!} \tag{21}$$

where R is the particle radius and n_0 is the number of active-sites per unit area (i.e., areal density). For each active-site, the probability distribution of the surface area, $P_s(A)$, is log-normal, as follows:

$$P_s(A) = B\exp\left\{-\gamma^2\left[\ln\left(\frac{A}{A_0}\right)\right]^2\right\} \tag{22}$$

where A is the active-site area, A_0 is the minimum active-site area, B constrains the integral $\int_{A_0}^{4\pi R^2} P_s(A)dA = 1$, and γ is the width of the distribution (Fletcher, 1969). The probability, $P_g(A)$, of a critical embryo forming on an active-site of area A is given as follows:

$$P_g(A) = 1 - \exp\left[-A(j - j_0)\tau\right] \tag{23}$$

where j ($\mathrm{cm}^{-2}\,\mathrm{s}^{-1}$) is the heterogeneous nucleation rate over the active-site (see Eqn. 25), j_0 is the heterogeneous nucleation rate over a defect-free portion of the surface (i.e., a terrace as in Eqn. 10), and τ is the observation time. Based on Equations (21)-(23), Gorbunov and Kakutkina (1982) evaluated the fraction (i.e., probability), $\mathbb{F}$, of particles undergoing a phase transition in an ensemble of monodisperse particles, as follows:

$$\Phi = 1 - \exp\left\{-4\pi R^2\left[j_0\tau + n_0\int_{A_0}^{4\pi R^2} P_s(A)P_g(A)dA\right]\right\} \tag{24}$$

For the infrared detection technique employed in Figure 19, the threshold sensitivity to the phase transition is $\mathbb{F} = 0.5$. The term j is calculated by a reduction in the free energy barrier due to an improved efficiency over the active site, as follows:

$$j = n\frac{kT}{h}\exp\left(-\frac{f(m)\Delta G_{germ} - A(m_1 - m)\sigma}{kT}\right) \tag{25}$$

where σ is the surface tension of the ammonium sulfate embryo/aqueous solution interface and m_1 describes the efficacy of heterogeneous nucleation at the active site (cf.

Eqn. 8). We assume perfect active sites (i.e., $m_1 = 1$) as done by Fletcher (1969). The active-site model embodied in Equation (24) rationalizes the data shown in Figure 19 for surfaces described as follows: {<0, 10.4 ± 0.4, 0.85 ± 0.15, 3 ± 1 × 10^{-15}} for α-Al_2O_3 and {0.04, 9.0 ± 0.2, 0.55 ± 0.05, 3 ± 1 × 10^{-15}} for α-Fe_2O_3 in the format {m, Log_{10} n_0 (site/cm^2), γ, A_0 (cm^2)}.

The values for α-Al_2O_3 indicate that the maximum likelihood distribution for 100 particles of 10-nm diameter (Eqn. 21) is that 73 particles have no active sites, 23 have one site, 4 have two sites, and 1 has three or more sites. Each category of particle exhibits strikingly different efficiency as heterogeneous nuclei. Most notable is that those particles having no active sites yield nucleation rates no faster than homogeneous nucleation. In contrast, in a population of 1-μm particles, over 99% of the particles have 3150 ± 100 active sites. The result is a strong nonlinearity in the heterogeneous nucleation properties in scaling from nanoparticles to micron-sized particles.

Figure 19 empirically demonstrates the divergence of nanoparticle properties from bulk properties. At sufficiently large size (i.e., extrapolation beyond the micron), every surface contains a number of active sites and the hysteresis gap between deliquescence and efflorescence approaches a limiting value of zero. However, when the particles move into the nanoregime, the distribution statistics shown by the Poisson distribution in Equation (21) indicate that there are perceptible differences from one particle to the next in terms of how many active sites are on an individual particle. For the smallest particles (e.g., 10 nm), over half of the particles have no active sites at all and are very ineffective heterogeneous nuclei.

Effect of size on deliquescence relative humidities. For particle diameters below 1 μm, free energy is affected increasingly by the surface energy contribution. The result is a shift in the deliquescence relative humidity for small particle sizes (Hameri et al. 2000; Mirabel et al. 2000; LM Russell, unpublished results). Work in this area is new, and the experimental and theoretical results have not yet led to agreed-upon conclusions, i.e., whether decreasing particle size leads to higher or lower values of the deliquescence RH (DRH). A theoretical framework can be developed, as follows (Mirabel et al. 2000). The DRH value is the water activity at which the free energies are equal for water and salt molecules arranged as either vapor and crystalline salt or vapor and aqueous salt (Martin 2000). The respective free energy formulations are as follows:

$$G_{vapor/crystal} = N_{total}^{H_2O}\mu_{vapor}^{H_2O} + \left(N_{solute}\mu_{solute,bulk}^{crystal} + \sigma^{crystal/vapor}A^{crystal}\right)$$

$$G_{vapor/aqueous} = \left(\left(N_{total}^{H_2O} - N_{aqueous}^{H_2O}\right)\mu_{vapor}^{H_2O}\right) + \left(N_{solute}\mu_{solute,bulk}^{aqueous}(x) + N_{aqueous}^{H_2O}\mu_{H_2O,bulk}^{aqueous}(x) + \sigma^{aqueous/vapor}(x)A^{aqueous}\right) \quad (26)$$

The definitions of the symbols are: free energy (G), number of molecules (N), chemical potentials in the bulk (μ), surface area (A), surface tension (σ), and mole fraction composition (x). Equation (26) is developed by Mirabel et al. (2000) by assuming that particles are spherical (even when crystalline), that the solute is not volatile, that the vapor phase reservoir of water is infinite, and that all chemical potentials behave ideally with respect to x. Note that the first and fourth approximations are gross.

Figure 20 shows the solution to Equation (26) for several different assumed $\sigma^{crystal/vapor}$ values in the $NaCl/H_2O$ system. The y-axis is the ratio of the DRH value anticipated from Equation (26) to the DRH value of a bulk system (DRH_{bulk} = 75% at 298 K) as a function of the number of solute molecules in the particle. In the nanosize regime, the DRH value is predicted to be shifted to much lower values in most cases. This result

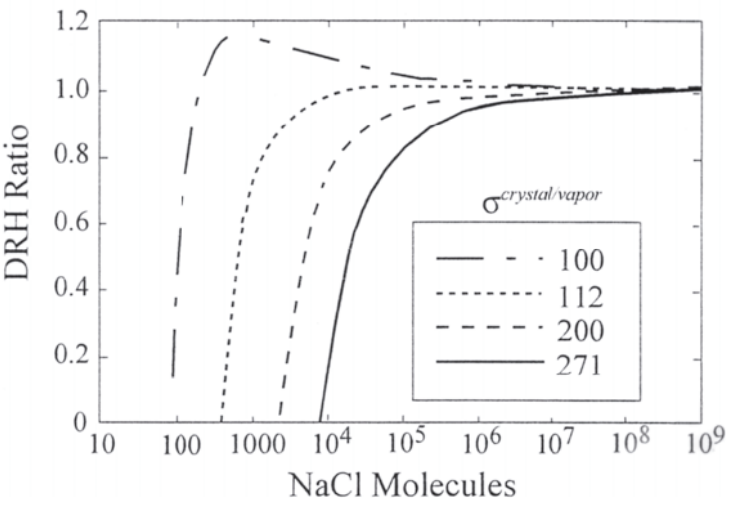

Figure 20. Plots of DRH relative to bulk crystal (viz. 75%) versus crystal size for various values of crystal/vapor surface tensions. Note the sensitivity of DRH to surface tension. Adapted from Mirabel et al. (2000). Used by permission of the American Chemical Society.

is driven primarily by the difference between $\sigma^{crystal/vapor}$ and $\sigma^{aqueous/vapor}$ (taken as 70 mJ m^{-2} independent of x in these calcuations). Because $\Delta\sigma > 0$ for normally behaving materials (i.e., surface tensions of solids against vapor are greater than liquids against vapor), there is a thermodynamic driving force to favor the aqueous state when sizes are small enough that the surface energy makes a significant contribution to the overall free energy of the particle. In a few cases (e.g., $\sigma^{crystal/vapor}$ = 100 mJ m^{-2}), a maximum is seen in Figure 20 where DRH of nanoparticles is greater than the bulk value. This subtle effect, which is explained in detail by Mirabel et al. (2000), arises because H_2O is volatile and NaCl is not volatile. In this case, the mole fraction composition of the smallest aqueous droplets are enriched in NaCl because the Kelvin effect drives the evaporation of water. The net effect on the free energies is that DRH increases as compared to bulk values.

Because NaCl is known to adsorb multilayers of water prior to the DRH value, the physical description of the chemical system given by Mirabel et al. (2000) may not be accurate. The multilayer of adsorbed water is believed to be ordered and relatively pure, i.e., free of ions. This interesting phenomenon is under investigation, i.e., pure water whose chemical potential is under unity (Peters and Ewing 1997a,b). The above formulation for the free energy of the system (Eqn. 26) can be revised for a multilayer interface involving the surface tensions of the water layer against the vapor and of the crystal against the water layer, as follows:

$$\begin{aligned} G_{vapor/adsorbed/crystal} &= \left(N_{total}^{H_2O} - N_{adsorbed}^{H_2O}\right)\mu_{vapor}^{H_2O} + \left(N_{adsorbed}^{H_2O}\mu_{adsorbed}^{H_2O} + \sigma^{vapor/adsorbed}A^{adsorbed}\right) \\ &\quad + \left(N_{solute}\mu_{solute,bulk}^{crystal} + \sigma^{adsorbed/crystal}A^{crystal}\right) \\ G_{vapor/aqueous} &= \left(\left(N_{total}^{H_2O} - N_{aqueous}^{H_2O}\right)\mu_{vapor}^{H_2O}\right) + \\ &\quad \left(N_{solute}\mu_{solute,bulk}^{aqueous}(x) + N_{aqueous}^{H_2O}\mu_{H_2O,bulk}^{aqueous}(x) + \sigma^{aqueous/vapor}(x)A^{aqueous}\right) \end{aligned} \quad (27)$$

A key point is that both $\sigma^{vapor/absorbed}$ and $\sigma^{absorbed/crystal}$ are less than $\sigma^{crystal/vapor}$. Recent work (LM Russell, unpublished results) has shown that for soluble salts that adsorb water below their deliquescence point (including NaCl), the DRH values increase with decreasing particle size for typical values of $\sigma^{vapor/absorbed}$ and $\sigma^{absorbed/crystal}$. This conclusion differs markedly from the formulation given in Equation (26) and shown in Figure 20, where the limiting value of DRH is zero at small particle sizes. These differences highlight the uncertainty and need for further theoretical and laboratory work on the effect of particle size on DRH values.

Chemical reactivity

Chemical reactions involving atmospheric nanoparticles are potentially important for at least two reasons: (1) reactions might alter the chemical composition and thus the physicochemical properties of nanoparticles and (2) reactions might change the composition of the gas-phase. For example, reactions with O_3 make soot particles more hydrophilic, which should enhance their ability to act as cloud condensation nuclei (Kotzick et al. 1997). Although it has been speculated that nanoparticle reactions also alter gas-phase composition, this is probably quite uncommon except perhaps in aerosols with very high nanoparticle surface areas. Even so, in some specific cases there might be a unique role for nanoparticles in atmospheric chemistry. Such cases could occur, for example, if a nanoparticle reaction is fast compared to the equivalent reaction in the gas-phase or in/on other condensed phases such as cloud drops or larger aerosol particles. Nanoparticles could also significantly alter the composition of the gas phase if the nanoparticle reaction is unique in terms of the reactants destroyed or products produced. To the best of our knowledge, there are no identified instances of nanoparticle reactions in the atmosphere where either of these two criteria is satisfied. However, this field is largely unexplored at the time of this writing.

As a first step in assessing the potential importance of nanoparticle reactions, we compare the volume and surface areas of these particles with the same values from other condensed phases with known chemical effects. We first consider nanoparticle volumes. As an upper limit, we consider an urban air parcel containing 20-nm diameter nanoparticles at a number concentration of 10^5 cm^{-3}. Under this scenario, the nanoparticle volume is a small fraction (10^{-13}) of the total air parcel volume. Thus the nanoparticle reaction rate (in units of mol m^{-3}-air s^{-1}) would have to be ca. 10^{13} times as fast as the equivalent gas phase reaction (mol m^{-3}-air s^{-1}) to have a comparable overall rate in the air parcel. For comparison, clouds typically have liquid water contents of 10^{-7} to 10^{-6} (volume fraction) and can have significant effects upon atmospheric chemistry (Seinfeld and Pandis 1998). For simplicity of argument, if the medium of the cloud droplets and nanoparticles are assumed similar (e.g., dilute aqueous), then the fundamental rate constants in each medium are similar. Under this condition, reactant concentrations in the nanoparticles would need to be enhanced by 10^6, as compared to the cloud droplets, to have equal rates. Based on this analysis, it appears unlikely that reactions occurring in the bulk of nanoparticles could affect the composition of the gas phase.

The other possibility is a reaction at the surface of the nanoparticles. For the assumed urban scenario above, the nanoparticle surface area concentration is approximately 100 μm^2 per cm^3-air. At this surface area loading, nanoparticle reactions could plausibly affect the composition of the gas phase. For example, de Reus et al. (2000a) report that plumes of mineral dust particles (primarily in the accumulation mode), with surface area concentrations of ca. 100 μm^2 cm^{-3}, significantly reduce mixing ratios of ozone and nitric acid. While this comparison suggests nanoparticle surface reactions could be significant in urban atmospheres, the conclusion depends on a number of factors, including high particle number concentrations (which are unlikely outside of urban areas), a reactive particle surface with sufficiently high uptake coefficients for trace gases, and surface renewal during the course of the reaction.

In the remaining portion of this section we examine several nanoparticle types and reactions that could potentially be significant in the atmosphere. Of course, until the chemical composition, morphology, and reactivity of nanoparticles are better characterized, it is not possible to assess accurately the significance of these or other reactions.

Concentrated H_2SO_4. Sulfuric acid is an important participant in the nucleation and the growth of new particles in the troposphere. The mole fraction acidity (viz. H_2SO_4 content) of these particles is believed to be high. It is likely that the presence of this strong sulfate acidity influences the chemistry of nanoparticles because sulfuric acid promotes a number of organic reactions that otherwise either do not occur or occur much more slowly (Liler 1971). We will consider several of these reaction classes here with a focus on those involving organic species common in the atmosphere.

One class of organic reactions in sulfuric acid is hydrolysis, which affects functional groups such as ethers, esters, nitriles, halogenated organics, and converts amides to the corresponding carboxylic acid, as follows:

$$RC(O)NH_2 + H_2SO_4 + H_2O \rightarrow RC(O)OH + NH_4^+ + HSO_4^- \quad (28)$$

In addition, concentrated sulfuric acid catalyzes the decarbonylation of aldehydes, aromatic acids, and aliphatic carboxylic acids, such as formic acid:

$$HC(O)OH + H_2SO_4 \rightarrow CO + H_2O + H_2SO_4 \quad (29)$$

Other classes of reactions are the dehydrations and condensations, such as the conversion of acetone to protonated mesityl oxide, as follows:

$$2\ CH_3C(O)CH_3 + H_2SO_4 \rightarrow (CH_3)_2C{=}CHC(OH^+)CH_3 + H_2O + HSO_4^- \quad (30)$$

Finally, a number of commonly occurring atmospheric trace species are converted to reactive electrophiles in concentrated sulfuric acid solutions. For example, nitric acid is converted to NO_2^+, which is a potent nitrating agent for aromatic compounds (Liler 1971), and hydrogen peroxide can be converted to peroxymonosulfuric acid ($HOOSO_2OH$), which is a strong oxidant (Mozurkewich 1995; Dalleska et al. 2000).

Studies of these reactions have typically been carried out in very concentrated sulfuric acid solutions (85 to 100 wt % H_2SO_4) (Liler 1971). More recent work examines whether similar types of reactions occur at lower sulfuric acid concentrations. Roberts and co-workers, for example, examine the condensation reactions of acetone in thin films of 70 to 96 wt % H_2SO_4 at temperatures found in the upper troposphere and lower stratosphere (180-220 K) (Duncan et al. 1998, 1999). According to this work, acetone is protonated in 70 wt % H_2SO_4, undergoes condensation to mesityl oxide (Eqn. 30) above 75 wt % H_2SO_4, and undergoes further condensation to trimethylbenzene above 85% H_2SO_4. Thus acetone condensation to larger carbon products requires quite high acidities. It has not yet been investigated how the rates and extents of the other reactions discussed above vary at lower sulfate acidities.

The weight percent of H_2SO_4 in stratospheric sulfuric acid particles is typically between 40 and 80% and stratospheric temperatures are generally between 210 and 240 K (Shen et al. 1995; Tabazadeh et al. 1997, 2000; Finlayson-Pitts and Pitts 2000). On the other hand, tropospheric sulfuric acid particles typically contain less than 75 wt % H_2SO_4 (this concentration is in equilibrium with a RH value of less than 1% at 298 K), and temperatures are typically above 230 K. For example, at 298 K pure sulfuric acid-water droplets ($D_p > 100$ nm) contain 42.5 wt % H_2SO_4 at a relative humidity of 50% (Seinfeld and Pandis 1998). Thus it is not known whether the reactions mentioned above occur to any appreciable extent in the troposphere or stratosphere. In the troposphere, nanoparticles of sulfuric acid may be much more acidic than larger sulfuric acid particles due to an increase in water vapor pressure with decreasing particle size (i.e., the Kelvin effect) (Fig. 21). For example, at 50% RH the weight percent of H_2SO_4 is 1.7 times

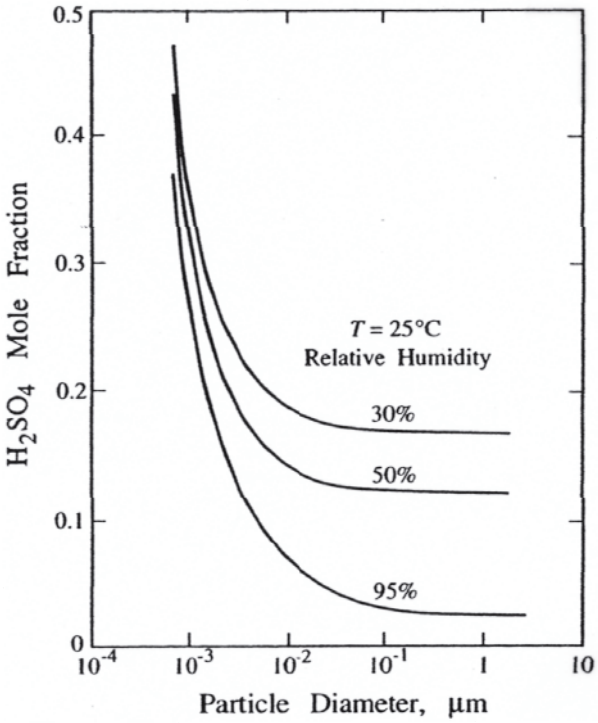

Figure 21. Mole fraction of H_2SO_4 ($x_{H_2SO_4}$) in a spherical drop of sulfuric acid and water as a function of relative humidity and drop diameter. The weight percent (wt %) of H_2SO_4 in solution is related to the mole fraction by: wt % = $\{MW_{H_2SO_4} / [(MW_{H_2O}(1/x_{H_2SO_4} - 1) + MW_{H_2SO_4}]\} \times 100\%$, where $MW_{H_2SO_4}$ and MW_{H_2O} are the molecular weights of sulfuric acid and water, respectively. From Seinfeld and Pandis (1998). Used by permission of Wiley-Interscience.

greater for a 1-nm particle (72 wt %) as compared to a 100-nm particle (43 wt %). Thus, organic reactions in sulfuric acid, such as those described above, are more likely to occur in nanoparticles and under conditions of low relative humidity. Because some reactions, such as the condensation of aldehydes (e.g., Eqn. 30), produce organic products that are of higher molecular weight and lower volatility than the initial organic compound, these chemical pathways could contribute to the growth of nanoparticles.

Soot. Combustion particles containing elemental carbon with variable amounts of organic carbon and trace metals (i.e., soot) consist of 30- to 40-nm diameter nanoparticles agglomerated in chains with typical lengths of a few hundred nanometers (Kennedy 1997; Seinfeld and Pandis 1998; Clague et al. 1999). In the past five years there has been growing interest in atmospheric reactions involving soot. Much of the attention has focused on reactions with O_3 and nitrogen oxides (i.e., NO and NO_2) because of the importance of these species as air pollutants.

The most significant soot reaction identified to date is the conversion of nitrogen dioxide (NO_2) to nitrous acid (HONO) and smaller amounts of nitric oxide (NO) (Ammann et al. 1998; Gerecke et al. 1998; Kalberer et al. 1999; Longfellow et al. 1999; Al-Abadleh and Grassian 2000; Alcala-Jornod et al. 2000; Stadler and Rossi 2000; Saathoff et al. 2001), as follows:

$$NO_2 + \text{soot} \rightarrow\rightarrow \text{HONO} + \text{NO} \qquad (31)$$

This reaction is of interest because current models underestimate the production of HONO, which is an important photolytic source of hydroxyl radical (Ammann et al. 1998; Finlayson-Pitts and Pitts 2000). This reaction could also be important as a reductive pathway for nitrogen species in the atmosphere, which is in contrast to most atmospheric reactions which tend to oxidize trace gases (e.g., the conversion of SO_2 to H_2SO_4). Molar yields of HONO via Equation (31) (relative to the moles of NO_2 lost) typically range from 50 to 100%, while yields of NO are 4 to 30% (Gerecke et al. 1998; Stadler and Rossi 2000). It appears that the formation of NO results from the secondary reaction of HONO at the surface of the soot (Stadler and Rossi 2000). The mechanism of

this reaction is not known, but water vapor appears to play a significant role (Longfellow et al. 1999). There is also some evidence that the reaction involves organic compounds that can be solvent-extracted from the soot (Stadler and Rossi 2000). There is no consensus on whether this reaction is a significant source of HONO in the polluted troposphere (Ammann et al. 1999; Kalberer et al. 1999; Kirchner et al. 2000; Saathoff et al. 2001) because there is uncertainty whether reactive sites on soot are catalytic (Longfellow et al. 1999) or are deactivated during the reaction (Kalberer et al. 1999; Kirchner et al. 2000).

A number of other atmospheric gases also react with soot. For example, ozone is destroyed on soot to form O_2, CO, and CO_2 (Gao et al. 1998; Kamm et al. 1999), while HNO_3 is reduced either to NO or NO_2 on soot (Choi and Leu 1998; Disselkamp et al. 2000a) or is simply physically adsorbed (Longfellow et al. 2000). In any case, the uptake coefficients for O_3 and HNO_3 are small enough that these soot reactions are not important as sinks for these gases or as a source of NO and NO_2 (Choi and Leu 1998; Gao et al. 1998; Kamm et al. 1999; Disselkamp et al. 2000a, 2000b; Longfellow et al. 2000). There is some evidence that the soot uptake of hydroperoxyl radical ($HO_2^{\bullet}$), which is a key component of ozone (smog) chemistry in the troposphere, is large enough to reduce O_3 mixing ratios in heavily polluted areas (Saathoff et al. 2001).

Although these O_3 and HNO_3 reactions are not important as sinks for the gases, they are likely important as pathways that chemically transform the surface of soot. For example, exposure of soot to HNO_3 or NO_2 produces surface species such as R-C=O, R-NO_2, R-ONO_2, and R-ONO (Al-Abadleh and Grassian 2000; Kirchner et al. 2000), while exposure to O_3 produces oxygen-containing functional groups such as -OH, R-C=O, and R-C-O (Kotzick et al. 1997; Al-Abadleh and Grassian 2000; Kirchner et al. 2000). These reactions are important because they make the surface of soot particles more polar, which increase soot's efficiency as a cloud condensation nucleus (Kotzick et al. 1997). These reactions might also affect the toxicity of soot particles. Given that soot is also an important reservoir of atmospheric polycylic aromatic hydrocarbons (PAHs) (Dachs and Eisenreich 2000), reactions of trace gases such as O_3 with soot may also be important in the transformation and destruction of these toxic molecules (Finlayson-Pitts and Pitts 2000; Poschl et al. 2001).

Although a number of studies have used commercially available carbon black as a surrogate for soot, there are large differences in the composition, and therefore probably in the chemistry, between these two types of materials (Watson and Valberg 2001). Diesel soot, for example, is much more oxygenated, has a more polar surface, and contains higher amounts of trace species such as Fe, S, and Ca than carbon black (Clague et al. 1999). Similarly, even with authentic soots there can be large differences in chemistry, both as a result of different fuels as well as different fuel/air ratios during soot formation (Alcala-Jornod et al. 2000; Kirchner et al. 2000; Stadler and Rossi 2000).

Metal oxides. Although most published chemical studies with prepared nanoparticles involve reactants bearing little or no relevance to the atmosphere, there are a number of reports of reactions involving metal or metal oxide nanoparticles that might have analogues in the atmosphere. For example, Klabunde and co-workers report that halocarbons, which are a significant class of anthropogenic atmospheric pollutants, are destroyed by nanoparticles of calcium oxide and magnesium oxide to form products such as CO, CO_2, elemental carbon, and the corresponding metal chloride (Koper et al. 1993, 1997; Li et al. 1994; Koper and Klabunde 1997). However, these reactions are likely insignificant in the atmosphere because they require high temperatures (typically above 600 K). It has also been shown that gases such as NO, HCl, SO_2, and CO_2 adsorb on the surface of MgO and in some cases react at room temperature (Stark and Klabunde 1996;

Stark et al. 1996). However, for these CaO and MgO reactions, the metal oxides are stoichiometrically consumed during the process. Thus even if the reactions could stoichiometrically destroy pollutant gases at atmospheric temperatures, their importance in the atmosphere should be limited by the small available masses of nanoparticulate CaO and MgO.

This stoichiometric constraint on reactivity is eliminated for catalytic or photocatalytic reactions involving nanoparticles. Although no quantitative investigations have yet been performed in either laboratory experiments or modeling, a reasonable speculation is that metals or metal oxides embedded in individual atmospheric nanoparticles might serve as catalysts for oxidation and reduction reactions in the atmosphere, as suggested by José-Yacamán (1998). In support of this view, synthesized nanoparticles containing Fe, Cr, Cu, Ti and other metals are typically very reactive, often catalytically, in reduction and oxidation reactions involving atmospheric pollutants such as CO, CH_4, and larger organic gases (Park and Ledford 1997, 1998; Zhang et al. 1998; Perkas et al. 2001). Furthermore, the rates and the efficiencies of reactions of metal oxide nanoparticles are often enhanced relative to the bulk material due to different surface structures (Stark et al. 1996; Jefferson 2000). However, it is unclear whether the reactivities of nanoparticles used in these studies are comparable to metal and metal oxide nanoparticles in the atmosphere. Moreover, given their small amounts, it is unclear whether reactions involving metal and metal oxide nanoparticles are as significant as similar reactions that might occur on accumulation and coarse mode mineral dusts.

Electronic. Several minerals, including oxides of Fe, Si, Ti, or Zn, have been investigated as active heterogeneous photocatalysts in the atmosphere. Gas/solid reactions have been investigated, for example, as tropospheric sinks for chlorofluorocarbons on mineral dusts (Ausloos et al. 1977; Benzoni and Garbassi, 1984; Filby et al. 1981; Zakharenko 1997). Photochemical conversions of aqueous species at the surface of iron oxyhydroxides (e.g., hematite, goethite, lepicrodocite, or ferrihydrite) contained within cloud droplets have also been the focus of considerable study (Sulzberger et al. 1988; Behra and Sigg 1990; Pehkonen et al. 1993, 1995; Litter et al. 1994; Siefert et al. 1994). These reactions favor the formation of oxidized species, both inorganic and organic, within cloud droplets.

The photochemical mechanism is worked out most completely for hematite. This semiconducting mineral generates electron-hole pairs when irradiated with sunlight (Sulzberger 1990; Hoffmann et al. 1995). The valence band holes oxidize adsorbed organics such as oxalate to carbon dioxide and other reduced species such as bisulfite to sulfate. As a by-product, ferrous iron is released to the aqueous solution from the ferric oxide matrix of the mineral. Although the absorption spectrum of hematite is in the red, this color arises mostly from *d*-orbital transitions in the band structure (2.2 eV) (Finklea 1988). The photoaction spectrum does not show significant activity until 3 eV (Siffert and Sulzberger 1991), which is explained by the band structure. Transitions begin at 3 eV from the occupied O(2*p*) valence band to the empty conduction band, which is composed of Fe centered *d*-orbitals. The photochemistry is explained either by hole scavenging by adsorbates or by direct charge transfer from localized orbitals of the oxygen atoms of adsorbed ligands into the conduction band.

The general process of mineral dissolution by photochemical reduction, as well as by pH-dependent non-oxidative thermal dissolution of other minerals in cloud waters (Desboeufs et al. 1999), yields the formation of dissolved aqueous species. Upon cloud droplet evaporation, one reasonable fate we can suggest for these species is reoxidation by abundant atmospheric O_2 followed by recrystallization into nanoparticles (since oxidized ions in general have lower solubility (Stumm and Morgan 1996)). There are two

assumptions inherent in this suggestion: (1) since acidic media dissolve minerals and thus disfavor precipitation of nanoparticles, the acidic cloud drop needs to be neutralized (e.g., by alkaline mineral constituents or ammonia) and (2) mineral precipitation forms new nanoparticles, possibly as accessory minerals, rather than growing material on preexisting surfaces of the same or similar minerals. Furthermore, Ostwald's rule of stages suggests amorphous phases with less developed band structures would be favored, at least initially, over more crystalline phases (Lasaga 1998). Under conditions favorable with respect to these assumptions, we offer the speculation that nanocrystalline mineral particles crystallize from cloud droplets.

Due to their small size, if these nanoparticles form they should possess altered electronic properties (Brus 1983), including a wider bandgap and thus a blue-shifted photoaction spectrum. Although this effect reduces the sunlight absorbed, the holes formed in the valence band have a higher thermodynamic driving force to promote chemical reactions. Novel chemical channels may then be opened or, alternatively, rates of chemical conversion may be increased for known channels. The idea of the formation of nanocrystalline particles with unique properties within cloud droplets is at best speculative at this time. Even so, it seems appropriate within the aims of this chapter to provide a perspective on possible properties and occurrence of atmospheric nanoparticles with electronic properties different from the bulk. Another occurrence may be in the stratosphere where 50% of the particles are estimated to contain 0.5 to 1 (w/w) iron oxide (Cziczo et al. 2001). It is unknown if the thermodynamics of highly acidic particles (60-80 wt % H_2SO_4) at extremely low temperatures (210-225 K) favors a dissolved or precipitated state for the iron. However, if crystalline, the iron should exhibit size-quantization effects in its band structure.

OUTLOOK

Many critical uncertainties must still be addressed to assess quantitatively the sources and sinks of atmospheric nanoparticles, their physical and chemical evolution during atmospheric aging, their direct and indirect impacts on atmospheric chemistry and physics, and their connections to adverse effects on human health. Several important and complex areas that need much additional study include:

1. New particle formation and growth. These processes are important sources of new particles and CCN, but field observations suggest that current theories relying on H_2SO_4 and H_2O are often inadequate to explain nucleation or growth. The role of NH_3 in a possible ternary nucleation mechanism needs to be examined quantitatively at more field sites. The identities of nonvolatile and low-volatile organic species involved in nucleation and growth should be further examined. To do so, highly sensitive and specific analytical techniques must be developed. In theoretical work, contemporary nonclassical theories of homogeneous nucleation are promising, but they are urgently in need of further data on the kinetics of cluster formation from laboratory studies.
2. Particle composition and morphology. Understanding the adverse health effects and possible chemical reactivity of atmospheric nanoparticles requires knowing their chemical composition and morphology. Quantitative measurements of the composition of ambient nanoparticles, as well as of nanoparticles from emission sources, are needed. Both traditional fine particle emission sources (e.g., combustion) as well as coarse particle emission sources (e.g., oceanic sea-salt and mineral dust) should be examined. Real-time single-particle compositional analysis, albeit still qualitative, has occurred through impressive instrumentation advances in the last few years. These advances highlight the need for commensurate progress in techniques sensitive not

only to overall particle morphology but also to internal structures such as water pockets, grain structures, surfactant layers, or radial compositional layering. In most cases, investigators must be cognizant of the overriding role of relative humidity in affecting morphology.

3. Chemical and photochemical reactions. Evaluating the potential effects of nanoparticles on atmospheric chemistry and composition will require much additional laboratory and modeling work. Experiments need to be performed to measure uptake coefficients, reaction rates, and products formed from the interaction of atmospheric trace gases with authentic or representative nanoparticles. Special attention should be given to important reactions in urban areas (e.g., ozone formation) where nanoparticle concentrations are typically greatest. An additional focus should be to examine reactions with important species that are destroyed only slowly in the gas-phase (e.g., CO or CH_4) since in these cases nanoparticle reactions might be fast enough to compete effectively with the gas-phase reactions. With these data it should then be possible to model atmospheric nanoparticle reactions and their significance.
4. Health effects. More epidemiological and clinical studies are needed to further examine the hypothesis that nano- and ultrafine particles are responsible for adverse human health effects. It will be especially valuable to perform experiments that allow elucidation of the particle properties that are responsible for toxicity, such as number concentration, surface area concentration, or specific chemical species.
5. Unique size-dependent properties. Although it is known that nanosized objects have properties diverging from the bulk, as highlighted in contemporary work on the electronic properties of semiconductors, unique chemical and physical properties in systems relevant to atmospheric nanoparticles are mostly speculative at this time and poorly informed by data. However, further intensive work is warranted based upon available data such as observations that heterogeneous nucleation properties depend on size and reach a critical regime at small size due to the statistics of small numbers, e.g., not every particle has an active site. Deliquescence relative humidities of salts depend critically on size at the nanoscale due to significant contributions of surface energies to the overall free energies. Electronic properties, including photochemistry, of metallic and semiconducting particles present in the atmosphere are strongly altered in nanosized objects. These objects may be spatially separate individual particles or they may instead be a single grain or inclusion embedded within a larger particle. These possible properties and their effects on atmospheric processes need to be investigated through additional laboratory work.

ACKNOWLEDGMENTS

This chapter is dedicated to the memory of Glen Cass and his many important contributions to atmospheric aerosol science.

We gratefully acknowledge assistance from the authors who provided us access to their unpublished manuscripts: V.H. Grassian, M.V. Johnston, L.M. Russell, and A.S. Wexler. We are also grateful to A.S. Wexler, A. Navrotsky, H.M. Hung, J. Schlenker, and A. Fillinger for valuable comments on the manuscript. C.A. appreciates the help of J. Chan, I. George, and Q. Zhang in completing this project, as well as funding from the National Science Foundation Atmospheric Chemistry Program through a CAREER award (ATM-9701995), the NIEHS through the University of Calfifornia-Davis Superfund Program, and the NSF-funded NEAT (Nanophases in the Environment, Agriculture and Technology) IGERT at UC-Davis. S.M. is grateful for support received from the NSF Atmospheric Chemistry Program, a Presidential Early Career Award in Science and Engineering (PECASE), and the New York Community Trust Merck Fund.

REFERENCES

Abbatt J, Molina MJ (1993) Status of stratospheric ozone depletion. Ann Rev Energy Environ 18:1-29

Ackerman AS, Toon OB, Stevens DE, Heymsfield AJ, Ramanathan V, Welton EJ (2000) Reduction of tropical cloudiness by soot. Science 288:1042-1047

Al-Abadleh HA, Grassian VH (2000) Heterogeneous reaction of NO_2 on hexane soot: A Knudsen cell and FT-IR study. J Phys Chem A 104:11926-11933

Albrecht BA (1989) Aerosols, cloud microphysics, and fractional cloudiness. Science 245:1227-1230

Alcala-Jornod C, van den Bergh H, Rossi MJ (2000) Reactivity of NO_2 and H_2O on soot generated in the laboratory: A diffusion tube study at ambient temperature. Phys Chem Chem Phys 2:5584-5593

Ammann M, Kalberer M, Jost DT, Tobler L, Rossler E, Piguet D, Gaggeler HW, Baltensperger U (1998) Heterogeneous production of nitrous acid on soot in polluted air masses. Nature 395:157-160

Ammann M, Madronich S, Kalberer M, Baltensperger U, Hauglustaine D, Brocheton F (1999) On the NO_2 plus soot reaction in the atmosphere. J Geophys Res 104:1729-1736

Anderson JG (1995) Polar processes in ozone depletion. *In* Progress and Problems in Atmospheric Chemistry. Barker JR (ed) p 744-770. Singapore: World Scientific

Andreae MO, Crutzen PJ (1997) Atmospheric aerosols: Biogeochemical sources and role in atmospheric chemistry. Science 276:1052-1058

Arts JHE, Spoor SM, Muijser H (2000) Short-term inhalation exposure of healthy and compromised rats and mice to fine and ultrafine carbon particles. Inhal Toxicol 12 (Suppl 1):261-266

Ausloos P, Rebbert RE, Glasgow L (1977) Photo-decomposition of chloromethanes adsorbed on silica surfaces. J Res Nat Bur Stand 82:1-8

Bagley ST, Baumgard KJ, Gratz LG, Johnson JH, Leddy DG (1996) Characterization of fuel and aftertreatment device effects on diesel emissions. Research Report 76. Cambridge, Massachusetts: Health Effects Institute (HEI)

Ball SM, Hanson DR, Eisele FL, McMurry PH (1999) Laboratory studies of particle nucleation: Initial results for H_2SO_4, H_2O, and NH_3 vapors. J Geophys Res 104:23709-23718

Barnett TP, Hasselmann K, Chelliah M, Delworth T, Hegerl G, Jones P, Rasmusson E, Roeckner E, Ropelewski C, Santer B, Tett S (1999) Detection and attribution of recent climate change: A status report. Bull Am Meterol Soc 80:2631-2659

Barraclough PB, Hall PB (1974) Adsorption of water-vapor by lithium-fluoride, sodium-fluoride, and sodium-chloride. Surf Sci 46:393

Barthelmie RJ, Pryor SC (1999) A model mechanism to describe oxidation of monoterpenes leading to secondary organic aerosol: 1. Alpha-pinene and beta-pinene. J Geophys Res 104:23657-23669

Becker EJ, O'Dowd CD, Hoell C, Aalto P, Mäkelä JM, Kulmala M (1999) Organic contribution to sub-micron aerosol evolution over a boreal forest: A case study. Phys Chem Chem Phys 1:5511-5516

Behra P, Sigg L (1990) Evidence for redox cycling of iron in atmospheric water droplets. Nature 344: 419-421

Benzoni L, Garbassi F (1984) Reactivity of fluorochloromethanes with desert sands. Ber Bunsen Phys Chem 88:379-382

Berg OH, Swietlicki E, Krejci R (1998) Hygroscopic growth of aerosol particles in the marine boundary layer over the Pacific and Southern Oceans during the First Aerosol Characterization Experiment (ACE 1). J Geophys Res 103:16535-16545

Boer GJ, Flato G, Ramsden D (2000a) A transient climate change simulation with greenhouse gas and aerosol forcing: Projected climate to the twenty-first century. Clim Dynam 16:427-450

Boer GJ, Flato G, Reader MC, Ramsden D (2000b) A transient climate change simulation with greenhouse gas and aerosol forcing: Experimental design and comparison with the instrumental record for the twentieth century. Clim Dynam 16:405-425

Borensen C, Kirchner U, Scheer V, Vogt R, Zellner R (2000) Mechanism and kinetics of the reactions of NO_2 or HNO_3 with alumina as a mineral dust model compound. J Phys Chem A 104:5036-5045

Borys RD, Lowenthal DH, Mitchell DL (2000) The relationships among cloud microphysics, chemistry, and precipitation rate in cold mountain clouds. Atmos Environ 34:2593-2602

Bowles RK, McGraw R, Schaaf P, Senger B, Voegel JC, Reiss H. (2000) A molecular based derivation of the nucleation theorem. J Chem Phys 113:4524-4532

Boyd PW, Watson AJ, Law CS, Abraham ER, Trull T, Murdoch R, Bakker DCE, Bowie AR, Buesseler KO, Change H, Charette M, Croot P, Downing K, Frew R, Gall M, Hadfield M, Hall J, Harvey M, Jameson G, LaRoche J, Liddicoat M, Ling R, Maldonado MT, McKay RM, Nodder S, Pickmere S, Pridmore R, Rintoul S, Safi K, Sutton P, Strzepek R, Tanneberger K, Turner S, Waite A, Zeldis J (2000) A mesoscale phytoplankton bloom in the polar Southern Ocean stimulated by iron fertilization. Nature 407:695-702

Brock CA, Schröder F, Kärcher B, Petzold A, Busen R, Fiebig M (2000) Ultrafine particle size distributions measured in aircraft exhaust plumes. J Geophys Res 105:26555-26567

Brunekreef B (2000) SESSION 2: What properties of particulate matter are responsible for health effects? Inhal Toxicol 12 (Suppl 1):15-18

Brus LE (1983) A simple model for the ionization potential, electron affinity, and aqueous redox potentials of small semiconductor crystallites. J Chem Phys 79:5566

Burtscher H, Kunzel S, Huglin C (1998) Characterization of particles in combustion engine exhaust. J Aerosol Sci 29:389-396

Buseck PR, Pósfai M (1999) Airborne minerals and related aerosol particles: Effects on climate and the environment. Proc Nat Acad Sci USA 96:3372-3379

Buseck PR, Jacob DJ, Pósfai M, Li J, Anderson JR (2000) Minerals in the air: An environmental perspective. Int Geol Rev 42:577-593

Carson PG, Johnston MV, Wexler AS (1997) Laser desorption/ionization of ultrafine aerosol particles. Rapid Commun Mass Spectrom 11:993-996

Cass GR, Hughes LA, Bhave P, Kleeman MJ, Allen JO, Salmon LG (2000) The chemical composition of atmospheric ultrafine particles. Phil Trans Roy Soc Lond A 358:2581-2592

Chameides WL, Stelson AW (1992) Aqueous-phase chemical processes in deliquescent sea-salt aerosols—A mechanism that couples the atmospheric cycles of S and sea salt. J Geophys Res 97:20565-20580

Chameides WL, Lindsay RW, Richardson J, Kiang CS (1988) The role of biogenic hydrocarbons in urban photochemical smog: Atlanta as a case study. Science 241:1473-1475

Charlesworth DH, Marshall WR (1960) Evaporation from drops containing dissolved solids. Am Inst Chem Engin J 6:9-23

Charlson RJ, Heintzenberg J (eds) (1994) Aerosol Forcing of Climate. New York: Wiley

Charlson RJ, Schwartz SE, Hales JM, Cess RD, Coakley JA, Hansen JE, Hofmann DJ (1992) Climate forcing by anthropogenic aerosols. Science 255:423-430

Chen DR, Pui DYH (1997) Numerical modeling of the performance of differential mobility analyzers for nanometer aerosol measurements. J Aerosol Sci 28:985-1004

Chiapello I, Prospero JM, Herman JR, Hsu NC (1999) Detection of mineral dust over the north Atlantic ocean and Africa with the Nimbus 7 TOMS. J Geophys Res 104:9277-9291

Choi W, Leu MT (1998) Nitric acid uptake and decomposition on black carbon (soot) surfaces: Its implications for the upper troposphere and lower stratosphere. J Phys Chem A 102:7618-7630

Clague ADH, Donnet J, Wang TK, Peng JCM (1999) A comparison of diesel engine soot with carbon black. Carbon 37:1553-1565

Claquin T, Schulz M, Balkanski YJ (1999) Modeling the mineralogy of atmospheric dust sources. J Geophys Res 104:22243-22256

Clarke AD, Davis D, Kapustin VN, Eisele F, Chen G, Paluch I, Lenschow D, Bandy AR, Thornton D, Moore K, Mauldin L, Tanner D, Litchy M, Carroll MA, Collins J, Albercook G (1998) Particle nucleation in the tropical boundary layer and its coupling to marine sulfur sources. Science 282:89-92

Clarke AD, Kapustin VN, Eisele FL, Weber RJ, McMurry PH (1999) Particle production near marine clouds: Sulfuric acid and predictions from classical binary nucleation. Geophys Res Lett 26:2425-2428

Clegg SL, Brimblecombe P, Wexler AS (1998) Thermodynamic model of the system H^+-NH_4^+-Na^+-SO_4^{2-}-NO_3^--Cl^--H_2O at 298.15 K. J Phys Chem. A 102:2155-2171

Clement CF, Pirjola L, dal Maso M, Mäkelä JM, Kulmala M (2001) Analysis of particle formation bursts observed in Finland. J Aerosol Sci 32:217-236

Coffman DJ, Hegg DA (1995) A preliminary study of the effect of ammonia on particle nucleation in the marine boundary layer. J Geophys Res 100:7147-7160

Collings N, Graskow BR (2000) Particles from internal combustion engines—What we need to know. Phil Trans Roy Soc Lond A 358:2611-2622

Covert DS, Kapustin VN, Quinn PK, Bates TS (1992) New particle formation in the marine boundary-layer. J Geophys Res 97:20581-20589

Covert DS, Wiedensohler A, Aalto P, Heintzenberg J, McMurry PH, Leck C (1996) Aerosol number size distributions from 3 to 500-nm diameter in the Arctic marine boundary layer during summer and autumn. Tellus B-Chem Phys Meteorol 48:197-212

Craig A, McIntosh R (1952) The preparation of sodium chloride of large specific surface. Can J Chem 30:448

Crowley TJ (2000) Causes of climate change over the past 1000 years. Science 289:270-277

Cruz CN, Pandis SN (2000) Deliquescence and hygroscopic growth of mixed inorganic-organic atmospheric aerosol. Environ Sci Technol 34:4313-4319

Cziczo DJ, Nowak JB, Hu JH, Abbatt JPD (1997) Infrared spectroscopy of model tropospheric aerosols as a function of relative humidity: Observation of deliquescence and crystallization. J Geophys Res 102:18843-18850

Cziczo DJ, Thomson DS, Murphy DM (2001) Ablation, flux, and atmospheric implications of meteors inferred from stratospheric aerosol. Science 291:1772-1775

Dachs J, Eisenreich SJ (2000) Adsorption onto aerosol soot carbon dominates gas-particle partitioning of polycyclic aromatic hydrocarbons. Environ Sci Technol 34:3690-3697

Dalleska NF, Colussi AJ, Hyldahl AM, Hoffmann MR (2000) Rates and mechanism of carbonyl sulfide oxidation by peroxides in concentrated sulfuric acid. J Phys Chem A 104:10794-10796

D'Almeida GA, Schütz L (1983) Number, mass, and volume distributions of mineral aerosol and soils of the Sahara. J Clim Appl Meteorol 22:233-243

De Haan DO, Brauers T, Oum K, Stutz J, Nordmeyer T, Finlayson-Pitts BJ (1999) Heterogeneous chemistry in the troposphere: Experimental approaches and applications to the chemistry of sea salt particles. Int'l Rev Phys Chem 18:343-385

de Reus M, Ström J, Kulmala M, Pirjola L, Lelieveld J, Schiller C, Zoger M (1998) Airborne aerosol measurements in the tropopause region and the dependence of new particle formation on preexisting particle number concentration. J Geophys Res 103:31255-31263

de Reus M, Dentener F, Thomas A, Borrmann S, Ström J, Lelieveld J (2000a) Airborne observations of dust aerosol over the North Atlantic ocean during ACE 2: Indications for heterogenous ozone destruction. J Geophys Res 105:15263-15275

de Reus M, Ström J, Curtius J, Pirjola L, Vignati E, Arnold F, Hansson HC, Kulmala M, Lelieveld J, Raes F (2000b) Aerosol production and growth in the upper free troposphere. J Geophys Res 105: 24751-24762

Dentener FJ, Carmichael GR, Zhang Y, Lelieveld J, Crutzen PJ (1996) Role of mineral aerosol as a reactive surface in the global atmosphere. J Geophys Res 101:22869-22889

Desboeufs KV, Losno R, Vimeux F, Cholbi S (1999) The pH-dependent dissolution of wind-transported Saharan dust. J Geophys Res 104:21287-21299

Disselkamp RS, Carpenter MA, Cowin JP (2000a) A chamber investigation of nitric acid-soot aerosol chemistry at 298 K. J Atmos Chem 37:113-123

Disselkamp RS, Carpenter MA, Cowin JP, Berkowitz CM, Chapman EG, Zaveri RA, Laulainen NS (2000b) Ozone loss in soot aerosols. J Geophys Res 105:9767-9771

Dixon JB, Weed SB (eds) (1989) Minerals in Soil Environments. Madison, Wisconsin: Soil Science Society of America

Dockery DW, Pope CA, Xu XP, Spengler JD, Ware JH, Fay ME, Ferris BG, Speizer FE (1993) An association between air pollution and mortality in 6 United States cities. N Engl J Med 329:1753-1759

Donaldson K, Li XY, MacNee W (1998) Ultrafine (nanometre) particle mediated lung injury. J Aerosol Sci 29:553-560

Donaldson K, Stone V, Gilmour PS, Brown DM, MacNee W (2000) Ultrafine particles: mechanisms of lung injury. Phil Trans Roy Soc Lond A 358:2741-2748

Donaldson K, Stone V, Clouter A, Renwick L, MacNee W (2001) Ultrafine particles. Occup Environ Med 58:211-216

Doremus RH (1985) Rates of Phase Transformations. New York: Academic Press

Dreher KL, Jaskot RH, Lehmann JR, Richards JH, McGee JK, Ghio AJ, Costa DL (1997) Soluble transition metals mediate residual oil fly ash induced acute lung injury. J Toxicol Environ Health 50:285-305

Duce RA (1969) On the source of gaseous chlorine in marine atmosphere. J Geophys Res 74:4597

Duce RA, Unni CK, Ray BJ, Prospero JM, Merrill JT (1980) Long-range atmospheric transport of soil dust from Asia to the tropical north Pacific: Temporal variability. Science 209:1522-1524

Duncan JL, Schindler LR, Roberts JT (1998) A new sulfate-mediated reaction: Conversion of acetone to trimethylbenzene in the presence of liquid sulfuric acid. Geophys Res Lett 25:631-634

Duncan JL, Schindler LR, Roberts JT (1999) Chemistry at and near the surface of liquid sulfuric acid: A kinetic, thermodynamic, and mechanistic analysis of heterogeneous reactions of acetone. J Phys Chem B 103:7247-7259

Eisele FL, Hanson DR (2000) First measurement of prenucleation molecular clusters. J Phys Chem A 104:830-836

Elder ACP, Gelein R, Finkelstein JN, Cox C, Oberdörster G (2000) Pulmonary inflammatory response to inhaled ultrafine particles is modified by age, ozone exposure, and bacterial toxin. Inhal Toxicol 12 (Suppl 1):227-246

Eldering A, Cass GR, Moon KC (1994) An air monitoring network using continuous particle size distribution monitors–Connecting pollutant properties to visibility via Mie scattering calculations. Atmos Environ 28:2733-2749

Ellison GB, Tuck AF, Vaida V (1999) Atmospheric processing of organic aerosols. J Geophys Res 104:11633-11641

Fahey DW, Gao RS, Carslaw KS, Kettleborough J, Popp PJ, Northway MJ, Holecek JC, Ciciora SC, McLaughlin RJ, Thompson TL, Winkler RH, Baumgardner DG, Gandrud B, Wennberg PO, Dhaniyala S, McKinney K, Peter T, Salawitch RJ, Bui TP, Elkins JW, Webster CR, Atlas EL, Jost H, Wilson JC, Herman RL, Kleinböhl A, von König M (2001) The detection of large HNO_3-containing particles in the winter Arctic stratosphere. Science 291:1026-1031

Fan CW, Zhang JJ (2001) Characterization of emissions from portable household combustion devices: Particle size distributions, emission rates and factors, and potential exposures. Atmos Environ 35:1281-1290

Faust BC (1994) A review of the photochemical redox reactions of iron(III) species in atmospheric, oceanic, and surface waters: Influences on geochemical cycles and oxidant formation. *In* Aquatic and Surface Photochemistry. RG Zepp, DG Crosby, GR Helz (eds) p 3-37. Boca Raton, Florida: Lewis Publishers

Fenter FF, Caloz F, Rossi MJ (1995) Experimental-evidence for the efficient dry deposition of nitric-acid on calcite. Atmos Environ 29:3365-3372

Filby WG, Mintas M, Gusten H (1981) Heterogeneous catalytic degradation of chlorofluoromethanes on zinc-oxide surfaces. Ber Bunsen Phys Chem 85:189-192

Finklea HO, 1988. Semiconductor Electrodes. New York: Elsevier

Finlayson-Pitts BJ, Hemminger JC (2000) Physical chemistry of airborne sea salt particles and their components. J Phys Chem A 104:11463-11477

Finlayson-Pitts BJ, Pitts JN (2000) Chemistry of the Upper and Lower Atmosphere: Theory, Experiments, and Applications. San Diego: Academic Press

Finlayson-Pitts BJ, Ezell MJ, Pitts JN (1989) Formation of chemically active chlorine compounds by reactions of atmospheric NaCl particles with gaseous N_2O_5 and $ClONO_2$. Nature 337:241-244

Fletcher NH (1969) Actives sites and ice crystal nucleation. J Atmos Sci 26:1266-1271

Forstner HJL, Flagan RC, Seinfeld JH (1997) Secondary organic aerosol from the photooxidation of aromatic hydrocarbons: Molecular composition. Environ Sci Technol 31:1345-1358

Foster KL, Plastridge RA, Bottenheim JW, Shepson PB, Finlayson-Pitts BJ, Spicer CW (2001) The role of Br_2 and BrCl in surface ozone destruction at polar sunrise. Science 291:471-474

Friedlander SK (2000) Smoke, Dust, and Haze: Fundamentals of Aerosol Dynamics. Topics in Chemical Engineering. New York: Oxford University Press

Gao RS, Kärcher B, Keim ER, Fahey DW (1998) Constraining the heterogeneous loss of O_3 on soot particles with observations in jet engine exhaust plumes. Geophys Res Lett 25:3323-3326

Ge Z, Wexler AS, Johnston MV (1996) Multicomponent aerosol crystallization. J Coll Interface Sci 183:68-77

Ge ZZ, Wexler AS, Johnston MV (1998) Laser desorption/ionization of single ultrafine multicomponent aerosols. Environ Sci Technol 32:3218-3223

Gerecke A, Thielmann A, Gutzwiller L, Rossi MJ (1998) The chemical kinetics of HONO formation resulting from heterogeneous interaction of NO_2 with flame soot. Geophys Res Lett 25:2453-2456

Ghio AJ, Stonehuerner J, Pritchard RJ, Piantadosi CA, Quigley DR, Dreher KL, Costa DL (1996) Humic-like substances in air pollution particulates correlate with concentrations of transition metals and oxidant generation. Inhal Toxicol 8:479-494

Gill PS, Graedel TE, Weschler CJ (1983) Organic films on atmospheric aerosol particles, fog droplets, cloud droplets, raindrops, and snowflakes. Rev Geophys Space Phys 21:903-920

Gong SL, Barrie LA, Blanchet JP (1997) Modeling sea-salt aerosols in the atmosphere. 1. Model development. J Geophys Res 102:3805-3818

Goodman AL, Underwood GM, Grassian VH (2000) A laboratory study of the heterogeneous reaction of nitric acid on calcium carbonate particles. J Geophys Res 105:29053-29064

Gorbunov BZ, Kakutkina NA (1982) Ice crystal formation on aerosol particles with a non-uniform surface. J Aerosol Sci 13:21-28

Graedel TE, Hawkins DT, Claxton LD (1986) Atmospheric Chemical Compounds: Sources, Occurrence, and Bioassay. Orlando, Florida: Academic Press

Griffin RJ, Cocker DR, Seinfeld JH, Dabdub D (1999) Estimate of global atmospheric organic aerosol from oxidation of biogenic hydrocarbons. Geophys Res Lett 26:2721-2724

Hameri K, Vakeva M, Hansson HC, Laaksonen A (2000) Hygroscopic growth of ultrafine ammonium sulphate aerosol measured using an ultrafine tandem differential mobility analyzer. J Geophys Res 105:22231-22242

Han J, Martin ST (1999) Heterogeneous nucleation of the efflorescence of $(NH_4)_2SO_4$ particles internally mixed with Al_2O_3, TiO_2, and ZrO_2. J Geophys Res 104:3543-3553

Han JH, Hung HM, Martin ST (2001) The size effect of hematite and corundum inclusions on the efflorescence relative humidities of aqueous ammonium nitrate particles. J Geophys Res (submitted)
Hanisch F, Crowley JN (2001) Heterogeneous reactivity of gaseous nitric acid on Al_2O_3, $CaCO_3$, and atmospheric dust samples: A Knudsen cell study. J Phys Chem A 105:3096-3106
Harrison RM, Shi JP, Xi SH, Khan A, Mark D, Kinnersley R, Yin JX (2000) Measurement of number, mass and size distribution of particles in the atmosphere. Phil Trans Roy Soc Lond A 358:2567-2579
Harvey LDD (2000) Constraining the aerosol radiative forcing and climate sensitivity. Clim Change 44:413-418
Hauser R, Godleski JJ, Hatch V, Christiani DC (2001) Ultrafine particles in human lung macrophages. Arch Environ Health 56:150-156
Hemminger JC (1999) Heterogeneous chemistry in the troposphere: A modern surface chemistry approach to the study of fundamental processes. Int'l Rev Phys Chem 18:387-417
Herman JR, Bhartia PK, Torres O, Hsu C, Seftor C, Celarier E (1997) Global distribution of uv-absorbing aerosols from Nimbus 7/TOMS data. J Geophys Res 102:16911-16922
Hoffmann MR, Martin ST, Choi W, Bahnemann DW (1995) Environmental applications of semiconductor photocatalysis. Chem Rev 95:69-96
Holland HD (1978) The Chemistry of Atmospheres and Oceans. New York: Wiley
Huffman GP, Huggins FE, Shah N, Huggins R, Linak WP, Miller CA, Pugmire RJ, Meuzelaar HLC, Seehra MS, Manivannan A (2000) Characterization of fine particulate matter produced by combustion of residual fuel oil. J Air Waste Manage Assoc 50:1106-1114
Hughes LS, Cass GR, Gone J, Ames M, Olmez I (1998) Physical and chemical characterization of atmospheric ultrafine particles in the Los Angeles area. Environ Sci Technol V32:1153-1161
Husar RB, Prospero JM, Stowe LL (1997) Characterization of tropospheric aerosols over the oceans with the NOAA advanced very high resolution radiometer optical thickness operational product. J Geophys Res 102:16889-16909
IPCC (Intergovernmental Panel on Climate Change) (2001) Climate Change 2001: The Scientific Basis. Houghton JT, Ding Y, Griggs DJ, Noguer M, van der Linden PJ, Xiaosu D (eds) Cambridge: Cambridge University Press
Jacobson MZ (2001) Strong radiative heating due to the mixing state of black carbon in atmospheric aerosols. Nature 409:695-697
Jaecker-Voirol A, Mirabel P (1988) Nucleation rate in a binary mixture of sulfuric-acid and water- vapor. J Phys Chem 92:3518-3521
Jaecker-Voirol A, Mirabel P, Reiss H (1987) Hydrates in supersaturated binary sulfuric acid-water vapor—A re-examination. J Chem Phys 87:4849-4852
Jaques PA, Kim CS (2000) Measurement of total lung deposition of inhaled ultrafine particles in healthy men and women. Inhal Toxicol 12 (Suppl 1):715-731
Jefferson DA (2000) The surface activity of ultrafine particles. Phil Trans Roy Soc Lond A 358:2683-2692
José-Yacamán M (1998) The role of nanosized particles. A frontier in modern materials science, from nanoelectronics to environmental problems. Metall Mater Trans A 29:713-725
Kalberer M, Ammann M, Arens F, Gaggeler HW, Baltensperger U (1999) Heterogeneous formation of nitrous acid (HONO) on soot aerosol particles. J Geophys Res 104:13825-13832
Kamm S, Mohler O, Naumann KH, Saathoff H, Schurath U (1999) The heterogeneous reaction of ozone with soot aerosol. Atmos Environ 33:4651-4661
Kane DB, Johnston MV (2000) Size and composition biases on the detection of individual ultrafine particles by aerosol mass spectrometry. Environ Sci Technol 34:4887-4893
Kärcher B, Turco RP, Yu F, Danilin MY, Weisenstein DK, Miake-Lye RC, Busen R (2000) A unified model for ultrafine aircraft particle emissions. J Geophys Res 105:29379-29386
Kashchiev D (1982) On the relation between nucleation work, nucleus size, and nucleation rate. J Chem Phys 76:5098-5102
Kavouras IG, Mihalopoulos N, Stephanou EG (1999) Secondary organic aerosol formation vs primary organic aerosol emission: *In situ* evidence for the chemical coupling between monoterpene acidic photooxidation products and new particle formation over forests. Environ Sci Technol 33:1028-1037
Keene WC, Sander R, Pszenny AAP, Vogt R, Crutzen PJ, Galloway JN (1998) Aerosol pH in the marine boundary layer: A review and model evaluation. J Aerosol Sci 29:339-356
Kennedy IM (1997) Models of soot formation and oxidation. Prog Energ Combust Sci 23:95-132
Kerminen VM (1999) Roles of SO_2 and secondary organics in the growth of nanometer particles in the lower atmosphere. J Aerosol Sci 30:1069-1078
Kerminen VM, Wexler AS, Potukuchi S (1997) Growth of freshly nucleated particles in the troposphere: Roles of NH_3, H_2SO_4, HNO_3, and HCl. J Geophys Res 102:3715-3724
Kerminen VM, Virkkula A, Hillamo R, Wexler AS, Kulmala M (2000) Secondary organics and atmospheric cloud condensation nuclei production. J Geophys Res 105:9255-9264

Keywood MD, Ayers GP, Gras JL, Gillett RW, Cohen DD (1999) Relationships between size-segregated mass concentration data and ultrafine particle number concentrations in urban areas. Atmos Environ 33:2907-2913

Kiehl JT, Schneider TL, Rasch PJ, Barth MC, Wong J (2000) Radiative forcing due to sulfate aerosols from simulations with the National Center for Atmospheric Research Community Climate Model, Version 3. J Geophys Res 105:1441-1457

Kim TO, Ishida T, Adachi M, Okuyama K, Seinfeld JH (1998) Nanometer-sized particle formation from $NH_3/SO_2/H_2O$/air mixtures by ionizing irradiation. Aerosol Sci Tech 29:111-125

Kirchner U, Scheer V, Vogt R (2000) FTIR spectroscopic investigation of the mechanism and kinetics of the heterogeneous reactions of NO_2 and HNO_3 with soot. J Phys Chem A 104:8908-8915

Kittelson DB (1998) Engines and nanoparticles: A review. J Aerosol Sci 29:575-588

Kleeman MJ, Schauer JJ, Cass GR (1999) Size and composition distribution of fine particulate matter emitted from wood burning, meat charbroiling, and cigarettes. Environ Sci Technol 33:3516-3523

Kleeman MJ, Schauer JJ, Cass GR (2000) Size and composition distribution of fine particulate matter emitted from motor vehicles. Environ Sci Technol 34:1132-1142

Kolb CE, Worsnop DR, Zahniser MS, Davidovits P, Keyser LF, Leu MT, Molina MR, Hanson DR, Ravishankara AR (1995) Laboratory studies of atmospheric heterogeneous chemistry. *In* Progress and Problems in Atmospheric Chemistry. Barker JR (ed) p 771-875. Singapore: World Scientific

Koper O, Klabunde KJ (1997) Destructive adsorption of chlorinated hydrocarbons on ultrafine (nanoscale) particles of calcium oxide.3. Chloroform, trichloroethene, and tetrachloroethene. Chem Mater 9: 2481-2485

Koper O, Li YX, Klabunde KJ (1993) Destructive adsorption of chlorinated hydrocarbons on ultrafine (nanoscale) particles of calcium oxide. Chem Mater 5:500-505

Koper O, Lagadic I, Klabunde KJ (1997) Destructive adsorption of chlorinated hydrocarbons on ultrafine (nanoscale) particles of calcium oxide. 2. Chem Mater 9:838-848

Korhonen P, Kulmala M, Laaksonen A, Viisanen Y, McGraw R, Seinfeld JH (1999) Ternary nucleation of H_2SO_4, NH_3, and H_2O in the atmosphere. J Geophys Res 104:26349-26353

Kotzick R, Panne U, Niessner R (1997) Changes in condensation properties of ultrafine carbon particles subjected to oxidation by ozone. J Aerosol Sci 28:725-735

Krä mer L, Poschl U, Niessner R (2000) Microstructural rearrangement of sodium chloride condensation aerosol particles on interaction with water vapor. J Aerosol Sci 31:673-685

Kreidenweis SM, Tyndall GS, Barth MC, Dentener F, Lelieveld J, Mozurkewich M (1999) Aerosols and clouds. *In* Atmospheric Chemistry and Global Change. GP Brasseur, JJ Orlando, GS Tyndall (eds) p 117-155. New York: Oxford University Press

Kulmala M (1993) Condensational growth and evaporation in the transition regime: An analytical expression. Aerosol Sci Tech 19:381-388

Kulmala M, Vesala T, Wagner PE (1993) An analytical expression for the rate of binary condensational particle growth. Proc R Soc London A 441:589-605

Kulmala M, Kerminen VM, Laaksonen A (1995) Simulations on the effect of sulphuric acid formation on atmospheric aerosol concentrations. Atmos Environ 29:377-382

Kulmala M, Laaksonen A, Pirjola L (1998a) Parameterizations for sulfuric acid/water nucleation rates. J Geophys Res 103:8301-8307

Kulmala M, Toivonen A, Mä kelä JM, Laaksonen A (1998b) Analysis of the growth of nucleation mode particles observed in boreal forest. Tellus B 50:449-462

Kulmala M, Pirjola U, Mä kelä JM (2000) Stable sulphate clusters as a source of new atmospheric particles. Nature 404:66-69

Kusaka I, Wang ZG, Seinfeld JH (1998a) Direct evaluation of the equilibrium distribution of physical clusters by a grand canonical Monte Carlo simulation. J Chem Phys 108:3416-3423

Kusaka I, Wang ZG, Seinfeld JH (1998b) Binary nucleation of sulfuric acid-water: Monte Carlo simulation. J Chem Phys 108:6829-6848

Kusaka I, Oxtoby DW, Wang ZG (1999) On the direct evaluation of the equilibrium distribution of clusters by simulation. J Chem Phys 111:9958-9964

Laaksonen A, Talanquer V, Oxtoby DW (1995) Nucleation: Measurements, theory, and atmospheric applications. Ann Rev Phys Chem 46:489-524

Lasaga AC (1998) Kinetic Theory in the Earth Sciences. Princeton University Press, Princeton

Leinen M, Prospero JM, Arnold E, Blank M (1994) Mineralogy of aeolian dust reaching the North Pacific Ocean. 1. Sampling and analysis. J Geophys Res 99:21017-21023

Leong KH (1981) Morphology of aerosol-particles generated from the evaporation of solution drops. J Aerosol Sci 12:417-435

Li YX, Li H, Klabunde KJ (1994) Destructive adsorption of chlorinated benzenes on ultrafine (nanoscale) particles of magnesium oxide and calcium oxide. Environ Sci Technol 28:1248-1253

Li P, Perreau KA, Covington E, Song CH, Carmichael GR, Grassian VH, (2001) Heterogeneous reactions of volatile organic compounds on oxide particles of the most abundant crustal elements: Surface reactions of acetaldehyde, acetone, and propionaldehyde on SiO_2, Al_2O_3, Fe_2O_3, TiO_2, and CaO. J Geophys Res 106:5517-5529

Liler M (1971) Reaction Mechanisms in Sulphuric Acid and Other Strong Acid Solutions. London - New York: Academic Press

Linak WP, Miller CA (2000) Comparison of particle size distributions and elemental partitioning from the combustion of pulverized coal and residual fuel oil. J Air Waste Manage Assoc 50:1532-1544

Litter MI, Villegas M, Blesa MA (1994) Photodissolution of iron-oxides in malonic-acid. Can J Chem 72:2037-2043

Lohmann U, Feichter J (2001) Can the direct and semi-direct aerosol effect compete with the indirect effect on a global scale? Geophys Res Lett 28:159-161

Longfellow CA, Ravishankara AR, Hanson DR (1999) Reactive uptake on hydrocarbon soot: Focus on NO_2. J Geophys Res 104:13833-13840

Longfellow CA, Ravishankara AR, Hanson DR (2000) Reactive and nonreactive uptake on hydrocarbon soot: HNO_3, O_3, and N_2O_5. J Geophys Res 105:24345-24350

Loomis D (2000) Sizing up air pollution research. Epidemiology 11:2-4

MacTaylor RS, Castleman AW (2000) Cluster ion reactions: Insights into processes of atmospheric significance. J Atmos Chem 36:23-63

Mä kelä JM, Aalto P, Jokinen V, Pohja T, Nissinen A, Palmroth S, Markkanen T, Seitsonen K, Lihavainen H, Kulmala M (1997) Observations of ultrafine aerosol particle formation and growth in boreal forest. Geophys Res Lett 24:1219-1222

Marion GM, Farren RE (1999) Mineral solubilities in the Na-K-Mg-Ca-Cl-SO_4^{2-}-H_2O: A re-evaluation of the sulfate chemistry in the Spencer-Moller-Weare model. Geochim Cosmochim Acta 63:1305-1318

Marti JJ, Jefferson A, Cai XP, Richert C, McMurry PH, Eisele F (1997a) H_2SO_4 vapor pressure of sulfuric acid and ammonium sulfate solutions. J Geophys Res 102:3725-3735

Marti JJ, Weber RJ, McMurry PH, Eisele F, Tanner D, Jefferson A (1997b) New particle formation at a remote continental site: Assessing the contributions of SO_2 and organic precursors. J Geophys Res 102:6331-6339

Martin JH, Gordon RM (1988) Northeast Pacific iron distributions in relation to phytoplankton productivity. Deep-Sea Res 35:177-196

Martin ST (2000) Phase transitions of aqueous atmospheric particles. Chem Rev 100:3403-3453

Martin ST, Han JH, Hung HM (2001) The size effect of hematite and alumina inclusions on the efflorescence relative humidities of aqueous ammonium sulfate particles. Geophys Res Lett 28: 2601-2604

Mathai CV (1990) Visibility and fine particles. 4. A summary of the A&WMA EPA International Specialty Conference. J Air Waste Manage Assoc 40:1486-1494

Matteson MJ, Preiming O, Fox JF (1972) Density distribution of sodium-chloride aerosols formed by condensation. Nature-Phys Sci 238:61

Mattila T, Kulmala M, Vesala T (1997) On the condensational growth of a multicomponent droplet. J Aerosol Sci 28:553-564

McCaffrey MA, Lazar B, Holland HD (1987) The evaporation path of seawater and the coprecipitation of Br^- and K^+ with halite. J Sed Petrology 57:928-937

McInnes LM, Covert DS, Quinn PK, Germani MS (1994) Measurements of chloride depletion and sulfur enrichment in individual sea-salt particles collected from the remote marine boundary-layer. J Geophys Res 99:8257-8268

McMurry PH, Woo KS, Weber R, Chen DR, Pui DYH (2000) Size distributions of 3-10 nm atmospheric particles: Implications for nucleation mechanisms. Philos Trans Roy Soc Lond A 358:2625-2642

Merrill J, Arnold E, Leinen M, Weaver C (1994) Mineralogy of aeolian dust reaching the north pacific-ocean. 2. Relationship of mineral assemblages to atmospheric transport patterns. J Geophys Res 99:21025-21032

Miller RL, Tegen I (1998) Climate response to soil dust aerosols. J Climate 11:3247-3267

Mirabel P, Ponche JL (1991) Studies of gas-phase clustering of water on sulfuric-acid molecules. Chem Phys Lett 183:21-24

Mirabel P, Reiss H, Bowles RK (2000) A theory for the deliquescence of small particles. J Chem Phys 113:8200-8205

Mozurkewich M (1995) Mechanisms for the release of halogens from sea-salt particles by free radical reactions. J Geophys Res 100:14199-14207

Noble CA, Prather KA (1996) Real-time measurement of correlated size and composition profiles of individual atmospheric aerosol particles. Environ Sci Technol 30:2667-2680

Noble CA, Prather KA (2000) Real-time single particle mass spectrometry: A historical review of a quarter century of the chemical analysis of aerosols. Mass Spectrom Rev 19:248-274

Nolte CG, Schauer JJ, Cass GR, Simoneit BRT (2001) Highly polar organic compounds present in wood smoke and in the ambient atmosphere. Environ Sci Technol 35:1912-1919

Oberdörster G (2001) Pulmonary effects of inhaled ultrafine particles. Int Arch Occup Envir Health 74:1-8

O'Dowd C, McFiggans G, Creasey DJ, Pirjola L, Hoell C, Smith MH, Allan BJ, Plane JMC, Heard DE, Lee JD, Pilling MJ, Kulmala M (1999) On the photochemical production of new particles in the coastal boundary layer. Geophys Res Lett 26:1707-1710

Odum JR, Jungkamp TPW, Griffin RJ, Forstner HJL, Flagan RC, Seinfeld JH (1997) Aromatics, reformulated gasoline, and atmospheric organic aerosol formation. Environ Sci Technol 31:1890-1897

Oxtoby DW (1992) Homogeneous nucleation: Theory and experiment. J Phys: Condens Matter 4: 7627-7650

Oxtoby DW, Kashchiev D (1994) A general relation between the nucleation work and the size of the nucleus in multicomponent nucleation. J Chem Phys 100:7665-7671

Park PW, Ledford JS (1997) Characterization and CH_4 oxidation activity of Cr/Al_2O_3 catalysts. Langmuir 13:2726-2730

Park PW, Ledford JS (1998) Characterization and CO oxidation activity of $Cu/Cr/Al_2O_3$ catalysts. Indust Engin Chem Res 37:887-893

Pehkonen SO, Siefert R, Erel Y, Webb S, Hoffmann MR (1993) Photoreduction of iron oxyhydroxides in the presence of important atmospheric organic compounds. Environ Sci Technol 27:2056-2062

Pehkonen SO, Siefert RL, Hoffmann MR (1995) Photoreduction of iron oxyhydroxides and the photooxidation of halogenated acetic-acids. Environ Sci Technol 29:1215-1222

Pekkanen J, Timonen KL, Ruuskanen J, Reponen A, Mirme A (1997) Effects of ultrafine and fine particles in urban air on peak expiratory flow among children with asthmatic symptoms. Environ Res 74:24-33

Penner JE, Chuang CC, Grant K (1998) Climate forcing by carbonaceous and sulfate aerosols. Clim Dynam 14:839-851

Perkas N, Koltypin Y, Palchik O, Gedanken A, Chandrasekaran S (2001) Oxidation of cyclohexane with nanostructured amorphous catalysts under mild conditions. Appl Catal A 209:125-130

Peter T (1997) Microphysics and heterogeneous chemistry of polar stratospheric clouds. Ann Rev Phys Chem 48:785-822

Peter T (1999) Physico-chemistry of polar stratospheric clouds. *In* Ice Physics and the Natural Environment. Wettlaufer JS (ed) p 143-167. Berlin: Springer-Verlag

Peters SJ, Ewing GE (1997a) Thin film water on NaCl(100) under ambient conditions: An infrared study. Langmuir 13:6345-6348

Peters SJ, Ewing GE (1997b) Water on salt: An infrared study of adsorbed H_2O on NaCl(100) under ambient conditions. J Phys Chem B 101:10880-10886

Peters A, Wichmann HE, Tuch T, Heinrich J, Heyder J (1997) Respiratory effects are associated with the number of ultrafine particles. Am J Respir Crit Care Med 155:1376-1383

Phares DJ, Rhoades KP, Wexler AS (2001a) Performance of a single-ultrafine-particle mass spectrometer. Aerosol Sci Tech (accepted)

Phares DJ, Rhoades KP, Johnston MV, Wexler AS (2001b) Size-resolved ultrafine particle composition analysis. Part 2: Houston. J Geophys Res (submitted)

Pilinis C (1989) Numerical simulation of visibility degradation due to particulate matter: Model development and evaluation. J Geophys Res 94:9937-9946

Pirjola L, Kulmala M (1998) Modelling the formation of H_2SO_4-H_2O particles in rural, urban and marine conditions. Atmos Res 46:321-347

Pirjola L, Laaksonen A, Aalto P, Kulmala M (1998) Sulfate aerosol formation in the Arctic boundary layer. J Geophys Res 103:8309-8321

Pirjola L, Kulmala M, Wilck M, Bischoff A, Stratmann F, Otto E (1999) Formation of sulphuric acid aerosols and cloud condensation nuclei: An expression for significant nucleation and model comparison. J Aerosol Sci 30:1079-1094

Pirjola L, O'Dowd CD, Brooks IM, Kulmala M (2000) Can new particle formation occur in the clean marine boundary layer? J Geophys Res 105:26531-26546

Pitchford ML, McMurry PH (1994) Relationship between measured water vapor growth and chemistry of atmospheric aerosol for Grand Canyon, Arizona, in winter 1990. Atmos Environ 28:827-839

Pope CA (2000) What do epidemiologic findings tell us about health effects of environmental aerosols? J Aerosol Med 13:335-354

Pope CA, Dockery DW, Schwartz J (1995a) Review of epidemiological evidence of health effects of particulate air pollution. Inhal Toxicol 7:1-18

Pope CA, Thun MJ, Namboodiri MM, Dockery DW, Evans JS, Speizer FE, Heath CW (1995b) Particulate air pollution as a predictor of mortality in a prospective study of US adults. Am J Respir Crit Care Med V151:669-674

Poschl U, Letzel T, Schauer C, Niessner R (2001) Interaction of ozone and water vapor with spark discharge soot aerosol particles coated with benzo[a]pyrene: O_3 and H_2O adsorption, benzo[a]pyrene degradation, and atmospheric implications. J Phys Chem A 105:4029-4041

Prospero JM (1999a) Long-range transport of mineral dust in the global atmosphere: Impact of African dust on the environment of the southeastern United States. Proc Natl Acad Sci 96:3396-3403

Prospero JM (1999b) Long-term measurements of the transport of African mineral dust to the southeastern United States: Implications for regional air quality. J Geophys Res 104:15917-15927

Pruppacher HR, Klett JD (1997) Microphysics of Clouds and Precipitation. Dordrecht: Kluwer

Pszenny AAP, Keene WC, Jacob DJ, Fan S, Maben JR, Zetwo MP, Springer-Young M, Galloway JN (1993) Evidence of inorganic chlorine gases other than hydrogen chloride in marine surface air. Geophys Res Lett 20:699-702

Pryor SC, Barthelmie RJ (2000) REVEAL II: Seasonality and spatial variability of particle and visibility conditions in the Fraser Valley. Sci Total Environ 257:95-110

Pye K (1987) Aeolian Dust and Dust Deposits. San Diego: Academic Press

Rhoades KP, Phares DJ, Wexler AS, Johnston MV (2001) Size-resolved ultrafine particle composition analysis. Part 1: Atlanta. J Geophys Res (submitted)

Richter H, Howard JB (2000) Formation of polycyclic aromatic hydrocarbons and their growth to soot: A review of chemical reaction pathways. Prog Energ Combust Sci 26:565-608

Rogge WF, Hildemann LM, Mazurek MA, Cass GR, Simonelt BRT (1991) Sources of fine organic aerosol. 1. Charbroilers and meat cooking operations. Environ Sci Technol 25:1112-1125

Rogge WF, Hildemann LM, Mazurek MA, Cass GR (1994) Sources of fine organic aerosol. 6. Cigarette smoke in the urban atmosphere. Environ Sci Technol 28:1375-1388

Rogge WF, Hildemann LM, Mazurek MA, Cass GR, Simoneit BRT (1998) Sources of fine organic aerosol. 9. Pine, oak and synthetic log combustion in residential fireplaces. Environ Sci Technol 32:13-22

Rosenfeld D (2000) Suppression of rain and snow by urban and industrial air pollution. Science 287: 1793-1796

Saathoff H, Naumann KH, Riemer N, Kamm S, Mohler O, Schurath U, Vogel H, Vogel B (2001) The loss of NO_2, HNO_3, NO_3/N_2O_5, and $HO_2/HOONO_2$ on soot aerosol: A chamber and modeling study. Geophys Res Lett 28:1957-1960

Samet JM (2000) What properties of particulate matter are responsible for health effects? Inhal Toxicol 12 (Suppl 1):19-21

Saxena P, Hildemann LM, McMurry PH, Seinfeld JH (1995) Organics alter hygroscopic behavior of atmospheric particles. J Geophys Res 100:18755-18770

Schauer JJ, Kleeman MJ, Cass GR, Simoneit BRT (1999) Measurement of emissions from air pollution sources. 2. C-1 through C-30 organic compounds from medium duty diesel trucks. Environ Sci Technol 33:1578-1587

Schauer JJ, Kleeman MJ, Cass GR, Simoneit BRT (2001) Measurement of emissions from air pollution sources. 3. C-1-C-29 organic compounds from fireplace combustion of wood. Environ Sci Technol 35:1716-1728

Schlesinger RB (2000) Properties of ambient PM responsible for human health effects: Coherence between epidemiology and toxicology. Inhal Toxicol 12 (Suppl 1):23-25

Schütz L (1989) Atmospheric mineral dust—properties and source markers. *In* Paleoclimatology and Paleometeorology: Modern and Past Patterns of Global Atmospheric Transport. Leinen M, Sarnthein M (eds) p 359-384. Dordrecht: Kluwer

Schütz L (1997) Mineral dust and source-relevant data. *In* Proceedings of the Alfred-Wegener-Conference: Sediment and Aerosol. von Hoyningen-Huene W, Tetzlaff G (eds) March 10-12, Leipzig, Germany. Cologne: Terra Nostra

Schütz L, Sebert M (1987) Mineral aerosols and source identification. J Aerosol Sci 18:1

Schwartz SE, Buseck PR (2000) Atmospheric science—Absorbing phenomen a. Science 288:989-990

Seinfeld JH, Pandis SN (1998) Atmospheric Chemistry and Physics: From Air Pollution to Climate Change. New York: Wiley

Senior CL, Helble JJ, Sarofim AF (2000) Emissions of mercury, trace elements, and fine particles from stationary combustion sources. Fuel Process Technol 65:263-288

Seto T, Nakamoto T, Okuyama K, Adachi M, Kuga Y, Takeuchi K (1997) Size distribution measurement of nanometer-sized aerosol particles using DMA under low-pressure conditions. J Aerosol Sci 28: 193-206

Shen T-L, Wooldridge PJ, Molina MJ (1995) Stratospheric pollution and ozone depletion. *In* Composition, Chemistry and Climate of the Atmosphere. HB Singh (ed) p 394-442. New York: Van Norstrand

Shi JP, Harrison RM (1999) Investigation of ultrafine particle formation during diesel exhaust dilution. Environ Sci Technol 33:3730-3736

Shi JP, Khan AA, Harrison RM (1999) Measurements of ultrafine particle concentration and size distribution in the urban atmosphere. Sci Total Environ 235:51-64

Siefert RL, Pehkonen SO, Erel Y, Hoffmann MR (1994) Iron photochemistry of aqueous suspensions of ambient aerosol with added organic-acids. Geochim Cosmochim Acta 58:3271-3279

Sievering H, Boatman J, Gorman E, Kim Y, Anderson L, Ennis G, Luria M, Pandis S (1992) Removal of sulphur from the marine boundary layer by ozone oxidation in sea-salt aerosols. Nature 360:571-573

Siffert C, Sulzberger B (1991) Light-induced dissolution of hematite in the presence of oxalate–A case-study. Langmuir 7:1627-1634

Simoneit BRT, Schauer JJ, Nolte CG, Oros DR, Elias VO, Fraser MP, Rogge WF, Cass GR (1999) Levoglucosan, a tracer for cellulose in biomass burning and atmospheric particles. Atmos Environ 33:173-182

Sloane CS, Watson J, Chow J, Pritchett L, Richards LW (1991) Size-segregated fine particle measurements by chemical species and their impact on visibility impairment in Denver. Atmos Environ A 25: 1013-1024

Smith KR, Aust AE (1997) Mobilization of iron from urban particulates leads to generation of reactive oxygen species in vitro and induction of ferritin synthesis in human lung epithelial cells. Chem Res Toxicol 10:828-834

Song CH, Carmichael GR (1999) The aging process of naturally emitted aerosol (sea-salt and mineral aerosol) during long range transport. Atmos Environ 33:2203-2218

Stadler D, Rossi MJ (2000) The reactivity of NO_2 and HONO on flame soot at ambient temperature: The influence of combustion conditions. Phys Chem Chem Phys 2:5420-5429

Stark JV, Klabunde KJ (1996) Nanoscale metal oxide particles/clusters as chemical reagents–Adsorption of hydrogen halides, nitric oxide, and sulfur trioxide on magnesium oxide nanocrystals and compared with microcrystals. Chem Mater 8:1913-1918

Stark JV, Park DG, Lagadic I, Klabunde KJ (1996) Nanoscale metal oxide particles/clusters as chemical reagents–Unique surface chemistry on magnesium oxide as shown by enhanced adsorption of acid gases (sulfur dioxide and carbon dioxide) and pressure dependence. Chem Mater 8:1904-1912

Stolzenburg MR, McMurry PH (1991) An ultrafine aerosol condensation nucleus counter. Aerosol Sci Tech 14:48-65

Stumm W, Morgan JJ (1996) Aquatic Chemistry. New York: Wiley

Sulzberger B (1990) Photoredox reactions at hydrous metal oxide surfaces: A surface coordination chemistry approach. *In* Aquatic Chemical Kinetics. Stumm W (ed) p 401-430. New York: Wiley

Sulzberger B, Siffert C, Stumm W (1988) Surface coordination chemistry and redox processes—Photoinduced iron (III) oxide dissolution. Chimia 42:257-261

Swap R, Garstang M, Greco S, Talbot R, Kallberg P (1992) Saharan dust in the Amazon basin. Tellus B 44:133-149

Tabazadeh A, Toon OB, Clegg SL, Hamill P (1997) A new parameterization of H_2SO_4/H_2O aerosol composition: Atmospheric implications. Geophys Res Lett 24:1931-1934

Tabazadeh A, Martin ST, Lin JS (2000) The effect of particle size and nitric acid uptake on the homogeneous freezing of sulfate aerosols. Geophys Res Lett 27:1111-1114

Tang IN, Tridico AC, Fung KH (1997) Thermodynamic and optical properties of sea salt aerosols. J Geophys Res 102:23269-23275

Tegen I, Fung I (1994) Modeling of mineral dust in the atmosphere–Sources, transport, and optical-thickness. J Geophys Res 99:22897-22914

Tegen I, Fung I (1995) Contribution to the atmospheric mineral aerosol load from land surface modification. J Geophys Res 100:18707-18726

Tegen I, Lacis A, Fung I (1996) The influence on climate forcing of mineral aerosols from disturbed soils. Nature 380:419-422

Tobias HJ, Ziemann PJ (2000) Thermal desorption mass spectrometric analysis of organic aerosol formed from reactions of 1-tetradecene and O_3 in the presence of alcohols and carboxylic acids. Environ Sci Technol 34:2105-2115

Tobias HJ, Beving DE, Ziemann PJ, Sakurai H, Zuk M, McMurry PH, Zarling D, Waytulonis R, Kittelson DB (2001) Chemical analysis of diesel engine nanoparticles using a nano-DMA/thermal desorption particle beam mass spectrometer. Environ Sci Technol 35:2233-2243

Tolbert MA, Toon OB (2001) Atmospheric science–Solving the PSC mystery. Science 292:61-63

Twomey S (1977) The influence of pollution on the shortwave albedo of clouds. J Atmos Sci 34:1149-1152

Underwood GM, Li P, Usher CR, Grassian VH (2000) Determining accurate kinetic parameters of potentially important heterogeneous atmospheric reactions on solid particle surfaces with a Knudsen cell reactor. J Phys Chem A 104:819-829

Underwood GM, Song CH, Phadnis M, Carmichael GR, Grassian VH (2001) Heterogeneous reactions of NO_2 and HNO_3 on oxides and mineral dust: A combined laboratory and modeling study. J Geophys Res (in press)

Utell MJ, Frampton MW (2000) SESSION 5: Who is susceptible to particulate matter and why? Inhal Toxicol 12 (Suppl 1):37-40

van Maanen JMS, Borm PJA, Knaapen A, van Herwijnen M, Schilderman PAEL, Smith KR, Aust AE, Tomatis M, Fubini B (1999) *In vitro* effects of coal fly ashes: Hydroxyl radical generation, iron release, and DNA damage and toxicity in rat lung epithelial cells. Inhal Toxicol 11:1123-1141

Vesala T, Kulmala M, Rudolf R, Vrtala A, Wagner PE (1997) Models for condensational growth and evaporation of binary aerosol particles. J Aerosol Sci 28:565-598

Vogt R, Crutzen PJ, Sander R (1996) A mechanism for halogen release from sea-salt aerosol in the remote marine boundary layer. Nature 383:327-330

Watson AY, Valberg PA (2001) Carbon black and soot: Two different substances. Am Indust Hyg Assoc J 62:218-228

Weber RJ, McMurry PH, Eisele FL, Tanner DJ (1995) Measurement of expected nucleation precursor species and 3-500 nm diameter particles at Mauna Loa Observatory, Hawaii. J Atmos Sci 52: 2242-2257

Weber RJ, Marti JJ, McMurry PH, Eisele FL, Tanner DJ, Jefferson A (1996) Measured atmospheric new particle formation rates: Implications for nucleation mechanisms. Chem Engin Commun 151:53-64

Weber RJ, Marti JJ, McMurry PH, Eisele FL, Tanner DJ, Jefferson A (1997) Measurements of new particle formation and ultrafine particle growth rates at a clean continental site. J Geophys Res 102:4375-4385

Weber RJ, McMurry PH, Mauldin L, Tanner DJ, Eisele FL, Brechtel FJ, Kreidenweis SM, Kok GL, Schillawski RD, Baumgardner D (1998a) A study of new particle formation and growth involving biogenic and trace gas species measured during ACE-1. J Geophys Res 103:16385-16396

Weber RJ, Stolzenburg MR, Pandis SN, McMurry PH (1998b) Inversion of ultrafine condensation nucleus counter pulse height distributions to obtain nanoparticle (~3-10 nm) size distributions. J Aerosol Sci 29:601-615

Weber RJ, McMurry PH, Mauldin RL, Tanner DJ, Eisele FL, Clarke AD, Kapustin VN (1999) New particle formation in the remote troposphere: A comparison of observations at various sites. Geophys Res Lett 26:307-310

Weis DD, Ewing GE (1999) Water content and morphology of sodium chloride aerosol particles. J Geophys Res 104:21275-21285

Wexler AS, Lurmann FW, Seinfeld JH (1994) Modelling urban and regional aerosols—I. Model development. Atmos Environ 28:531-546

Wiedensohler A, Aalto P, Covert D, Heintzenberg J, McMurry PH (1994) Intercomparison of 4 methods to determine size distributions of low-concentration (~100 cm^{-3}), ultrafine aerosols ($3 < D(p) < 10$ nm) with illustrative data from the Arctic. Aerosol Sci Tech 21:95-109

Wiedensohler A, Hansson HC, Orsini D, Wendisch M, Wagner F, Bower KN, Chourlarton TW, Wells M, Parkin M, Acker K, Wieprecht W, Facchini MC, Lind JA, Fuzzi S, Arends BG, Kulmala M (1997) Night-time formation and occurrence of new particles associated with orographic clouds. Atmos Environ 31:2545-2559

Woo KS, Chen DR, Pui DYH, McMurry PH (2001) Measurement of Atlanta aerosol size distributions: Observations of ultrafine particle events. Aerosol Sci Tech 34:75-87

Wooldridge MS (1998) Gas-phase combustion synthesis of particles. Prog Energ Combust Sci 24:63-87

Wooldridge MS, Danczyk SA, Wu JF (1999) Demonstration of gas-phase combustion synthesis of nanosized particles using a hybrid burner. Nanostruct Mater 11:955-964

Wurzler S, Reisin TG, Levin Z (2000) Modification of mineral dust particles by cloud processing and subsequent effects on drop size distributions. J Geophys Res 105:4501-4512

Xie JY, Marlow WH (1997) Water vapor pressure over complex particles. 1. Sulfuric acid solution effect. Aerosol Sci Technol 27:591-603

Xiong Y, Kodas TT (1993) Droplet evaporation and solute precipitation during spray-pyrolysis. J Aerosol Sci. 24:893-908

Xiong JQ, Zhong M, Fang C, Chen LC, Lippmann M (1998) Influence of organic films on the hygroscopicity of ultrafine sulfuric acid aerosol. Environ Sci Technol 32:3536-3541

Yu JZ, Griffin RJ, Cocker DR, Flagan RC, Seinfeld JH, Blanchard P (1999) Observation of gaseous and particulate products of monoterpene oxidation in forest atmospheres. Geophys Res Lett 26:1145-1148

Zakharenko VS (1997) Photoadsorption and photocatalytic oxidation on the metal oxides—Components of tropospheric solid aerosols under the earth's atmosphere conditions. Catalysis Today 39:243-249

Zhang Y, Carmichael GR (1999) The role of mineral aerosol in tropospheric chemistry in East Asia—A model study. J Appl Meteorol 38:353-366

Zhang WX, Wang CB, Lien HL (1998) Treatment of chlorinated organic contaminants with nanoscale bimetallic particles. Catalysis Today 40:387-395

Zhuang Y, Biswas P (2001) Submicrometer particle formation and control in a bench-scale pulverized coal combustor. Energy & Fuels 15:510-516

Zondlo MA, Hudson PK, Prenni AJ, Tolbert MA (2000) Chemistry and microphysics of polar stratospheric clouds and cirrus clouds. Ann Rev Phys Chem 51:473-499